Restoration of $\mathbf{SU(2)_L \times SU(2)_R \times U(1)_A}$ and Emergence of $\mathbf{SU(4)}$ Symmetry in Hadrons

Mikhail Denissenya

Dissertation

zur Erlangung des Doktorgrades der naturwissenschaften
verfasst am Institut für Physik, FB Theoretische Physik,
an der Karl-Franzens-Universität Graz

Betreuer:

Assoz. Prof. Dr. Leonid Glozman

Graz, July 2015

Dedicated to Zhanna,
Yan and Alan

Abstract

Understanding the hadron spectrum is an open issue of fundamental importance in the modern theory of elementary particles. Studying the hadron spectrum opens a way to understand the physics of the strong force binding quarks and gluons into hadrons. The main subject of this thesis is the physics of hadrons composed of light quarks within the lattice approach to Quantum Chromodynamics (QCD). This work brings a new insight for a deeper understanding of chiral symmetry breaking effects in the hadron spectrum. We calculate the hadron masses upon elimination of chiral symmetry breaking dynamics. Our work covers a broad range of hadron channels including mesons and baryons for various angular momenta J. In particular, the analysis of $J = 0, 1$ isoscalar mesons, $J = 2$ tensor mesons, $N(J = 3/2)$ and $\Delta(J = 1/2)$ baryons states in the chirally restored regime is presented for the first time. We find that the hadron states with angular momenta $J > 0$ survive the chiral restoration. The energy levels of the hadron states with the same J are identical and independent of the isospin I, spatial parity P and charge conjugation C quantum numbers. To interpret these energy levels a notion of the QCD dynamical string is introduced. Finally, we propose a new emergent $SU(4)$ symmetry which explains multiple degeneracy of the hadron states of a given angular momentum $J > 0$ in the chirally restored regime. Results presented in this thesis are important in predicting the properties of hadronic matter close to phase transitions under extreme conditions such as high-temperature and high-density. The studies presented in this work are relevant for the understanding of the physics of confinement and can be used for the systematization of hadrons in phenomenology.

Declaration

The results presented in my thesis are based on the research carried out in the Department of Theoretical Physics, at the University of Graz, in Austria. The parts of this thesis present the original contribution of the author unless stated otherwise and a proper credit is given followed by the reference. No part of this thesis has been submitted elsewhere for any other degree or qualification.

My thesis is based on work primarily done by myself and joint contribution from L. Ya. Glozman, C. B. Lang, M. Pak and M. Schröck. Our fruitfull collaboration resulted in the following list of publications presented in the reversed chronological order:

- **"Emergence of the $SU(4)$ symmetry in the spectrum of N and Δ Baryons"**
  M. Denissenya, L. Ya. Glozman, C.B. Lang , M. Pak
  In preparation

[1] **"Evidence for a new $SU(4)$ symmetry with $J = 2$ mesons"**
M. Denissenya, L. Ya. Glozman, M. Pak, to appear in Phys. Rev. D92 (2015) [arXiv:1505.03285]

[2] **"Isoscalar mesons upon unbreaking of chiral symmetry "**
M. Denissenya, L. Ya. Glozman, C.B. Lang Phys.Rev. D91 (2015) 3, 034505 [arXiv:1410.8751]

[3] **"Mesons upon low-lying Dirac mode exclusion "**
M. Denissenya, L. Ya. Glozman, C.B. Lang PoS LATTICE 2014 (2014) 068 [arXiv:1309.0202]

[4] **" Symmetries of mesons after unbreaking of chiral symmetry and their string interpretation"**
M. Denissenya, L. Ya. Glozman, C.B. Lang Phys.Rev. D89 (2014) 7, 077502 [arXiv:1402.1887]

[5] **"Chiral symmetry breaking and the generation of light hadron masses**
M. Denissenya, L. Ya. Glozman [arXiv:1401.6034]

[6] **"Effects of low vs. high fermionic modes on hadron mass generation"**
M. Denissenya, L. Ya. Glozman, C.B. Lang, M. Schröck PoS LATTICE2013 115 [arXiv:1310.8584]

[7] **"More effects of Dirac low-mode removal "**
M. Denissenya, L. Ya. Glozman, C.B. Lang, M. Schröck PoS LATTICE2013 116 [arXiv:1309.0202]

Contents

Chapter 1

Introduction

The rise of Quantum Chromodynamics as the theory of strongly interacting quarks and gluons marked a new century of development in theoretical and experimental physics [8, 9]. Together with the theory of week interactions [10] it has become possible to explain the origin of the mass in the observable part of our Universe. In particular, the mass of any hadron composed of colored quarks and gluons is primarily due to the strong interactions. There are two intrinsically non-perturbative phenomena determining the shape of the hadron spectrum, confinement and dynamical chiral symmetry breaking. Confinement forbids the observation of a single quark or gluon and restricts all possible internal structure of hadrons so that we observe only colorless states in nature. Chiral symmetry breaking explains the dynamical quark mass generation, appearance of nearly massless pions and absence of the parity doublets in the low-lying part of the hadron spectrum. Both confinement and Spontaneous Chiral Symmetry Breaking (SχSB) are important for the hadron interactions.

Advanced and sophisticated techniques were developed to deepen our understanding of hadronic interactions including the Dyson-Schwinger approach [11, 12], Lattice QCD [13–15], QCD Sum Rules [16, 17], etc. However, no satisfactory explanation of confinement or SχSB is given in terms of the underlying quark and gluon dynamics. In particular, there is no consistent and systematic picture of the low-lying hadrons composed of light quarks.

Various phenomenological schemes and mass formulae are proposed to classify experimental data on the hadron masses over the region 1000–2400 MeV [18–20]. The hadron spectrum of the high-lying states above 1700 MeV exhibits a large degeneracy of states signalling of $SU(2)_L \times SU(2)_R$ and $U(1)_A$ symmetries restoration [21–24]. It turns out, that this large degeneracy is absent in the low-lying hadrons below 1700 - 1800 MeV. The spectrum of these low-lying hadrons is strongly affected by the SχSB effects. We

consider that the removal of the SχSB effects by hand enables us to explain such phenomenological observations in the low-lying as well as in the high-lying spectrum of hadrons. Thus, we hope to get a deeper insight into the physics of hadrons and shed light on the other interesting aspects of the low-energy regime of QCD.

Our work in this thesis is primarily devoted to the study of the hadron spectrum under removal of the chiral symmetry breaking dynamics and its implications. We use the lattice formulation of QCD with exact chiral symmetry to extract the information on hadron masses subject to unbreaking of chiral symmetry. The results presented in this work are contrasted to the similar studies performed in References [25–27] with approximate chiral symmetry on the lattice.

The thesis is organized as follows. Chapter 2 contains an introductory material necessary for the understanding of the lattice QCD approach with an emphasize on lattice chiral symmetry. Chapter 3 introduces the basic ideas and techniques to unbreak chiral symmetry on the lattice. In Chapter 4 we use hadron correlation functions to probe the symmetries of mesons on removal of the chiral symmetry breaking dynamics. This chapter contains separate sections for $J = 0$, $J = 1$ and $J = 2$ mesons. Each section includes a discussion on the model independent constraints based on the chiral symmetry group classification of mesons. Section 4.1 provides the first evidence for the restoration of $SU(2)_L \times SU(2)_R$ and $U(1)_A$ symmetries with $J = 0$ mesons. In Section 4.2 we show that the masses of $J = 1$ mesons depend only on the radial excitation number in the chirally restored regime. To explain our observations with $J = 1$ mesons a notion of the QCD dynamical string and emergent $SU(4)$ symmetry are introduced in the related subsections. Section 4.3.1 provides an additional evidence for $SU(4)$ symmetry with $J = 2$ mesons on the lattice. In Chapter 5 we present our results for the spectrum of light baryons and compare it with the chiral symmetry predictions. Information on the gauge ensemble used in our study is provided in Appendix A. Appendix B contains a description of the stochastic estimation techniques for the all-to-all-propagators. Discussion on the reweighting of the fermion determinant and its implications are presented in Appendix C. Appendix D discusses a diminishing role of the explicit chiral symmetry breaking due to a finite quark mass and presence of exact zero modes of the Dirac operator. Finally, numerical values for the hadron masses and corresponding statistics are summarized in tables of Appendix E.

Chapter 2

Formulation of Euclidean QCD on the Lattice

This chapter deals with the simplest formulation of Quantum Chromodynamics on the lattice [1]. For this formulation we have to find a discretized and gauge invariant analog for the continuum QCD action

$$S_E[\bar{\psi}, \psi, A_\mu] = \int d^4x \mathcal{L}_{QCD} \ , \tag{2.1}$$

where $\mathcal{L}_{QCD}$ is the Euclidean QCD Lagrangian with gluon A_μ and quark ψ degrees of freedom

$$\mathcal{L}_{QCD} = \bar{\psi}(\gamma_\mu D_\mu + M)\psi + \frac{1}{4g^2} F^a_{\mu\nu} F^a_{\mu\nu} \ , \tag{2.2}$$

The fermion part of the Lagrangian includes the quark mass matrix M and covariant derivative

$$D_\mu = \partial_\mu + iA_\mu \ , \tag{2.3}$$

where the gauge field A_μ is expressed in terms of the generators T_a in the fundamental representation of the $SU(3)_c$ group with c denoting color

$$A_\mu = \sum_{a=1}^{8} A^a_\mu T_a \ . \tag{2.4}$$

The gauge action contains the $F^a_{\mu\nu}$ gluon field-strength tensor constructed out of the gauge field components A^a_μ

$$F^a_{\mu\nu} = \partial_\mu A^a_\nu - \partial_\nu A^a_\mu - f_{abc} A^b_\mu A^c_\nu \ , \tag{2.5}$$

[1] We refer to the reference [28] for a pedagogical and systematic treatment of this subject.

where f_{abc} are the structure constants of the $SU(3)_c$ group.

In the first step of the lattice formulation of QCD a continuous four-dimensional Euclidean space is replaced by the hypercubic lattice

$$x_\mu \longrightarrow x_\mu = n_\mu a \ , \tag{2.6}$$

where $n_\mu = (n_1, n_2, n_3, n_4)$ labels the lattice *sites*. The line which connects two neighboring sites is called a link. A minimal distance a between these nearest sites a is called a *lattice spacing*. An integral over four-dimensional space is substitued by its lattice counterpart

$$\int d^4x \longrightarrow a^4 \sum_x \ . \tag{2.7}$$

The lattice disretization of the gauge and fermion part of the QCD action on this hypercubic lattice is non-trivial. We illustrate the main principles of such a construction in the next sections.

2.1 Gauge action

To construct any gluon gauge invariant action one uses a *gauge transporter* defined as

$$U(x_1, x_2) = \mathcal{P}\ \mathrm{e}^{\,i \int_{C_{x_1,x_2}} dl A_\mu(x)} \ , \tag{2.8}$$

where $\mathcal{P}$ denotes the path ordering and C_{x_1,x_2} is an arbitrary countour connecting the points x_1 and x_2.

Using (2.8) any gauge transporter connecting arbitrary points x_1 and x_2 on the lattice can be constructed from a simpler gauge transporters as follows

$$U_{x_1,x_2} = \prod_{j=0}^{N-1} U_{z_j,z_{j+1}} \ , \tag{2.9}$$

where z_j are all intermediate lattice points. For two neighboring points $z_j = x$ and $z_{j+1} = x + a\hat{\mu}$ and sufficiently small a, $U_{z_j,z_{j+1}}$ reduces to

$$U_{x,x+a\hat{\mu}} = 1 + iaA_\mu + \mathcal{O}(a^2) \ . \tag{2.10}$$

We see that it is natural to replace the gauge degree of freedom A_μ by the so-called link variable $U_{x,\mu} = \mathrm{e}^{iaA_\mu(x)}$. The latter is defined on the link of the lattice which starts at a point x and is oriented in the μ direction.

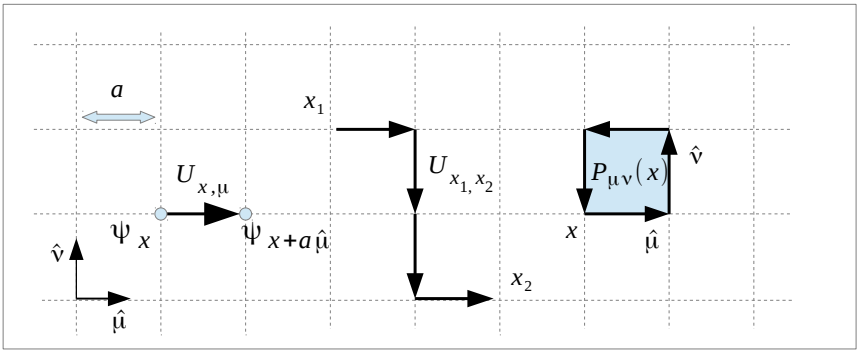

Figure 2.1: Illustration for the simplest gauge variant and gauge invariant objects on the two-dimensional lattice.

Under a gauge transformation (2.10) transforms as

$$U_{x,x+a\hat{\mu}} \longrightarrow \Omega_x U_{x,x+a\hat{\mu}} \Omega^{\dagger}_{x+a\hat{\mu}} \,, \tag{2.11}$$

where Ω_x is an element of the $SU(3)_c$ gauge group. Then the lattice gauge transporter obeys similar transformation property

$$U_{x_1,x_2} \longrightarrow \Omega_{x_1} U_{x_1,x_2} \Omega^{\dagger}_{x_2} \,. \tag{2.12}$$

This enables us to construct the following gauge invariant object involving only the gauge fields

$$\mathrm{tr}(U_{x_1,x_2} U_{x_2,x_3} U_{x_3,x_4} U_{x_4,x_1}) \,, \tag{2.13}$$

where tr is the trace over the color indices.

The so-called plaquette $P_{\mu\nu}(x)$ is the simplest form of (2.13)

$$P_{\mu\nu}(x) = U_{x,\mu} U_{x+a\hat{\mu},\nu} U_{x+a\hat{\mu}+a\hat{\nu},-\mu} U_{x+a\hat{\nu},-\nu} \,. \tag{2.14}$$

$P_{\mu\nu}(x)$ can be related to the field-strength tensor in the continuum limit $a \to 0$

$$P_{\mu\nu}(x) = \mathrm{e}^{ia^2 F_{\mu\nu}(x) + \ldots} \,. \tag{2.15}$$

Expanding (2.15) in powers of a^2, we get

$$P_{\mu\nu} = 1 + ia^2 F_{\mu\nu} - \frac{1}{2} a^4 F_{\mu\nu} F_{\mu\nu} + \ldots \,. \tag{2.16}$$

By comparing the terms on the *rhs* of (2.16) with (2.2) we obtain the famous Wilson action

$$S_G[U] = \frac{2}{g^2} \sum_x \sum_{\mu<\nu} \text{Re tr}(1 - P_{\mu\nu}(x)) \; . \tag{2.17}$$

Other gauge actions are constructed by considering more complicated closed loops of links.

2.2 Fermionic action

The quarks ψ_x live on the sites of the lattice. To construct the fermionic action we need to find a gauge invarint object involving quark degees of freedom. The gauge transformation properties of the fermion fields are the following

$$\begin{aligned} \psi_x &\rightarrow \Omega_x \psi_x \; , \\ \bar{\psi}_x &\rightarrow \bar{\psi}_x \Omega_x^\dagger \; . \end{aligned} \tag{2.18}$$

From the last section we know the transformation properties of the gauge transporter on the lattice, see (2.12). This enables us to deduce the second type of gauge invariant objects involving quark and gauge degrees of freedom, namely

$$\bar{\psi}_{x_1} U_{x_1,x_2} \psi_{x_2} \; . \tag{2.19}$$

Further, we use Equation (2.19) in the construction of the lattice fermion action. The descritization of the mass term $m\bar{\psi}\psi$ is obtained simply by setting $x_1 = x_2$ in (2.19). The descritization of the term with the covariant derivative (2.3) can be easily obtained by employing a symmetric definition of the partial derivative

$$\bar{\psi}(x)\gamma_\mu(\partial_\mu + iA_\mu)\psi(x) \rightarrow \bar{\psi}_x \gamma_\mu \frac{\psi_{x+a\hat{\mu}} - \psi_{x-a\hat{\mu}} + 2iaA_\mu\psi_x}{2a} \; . \tag{2.20}$$

Next, we can identify the terms on the *rhs* of (2.20) with the gauge invariant object of the form (2.19) up to order $\mathcal{O}(a^2)$ corrections

$$\begin{aligned} \bar{\psi}_x \gamma_\mu U_{x,x+a\hat{\mu}} \psi_{x+a\hat{\mu}} &= \bar{\psi}_x \gamma_\mu \psi_{x+a\hat{\mu}} + \bar{\psi}_x iaA_\mu \psi_x \; , \\ \bar{\psi}_x \gamma_\mu U_{x,x-a\hat{\mu}} \psi_{x-a\hat{\mu}} &= \bar{\psi}_x \gamma_\mu \psi_{x-a\hat{\mu}} - \bar{\psi}_x iaA_\mu \psi_x \; . \end{aligned} \tag{2.21}$$

Finally, we arrive at a "naive" fermion action

$$S_F[\psi, \bar{\psi}, U] = a^4 \sum_x \bar{\psi}_x (\gamma_\mu \frac{U_{x,x+a\hat{\mu}}\psi_{x+a\hat{\mu}} - U_{x,x-a\hat{\mu}}\psi_{x-a\hat{\mu}}}{2a} + m\psi_x) \; . \tag{2.22}$$

However, this fermion disretization suffers from a fermion doubling problem. To see this it is sufficient to take the free part of (2.22) and set m to zero

$$S_F[\psi, \bar{\psi}, U] = a^4 \sum_x \bar{\psi}_x D(x, y) \psi_y \ , \tag{2.23}$$

where the Dirac operator D has the following form

$$D(x, y) = \frac{1}{2a} \gamma_\mu (\delta_{y,x+a\hat{\mu}} - \delta_{y,x-a\hat{\mu}}) \ . \tag{2.24}$$

It turns out, that the inverse of D in momentum space is

$$D(p)^{-1} = \frac{-ia^{-1} \sum_\mu \gamma_\mu \sin(p_\mu a)}{a^{-2} \sum_\mu \gamma_\mu \sin^2(p_\mu a)} \ , \tag{2.25}$$

where $-\pi/a < p_\mu \leq \pi/a$, has 15 fictitious poles in addition to a physical one at $p = (0, 0, 0, 0)$. In the continuum limit, these spurious doublers cause unphysical effects. To remove such unwanted effects it is possible to introduce the so called Wilson term. However, this term breaks chiral symmetry explicitely even when $m \to 0$. In our study, it is crucial to preserve chiral symmetry in the fermion desritization. In the next section we introduce the basic ideas of how it can be done at a finite lattice spacing a.

2.3 Lattice Chiral Symmetry

The problem of preserving chiral symmetry on the lattice is far from being trivial. Every kind of fermionic descretization breaks chiral symmetry on the lattice in its own way

Chiral symmetry in the continuum

Chiral symmetry in the continuum is preserved automatically and expressed via the simple relation

$$\{\gamma_5, D\} = 0 \ . \tag{2.26}$$

However, there was an obstacle to obtain a discretization of the Dirac operator D such that this relation is preserved. A no-go theorem was formulated by Nilsen and Ninomiya in [29]. This theorem states that it is impossible to construct a local invertible Dirac operator that preserves chirality (2.26) and is free from fermion doublers on the lattice.

Ginsparg-Wilson Relation

Later, Ginsparg and Wilson found a way to bypass this no-go theorem [30]. In this work they seek for the answer to the folowing question: What is the remnant of chiral symmetry that is left when one starts from the continuum action and goes to a discrete one by the spin-block transformation? The answer to this question is summarized in the famous *Ginsparg-Wilson relation*:

$$\gamma_5 D + D\gamma_5 = aD\gamma_5 RD \ , \tag{2.27}$$

where R is a local term. This relation tells us that $\{\gamma_5, D\}$ is not exactly zero and chiral symmetry is broken on the lattice by a higher dimensional operator $aD\gamma_5 D$. The latter goes to zero as we approach the continuum limit of zero lattice spacing. Second, this relation holds exactly for any finite distance. To see this we rewrite this relation in terms of the quark propagator $S = D^{-1}$

$$\gamma_5 S(x,y) + S(x,y)\gamma_5 = a\gamma_5 R\delta(x,y) \ , \tag{2.28}$$

where the *rhs* is non-zero only when $|x-y| = 0$. This implies that any operator satisfying this relation is automatically chirally invariant at arbitrary distances $|x-y| = 0$ with corrections up to the order $\mathcal{O}(a)$.

Overlap Operator

The explicit construction of the Dirac operator that satisfies the Ginsparg-Wilson relation was found in [31, 32]. Such a construction is called the overlap operator. The latter is of the following form for the massless case

$$D_{ov}(0) = \frac{1}{\bar{a}}(1 + \frac{H_W}{\sqrt{H_W^\dagger H_W}}) \ , \tag{2.29}$$

where $\bar{a} = a/\rho$, $H_W = a\gamma_5 D_W(-\rho)$ is the hermitian Wilson-Dirac operator and ρ is the Wilson mass. It is easy to check that this operator fullfills the Ginsparg-Wilson relation taking $R = \delta_{x,y}/\rho$. There are a number of different operator constructions that satisfy this relation like domain wall [33, 34], etc.

Chiral rotations on the lattice

Chiral rotations in the continuum leave the massless QCD Lagrangian invariant. However, modified chiral rotations have to be introduced to preserve this property on the lattice [35]:

$$\begin{array}{lcl} \text{in continuum} & & \text{on the lattice} \\ \psi'(x) = \mathrm{e}^{i\,\theta^b\,T^b\gamma_5}\,\psi(x) & \longrightarrow & \psi'_x = \mathrm{e}^{i\,\theta^b\,T^b\gamma_5(1-\frac{a}{2}D)}\,\psi_x, \\ \bar{\psi}'(x) = \bar{\psi}(x)\,\mathrm{e}^{i\,\theta^b\,T^b\gamma_5} & \longrightarrow & \bar{\psi}'_x = \bar{\psi}_x\,\mathrm{e}^{i\,\theta^b\,T^b(1-\frac{a}{2}D)\gamma_5}\ . \end{array} \tag{2.30}$$

The lattice version of the chiral rotations reveals the physical content of the Ginsparg-Wilson relation. These transformations leave the discretized fermion action S_F invariant. The invariance of the QCD action under chiral rotations on the lattice is of crucial importance in our studies.

2.4 Path Integral Quantization

Quantization of the classical Euclidean QCD action S_{QCD} is achieved via the path integral prescription. Given the partition sum

$$Z = \int DA_\mu D\bar{\psi} D\psi\,\mathrm{e}^{-S_{QCD}}\ , \tag{2.31}$$

the path integral on the lattice is obtained by replacing the continuum measure with its discrete analog

$$\int DA_\mu D\bar{\psi} D\psi \longrightarrow \int DU D\bar{\psi} D\psi = \prod dU_{x,\mu} \prod d\bar{\psi}_x d\psi_x\ . \tag{2.32}$$

For a chosen discretization of the QCD action

$$S_{QCD}[U,\bar{\psi},\psi] = S_A[U] + S_F[U,\bar{\psi},\psi]\ , \tag{2.33}$$

any observable on the lattice can be computed via

$$< \mathcal{O} >= \frac{\int DU D\bar{\psi} D\psi\,\mathcal{O}[U,\bar{\psi},\psi]\,\mathrm{e}^{-S_A[U]-S_F[U,\bar{\psi},\psi]}}{\int DU_{x,\mu} D\bar{\psi} D\psi\,\mathrm{e}^{-S_A[U]-S_F[U,\bar{\psi},\psi]}}\ . \tag{2.34}$$

To perform numerical simulations the fermionic degrees of freedom are integrated out formally. As a result of such integration the fermion determinant is introduced for each

fermion flavour, e.g. in $N_f = 2$:

$$< \mathcal{O} >= \frac{\int DU\, \mathcal{O}[U, \bar{\psi}, \psi]\, (\mathrm{det}D[U])^2\, \mathrm{e}^{-S_A[U]}}{\int DU \mathrm{det}D_u[U] (\mathrm{det}D[U])^2\, \mathrm{e}^{-S_A[U]}}\ . \tag{2.35}$$

In practice, the Boltzmann weight factor $(\mathrm{det}D[U])^2 e^{-S_A[U]}$ is used to generate the gauge field configurations U at finite volume V. An ensemble of the generated gauge configurations is subsequently used to measure various observables and extract valuable information on QCD dynamics on the lattice

$$< \mathcal{O} >= \frac{1}{N} \sum_{i=1}^{N} O[U_i]\ . \tag{2.36}$$

The continuum $a \to 0$ and thermodynamic $V \to \infty$ limits have to be taken for the reliable comparison of the measured observable with the experiment or other approaches to QCD.

Chapter 3

Unbreaking Chiral Symmetry

3.1 SχSB and Banks-Casher Relation

In the limit of massless quarks the QCD Lagrangian exhibits the following global chiral properties. First, on the classical level it is invariant under $U(1)_A$ symmetry transformations of each quark flavor

$$\begin{aligned} \psi \to \psi' &= \mathrm{e}^{i\gamma_5\alpha}\,\psi \ , \\ \bar{\psi} \to \bar{\psi}' &= \bar{\psi}\,\mathrm{e}^{i\gamma_5\alpha} \ . \end{aligned} \tag{3.1}$$

However, this symmetry is broken by an anomaly on the quantum level due to the non-invariance of the fermion measure [36, 37] under these chiral rotations. Second, one can easily check that the same Lagrangian for $N_F = 2$ flavors is invariant under a global $SU(2)_L \times SU(2)_R$ symmetry transformation, the left-handed and right-handed components of the quark fields are rotated independently [38, 39]

$$\begin{aligned} \psi_L \to \psi'_L &= \mathrm{e}^{-i\frac{\tau^a}{2}\theta^a_L}\,\psi_L \ , \\ \psi_R \to \psi'_R &= \mathrm{e}^{-i\frac{\tau^a}{2}\theta^a_R}\,\psi_R \ . \end{aligned} \tag{3.2}$$

However, it is an experimental fact that the $SU(2)_L \times SU(2)_R$ chiral symmetry of the QCD Lagrangian is spontaneously broken by the formation of the quark condensate

$$\langle\bar{\psi}\psi\rangle = \langle\bar{\psi}_L\psi_R + \bar{\psi}_R\psi_L\rangle \neq 0 \ . \tag{3.3}$$

The symmetry group $SU(2)_L \times SU(2)_R$ is reduced to $SU(2)_V$. Non-zeroness of the quark condensate contributes to $U(1)_A$ symmetry breaking in addition to the axial anomaly. The breakdown of $SU(2)_L \times SU(2)_R \times U(1)_A$ and appearance of the quark condensate at the quantum level has an impact on the properties of the hadron spectrum. For

example, the appearance of the pions as the pseudo-Goldstone bosons and anomalously heavy η' meson in the spectrum, absence of the parity doublets in the low-lying part of the meson as well as the baryon spectra.

In Euclidean four-dimensional space the quark condensate can be defined as a trace of the quark propagator $S = D^{-1}$ in the chiral limit

$$\langle\bar{\psi}\psi\rangle = \text{Tr } S(x,x) = \sum_n \frac{1}{i\lambda_n}\langle x|\lambda_n\rangle\langle\lambda_n|x\rangle \ , \tag{3.4}$$

where λ_n are the eigenvalues and $|\lambda_n\rangle$ are the eigenmodes of the massless Dirac operator $D(0) = D(m_q \to 0)$. Due to anti-hermiticity of the Dirac operator its eigenvalues are purely imaginary or exactly zero

$$D(0)|\lambda_n\rangle = i\lambda_n|\lambda_n\rangle \ , \tag{3.5}$$

where λ_n is real.

It can be shown that a non-zero density of the eigenvalues λ close to zero is responsible for the appearance of the quark condensate in the theory. This statement is summarized in the following Banks-Casher formula

$$\langle 0|\overline{\psi}\psi|0\rangle = -\lim_{m_q\to 0}\lim_{V\to\infty}\int_0^\infty d\lambda\rho(\lambda)\frac{2m_q}{{m_q}^2+\lambda^2} = -\pi\rho(0) \ , \tag{3.6}$$

where $\rho(0)$ is the so called spectral density of the eigenvalues of the Dirac operator.

Notice the sequence of limits in Equation (3.6). Taking the chiral limit first with fixed volume would not produce the non-zero condensate. A large number of computations of the quark condensate by exploiting this definition are performed on the lattice [40–43] in a good agreement with the phenomenological value. On the lattice the Dirac eigenmodes with the near-zero eigenvalues are associated with the chiral symmetry breaking dynamics [44–49]. One might expect that removing exactly these low-lying eigenmodes in lattice simulations yields a decoupling of quarks from the quark condensate of the vacuum. The latter can be used to test the implications of artificial chiral symmetry restoration in hadron spectrum. This is done by excluding the lowest Dirac eigenmodes from the valence quarks. A procedure of the low-mode removal was introduced in [25–27] using the Chirally Improved Dirac operator D_{CI} on the lattice [50]. This fermion discretization does not preserve chiral symmetry exactly and suffers from the additive quark mass renormalization. In addition, the D_{CI} operator is non-normal and satisfies γ_5 - hermiticity

$$D_{\text{CI}}^\dagger = \gamma_5 D_{\text{CI}}\gamma_5 \ . \tag{3.7}$$

The γ_5 - hermiticity means that the eigenvalues of $D_{\rm CI}$ are either real or come in complex conjugate pairs. The corresponding eigenvalue spectrum is spread in the complex plain [27] which introduces an ambiguity in the ordering of the eigenvalues by the absolute value. This issue was resolved with the use of eigenvalues of the hermitian $\gamma_5 D_{\rm CI}$ operator. However, there is no one-to-one correspondence of the modes of this operator with the modes of the chirally-symmetric Dirac operator. A possible contribution from the exact zero-modes of $D_{\rm CI}$ operator is not excluded in the computation of the hadron observables. These difficulties do not occur if the Dirac operator preserves chiral symmetry on the lattice exactly. In our work we use the chirally invariant Overlap operator and advantages of using this operator on the lattice are emphasized in the next section.

3.2 Eigenvalue Spectrum of the Overlap Operator

The Overlap operator for a non-zero quark mass m_q has the following form

$$D_{\rm ov}(m_q) = (\rho + \frac{m_q}{2}) + (\rho - \frac{m_q}{2})\gamma_5 {\rm sign}(H_W) \ , \tag{3.8}$$

where H_W is the Wilson kernel, ρ is the Wilson mass parameter.

The Overlap operator (3.8) is γ_5 - hermitian and satisfies the Ginsparg-Wilson relation Equation (2.27). The latter implies that the non-zero eigenvalues $\lambda = x + iy$ of the Overlap operator are restricted on the complex plane by the following equation

$$\Big(x - \frac{\rho + \frac{m_q}{2}}{a}\Big)^2 + y^2 = \frac{(\rho - \frac{m_q}{2})^2}{a^2} \ . \tag{3.9}$$

According to Equation (3.9) the non-zero eigenvalues are distributed on the circle of the radius $\rho - m_q/2$ with a center displaced from the origin by $\rho + m_q/2$ for $a = 1$, as it is shown on Figure 3.1 (left). The eigenvalues come in complex conjugate pairs (λ, λ^*) and can be ordered by the magnitude of the imaginary ${\rm Im}\lambda$ or real part ${\rm Re}\lambda$ of the corresponding eigenvalue. There is a one-to-one correspondence between the complex eigenvalues $x+iy$ and eigenvectors of the operator with a finite mass $D_{\rm ov}(m_q)$ and purely imaginary eigenvalues at $m_q \to 0$, i.e.

$$D_{\rm ov}(0)|\lambda_n\rangle = \lambda_n(0)|\lambda_n\rangle \ , \tag{3.10}$$

$$D_{\rm ov}(m_q)|\lambda_n\rangle \overset{(3.8)}{=} [(1 - \frac{m_q}{2\rho})D_{\rm ov}(0) + m_q]|\lambda_n\rangle = \lambda_n(m_q)|\lambda_n\rangle \ , \tag{3.11}$$

where $\lambda_n(m_q) = (1 - \frac{m_q}{2\rho})\lambda_n(0) + m_q$. The eigenmode basis $\{\lambda_n\}$ of the $D_{\rm ov}(m_q)$ and $D_{\rm ov}(0)$ operators is the same and satisfies the orthogonality condition. The eigenmodes corresponding to the complex conjugate eigenvalues $|\lambda\rangle$ and $|\lambda^*\rangle$ are related by a γ_5

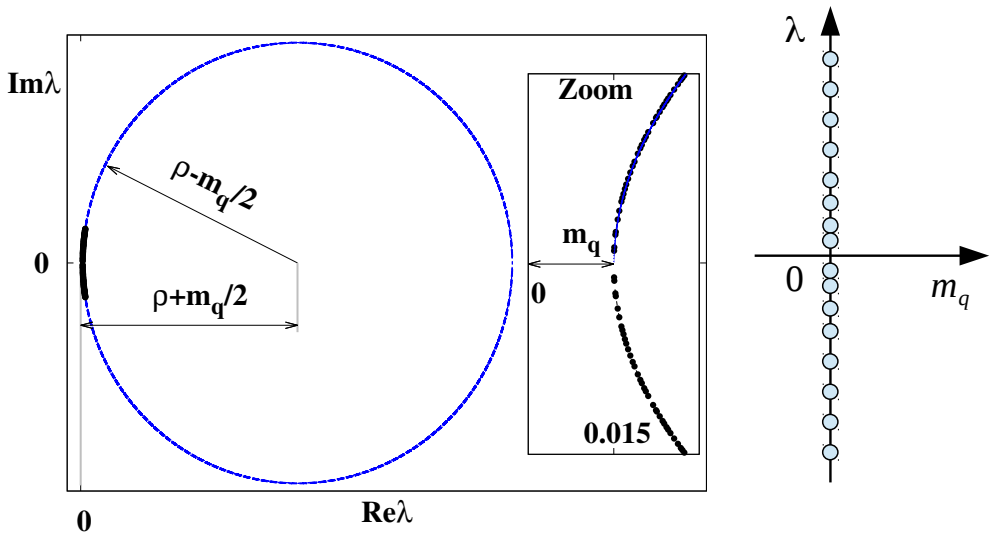

Figure 3.1: Eigenvalue spectrum of the Overlap operator (left) in the naive continuum limit (right)

transformation. The eigenvalue spectrum of the Overlap operator $D(m)$ reproduces the original eigenvalue spectrum (3.5) of the anti-hermitian Dirac operator D in the continuum and chiral limits

$$\lambda_n(m_q) \xrightarrow{m_q \to 0} i\lambda \ , \tag{3.12}$$

see Figure 3.1 (right).

A sample of numerically calculated 50 pairs of the lowest eigenvalues of the Overlap operator (3.8) is depicted on Figure 3.1 in the inset plot. These eigenvalues were computed on a single gauge configuration of an ensemble **A**, see Appendix A. The histogram $\mathrm{H}(|\mathrm{Im}\lambda|)$ of the eigenvalues computed on the same gauge ensemble and averaged over the number of the gauge configurations N_{conf} is shown on figure Figure 3.2. $\mathrm{H}(|\mathrm{Im}\lambda|)$ is the spectral density which a lattice analog for the Dirac spectral density $\rho(\lambda)$ in the continuum. By introducing an integrated spectral density we can assign the energy σ [1] which corresponds to any number of k lowest eigenmodes on the lattice. The curve depicted on Figure 3.2 (right) establishes the connection between the number of the lowest k modes and the energy σ they represent on the gauge ensemble A. For example, exclusion of the $k = 10$ and $k = 30$ lowest modes from the spectrum introduces the $\sigma = 65$ MeV and $\sigma = 180$ MeV energy gap in the Dirac eigenvalue spectrum, respectively.

[1] The scale here is plotted for the unrenormalized values of σ and quark mass m_q. To take into account the renormalization one needs to consider the definition of renormalized quark mass which goes as follows

$$m(\mu) = \lim_{a \to 0} Z(a\mu) m_q(a) \ .$$

We use $Z_m^{\overline{MS}}(2 \text{ GeV }) = 0.838(14)$ computed on the JLQCD gauge ensembles in Ref. [51].

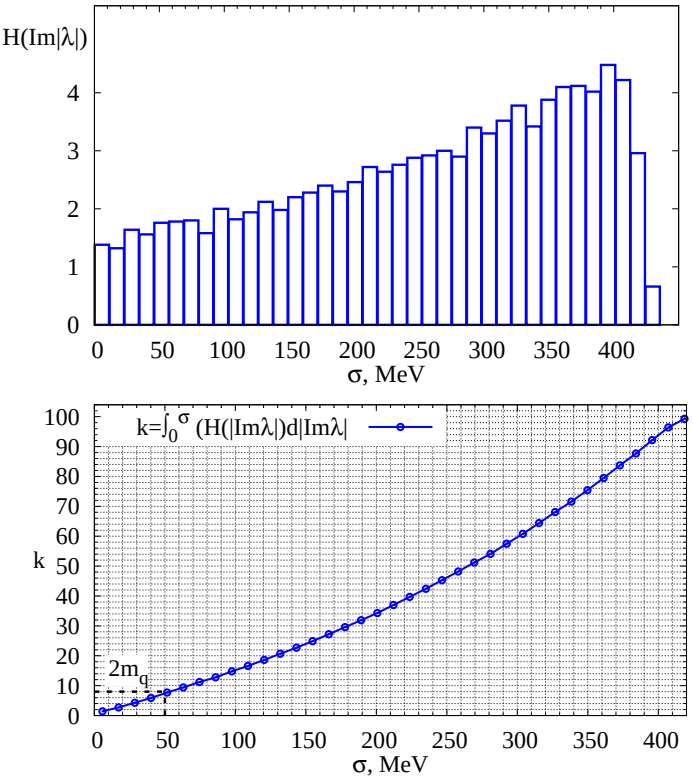

Figure 3.2: Spectral density (upper) and integrated spectral density (lower) of the eigenvalues of the Overlap operator on the ensemble A of the gauge field configurations.

In the next section we describe the methodology of how these low-lying eigenmodes can be used to remove the chiral symmetry breaking dynamics from the valence quark propagators.

3.3 Reduced Quark Propagators

In the full dynamical simulations the Dirac operator is used in the evaluation of the fermion determinant as well as in the computation of the quark propagator on a given gauge configuration. In our analysis, we leave the fermion determinant intact [2] and introduce modifications on the valence quark propagators. Our strategy of exclusion of the low-lying modes from the valence quarks is described below.

First, the full quark propagator is obtained by inverting the Overlap operator for a given quark mass m_q

$$S_{\text{Full}} = D_{\text{ov}}^{-1}(m_q) \; . \tag{3.13}$$

[2] Appendix C deals with the modification of the fermion determinant by means of the reweighting technique.

Then we compute the low-mode quark propagator $S_{\mathrm{LM}(k)}$ using the spectral decomposition

$$S_{\mathrm{LM}(k)} = \sum_{i=1}^{k} \frac{1}{\lambda_i(m_q)} |\lambda_i\rangle\langle\lambda_i| \ , \tag{3.14}$$

where k is the number of the lowest eigenvalues $\lambda_i(m_q)$ and eigenmodes $|\lambda_i\rangle$ of the massive Overlap operator $D_{\mathrm{ov}}(m_q)$.

In the last step, we define reduced quark propagators by subtracting the low-mode quark propagators from the full propagator

$$S_k = S_{\mathrm{Full}} - S_{\mathrm{LM}(k)} \ . \tag{3.15}$$

Given the one-to-one correspondence of $\lambda_i(m_q)$ and $|\lambda_i\rangle$ with the eigenvalues and eigenvectors at $m_q \to 0$ such a procedure decouples the valence quarks from the quark condensate. We expect that the exclusion of the low-lying modes reduces the effects of chiral symmetry breaking in the quark propagators S_k, where k value denotes the respective truncation level (2,4,6,...,100), $k = 0$ corresponds to the full quark propagator. The larger the amount of the excluded low-lying modes k, the larger is suppressed the effect of chiral symmetry breaking. Reduced quark propagators S_k are used in the computation of the hadron propagators at each level of truncation k. We then apply hadron spectroscopy methods to extract hadron masses on unbreaking chiral symmetry.

3.4 Hadron Spectroscopy

We study the hadron spectrum in the transition region from the chirally broken to a chirally restored regime. We have to ensure that our prescription is consistent and captures the main features of the hadron spectrum in both of these regimes. Below we discuss subtle issues related to the selection of hadron interpolators and the method used to extract hadron states before and after unbreaking of chiral symmetry.

3.4.1 Note on Interpolator Basis

In general , to extract the hadron states on the lattice one needs to construct an operator $\mathcal{O}_H$ that carries the quantum numbers I, J^{PC} of the state of interest. Such an operator is called an interpolating current or *interpolator* on the lattice. It is expected that a given hadron state can be created by acting with this interpolator onto the vacuum state of the theory. However, it can be shown that a single interpolator may couple to more than one state in a given quantum channel. So, what one actually gets is a superposition of

states n, i.e.

$$|'H'\rangle = \mathcal{O}_H|\text{vac}\rangle_{QCD} = \sum_{n=0} c_n|I, J^{PC}; n\rangle \ , \tag{3.16}$$

where

$$c_n = \langle I, J^{PC}; n|\mathcal{O}_H|\text{vac}\rangle_{QCD} \tag{3.17}$$

is the coupling of an interpolator $\mathcal{O}_H$ to a hadron state $|I, J^{PC}; n\rangle$.

Moreover, different interpolators with the same quantum numbers can couple to the same state. One can use only a finite basis of interpolators to study hadrons on the lattice. The latter is primarily due to finite computational resources. In our work we use only single particle interpolators.

Another important issue is related to the determination of the hadron spectrum in the chirally restored regime. It is expected that the left-handed and right-handed quarks decouple from each other and hadron states fall in to chiral multiplets in this regime. These chiral multiplets are labeled with an index r denoting the left and right isospin content (I_L, I_R) of a given hadron state. This implies that in the chirally restored regime in addition to the isospin I index of a given state a new quantum number has to be added, that is the index r of the chiral representation. This has an implication for the hadron spectroscopy in the chirally broken regime. In particular, the states from different chiral representations r and r' get mixed due to chiral symmetry breaking. For example,

$$|I, J^{PC}; n\rangle = \alpha\,|r, I, J^{PC}; n\rangle + \beta\,|r', I, J^{PC}; n\rangle \ , \tag{3.18}$$

where α and β are unknown mixing coefficients:

$$\alpha = \langle I, J^{PC}; n|\mathcal{O}^r_H|\text{vac}\rangle_{QCD}, \qquad \beta = \langle I, J^{PC}; n|\mathcal{O}^{r'}_H|\text{vac}\rangle_{QCD} \ . \tag{3.19}$$

$\mathcal{O}^r_H$ and $\mathcal{O}^{r\prime}_H$ are the interpolators belonging to different chiral representations r and r' with the same I, J^{PC} for mesons and I, J^P for baryons. We take into account this issue and incorporate interpolators $\mathcal{O}^r_H$ and $\mathcal{O}^{r'}_H$ into our interpolator basis for such specific quantum channels. We then take the interpolator basis $\{O^l_H\}^N_{l=1}$ as large as it is possible to extract corresponding ground and excited energy levels of hadrons.

3.4.2 Variational Method

We employ the standard variational method [52–54] which is a very efficient tool to determine the hadron spectrum on the lattice. For a given interpolator basis $\{O^l_H\}^N_{l=1}$,

we construct the cross-correlation matrices of the following from

$$C_{ij}(t) = \langle \mathcal{O}_i(t)\mathcal{O}_j^\dagger(0)\rangle \ . \tag{3.20}$$

Then we formulate a generalized eigenvalue problem

$$C(t)\vec{v}_n(t,t_0) = \lambda_n(t,t_0)C(t_0)\vec{v}_n(t,t_0) \ , \tag{3.21}$$

where $t_0 = 1$ is chosen as a reference time slice in our analysis. Solution to this eigenvalue problem enables us to determine the energy levels in a given quantum channel. We choose reasonable time ranges where the eigenvalues $\lambda(t,t_0)$ decay exponentially, i.e.

$$\lambda^{(n)}(t,t_0) \propto \mathrm{e}^{-E_n(t-t_0)}(1+\mathcal{O}(\mathrm{e}^{-\Delta E_n(t-t_0)}) \ , \tag{3.22}$$

and apply an exponential fit to extract masses E_n, where n labels the ground ($n = 1$) and excited ($n > 1$) energy levels. The eigenvector components v_n^k are used to determine the relative coupling of each interpolator in the basis $\{O_H^l\}_{l=1}^N$ to a specific state n.

Chapter 4

Restoration of $\mathbf{SU(2)_L \times SU(2)_R \times U(1)_A}$ Symmetry in Mesons

4.1 $J = 0$ Mesons

In this section we show how the lattice Euclidean correlators of $J = 0$ mesons are used to probe the restoration of $SU(2)_L \times SU(2)_R \times U(1)_A$ symmetry by the removal of the low-lying eigenmodes of the Dirac operator. Further, we present our results that confirm this symmetry restoration and discuss the resulting spectrum of $J = 0$ mesons in the chirally restored regime.

4.1.1 Probing Chiral Symmetry with Isoscalars

We expect that $J = 0$ mesons composed of two light quarks should fall into chiral multiplets of the parity chiral-group $SU(2)_L \times SU(2)_R \times C_i$ [22, 24, 55] if chiral symmetry is unbroken. This classification is depicted in Figure 4.1 for the $J = 0$ mesons with u and d quark flavors. Corresponding interpolating currents are given in brackets. The isovector-pseudoscalar interpolator is connected to the scalar-isoscalar interpolator via the $SU(2)_L \times SU(2)_R$ symmetry transformation within the $(1/2, 1/2)_a$ chiral multiplet. In other words, chiral symmetry requires the π and σ states to be mass degenerate, if they exist. A similar discussion applies to the η and a_0 states in the $(1/2, 1/2)_b$ chiral multiplet. In addition to this, the states in these two multiplets are related to each other by the $U(1)_A$ symmetry transformation. For instance, the π and a_0 isovector states are connected by this transformation. Restoration of the $SU(2)_L \times SU(2)_R \times U(1)_A$ symmetry implies that these four meson states have to be mass degenerate, if they exist. To claim the restoration of $SU(2)_L \times SU(2)_R \times U(1)_A$ symmetry it is sufficient to show that the two-point correlators of π, σ η and a_0 interpolators are identical.

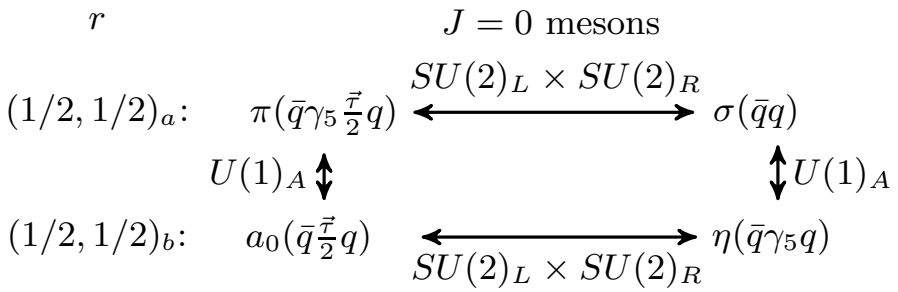

Figure 4.1: Symmetry relations among $J = 0$ mesons. r denotes the index of chiral representation.

4.1.2 Connected vs. Disconnected Correlators

There are two distinct contributions used in the construction of the meson two-point correlators on the lattice [56–58]. The isovector meson correlators include the so-called

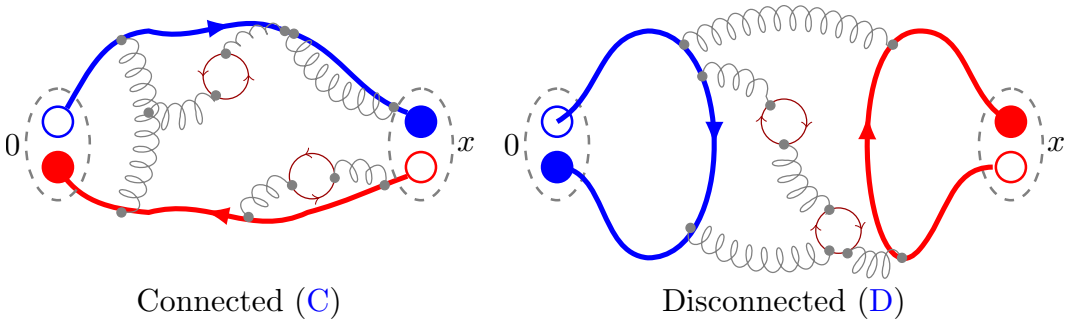

Figure 4.2: Connected (left) and disconnected (right) contributions to meson correlators.

connected contribution only

$$C = -\langle Tr(\Gamma S(x,z)\Gamma S(z,y))\rangle \ . \tag{4.1}$$

For the isoscalar correlators one needs in addition the following *disconnected contribution*

$$D = 2\langle Tr(\Gamma S(x,x)\Gamma S(y,y))\rangle \ , \tag{4.2}$$

where $S(x,y)$ is a quark propagator computed on a given gauge field configuration.

C and D can be represented by two topologically different diagrams shown in Figure 4.2. Thick lines represent the propagation of the valence quarks in a given quantum channel. Thin curvy gluon lines and closed quark loops are used to depict some virtual interactions taking place in the vacuum.

In our case, u and d quarks are mass degenerate and $S_u = S_d = S$. Hence, the full η isoscalar correlator is constructed as follows

$$F_\eta = C_\pi + D_\eta \ , \tag{4.3}$$

where C_π is the connected part which coincides with the pion correlator, D_η is the disconnected contribution. Similarly, we get the full σ correlator

$$F_\sigma = C_{a_0} + D_\sigma \ , \tag{4.4}$$

where C_{a_0} is the connected part, D_σ is the corresponding disconnected contribution.

It is sufficient to use one-to-all propagators to compute connected pieces of the mesons correlators. However, the disconnected contribution requires the use of all-to-all propagators. The latter are computationally unfeasible at large lattice sizes. Various computational technique is developed to tackle this problem like stochastic estimators [59], distillation [60], etc.

In our work we use stochastic all-to-all propagators obtained with the hydrid technique [61]. The latter means that the resulting all-to-all propagator is a sum of two parts, $S_{\rm LM}$ and $S_{\rm HM}$ respectively. The first part $S_{\rm LM}$ is constructed from a rather big set of lowest eigenmodes of the Dirac operator and computed exactly. Contribution from the high-lying modes $S_{\rm HM}$ is computed using the stochastic method [59]. In our case 100 lowest modes are computed exactly. We define the following reduced quark propagators

$$S_k(x,y) = \sum_{n=k+1}^{100} \frac{1}{\lambda_n} u_n(x) u_n^\dagger(y) + S_{\rm Stoch} \ , \tag{4.5}$$

where the k is the number of lowest-lying modes excluded from the full propagator. $S_{\rm Stoch}$ is a stochastic estimator for $S_{\rm HM}$. The full propagator $S_{\rm FULL}$ corresponds to S_k at $k = 0$. The propagators S_k are then used in (4.1)-(4.2) to compute the π, σ η and a_0 meson correlators. The details of the computation of the meson correlators using the stochastic all-to-all technique are given in Appendix B.

4.1.3 Isoscalar and Isovector Mesons on the Lattice

It is obvious from the definitions of the π, σ η and a_0 correlators given above, the disconnected contributions D_σ and D_η have to be identical to zero to claim the restoration of the $SU(2)_L \times SU(2)_R \times U(1)_A$ symmetry. In this section we show that this is exactly what happens when a sufficient number of the low-lying modes k is removed from the full quark propagators, see Equation (4.5).

It turns out that the disconnected contributions become negligibly small when we exclude an increasing amount of the low-lying modes k. The latter holds true for both η and σ disconnected contributions, as it is shown in Figure 4.3. We find that $D_\sigma(k = 10) \ll D_\sigma(k = 0)$ as well as $D_\eta(k = 10) \ll D_\eta(k = 0)$. Inclusion or exclusion of the stochastically estimated part of the propagator S_k produces a negligible effect on the magnitude of the disconnected contributions $D_\eta(D_\sigma)$, except for small fluctuations and sizes of the error bars. The latter are reduced drastically when $S_{\rm Stoch}$ is excluded. However, the situation is different with the connected parts C_π and C_{a_0}. There we see significant differences at small values of t for $k = 0, 10$. Moreover, the absolute values of C_π and C_{a_0} correlators are non-zero at any truncation level k.

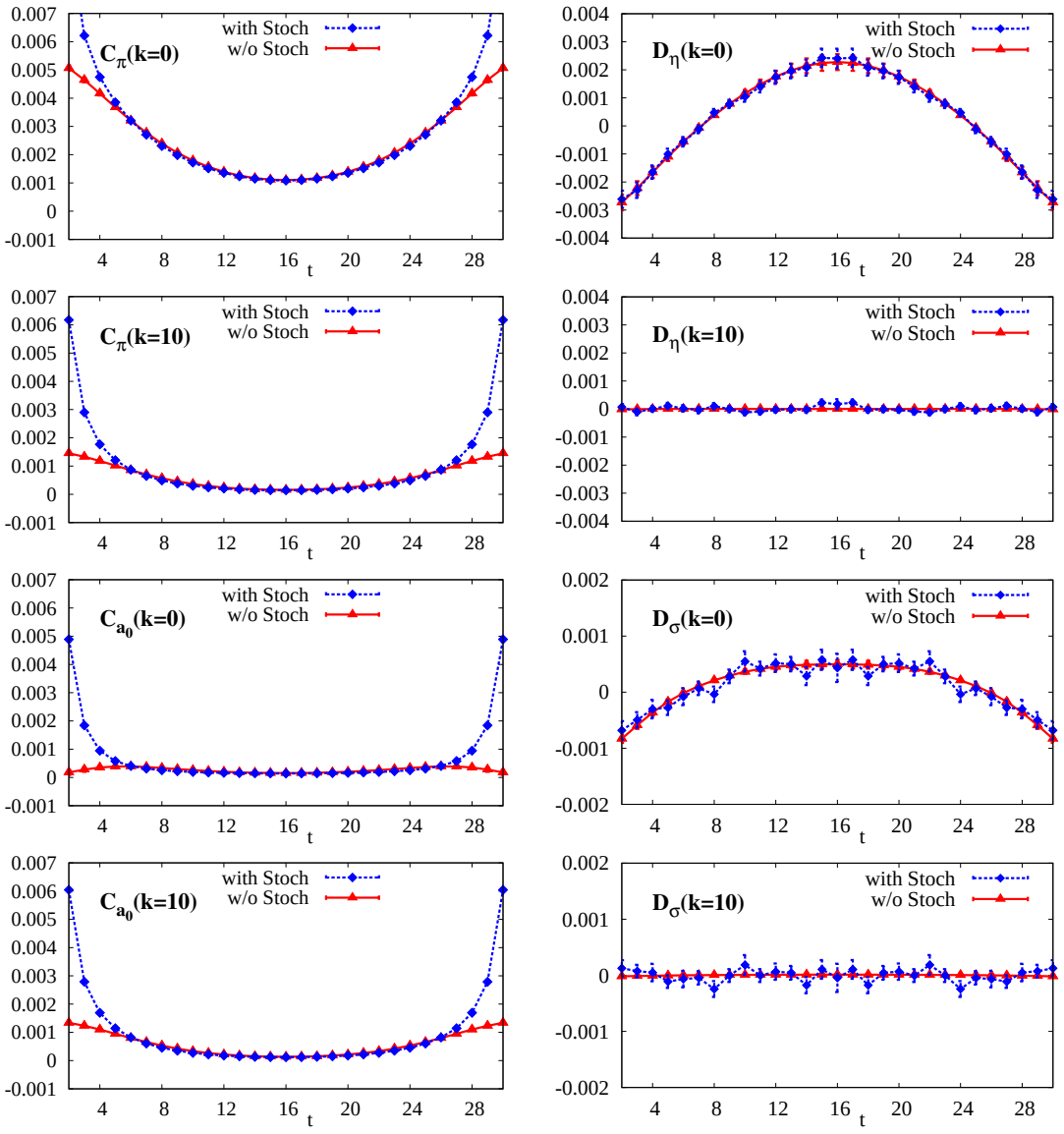

Figure 4.3: Connected (left panel) and disconnected (right panel) contributions to the η and σ meson correlators with included or excluded stochastically estimated part of the quark propagator, $k = 0, 10$.

Now, we combine all four correlators together and study their behavior upon exclusion of the low-lying modes. Figure 4.4 shows the snapshots of such a behavior on the logarithmic scale for the truncations $k = 0, 2, 10, 30$. It is clearly seen that C_π and C_{a_0} correlator become absolutely identical at $k = 30$. The latter we consider as a reliable signal for the $U(1)_A$ symmetry restoration. In addition, the contributions from the disconnected pieces D_η and D_σ become negligibly small and noisy at large values of t. Figure 4.5 shows the same set of correlators at $k = 30$ obtained when the stochastically estimated part of the propagator S_{Stoch} is omitted in the computation of D_η and D_σ pieces.

Now, we can clearly see in Figure 4.5 that the π, σ, a_0 and η correlators are identical.

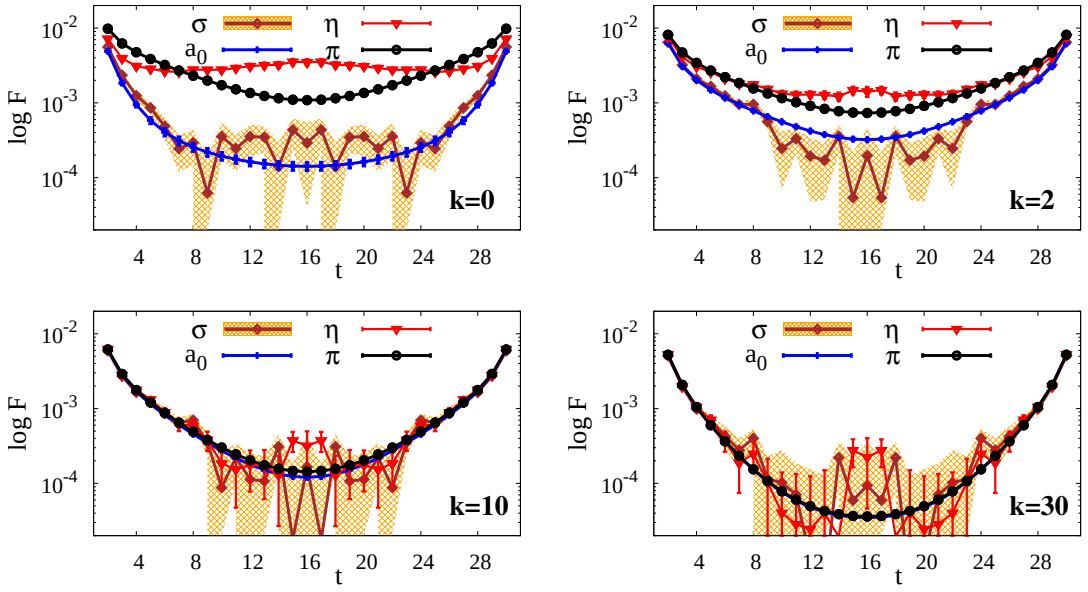

Figure 4.4: π, σ, a_0, η point-to-point correlators upon exclusion of the near-zero modes, $k = 0, 2, 10, 30$.

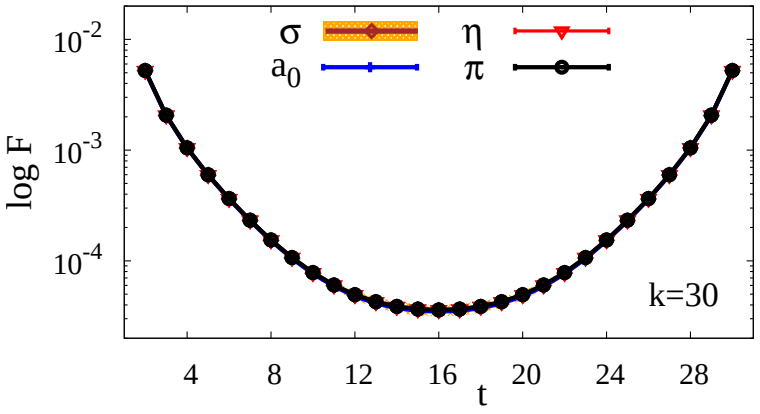

Figure 4.5: π, σ, a_0, η point-to-point correlators upon exclusion of the near-zero modes without the contribution from the stochastically estimated part of the propagator, $k = 30$.

Thus, the full $SU(2)_L \times SU(2)_R \times U(1)_A$ symmetry gets restored at the truncation $k = 30$. The restoration of $U(1)_A$ is consistent with the Instanton Liquid Model predictions where the instanton type of interactions are responsible for the $SU(2)_L \times SU(2)_R$ as well as for the $U(1)_A$ symmetry breaking [62–65].

The next natural question we ask : Do all the states π, σ, a_0 and η suvive this restoration of chiral symmetry? Now, we know that all correlators are identical and it is sufficient to consider a single π channel for the following reason. In the untruncated case we

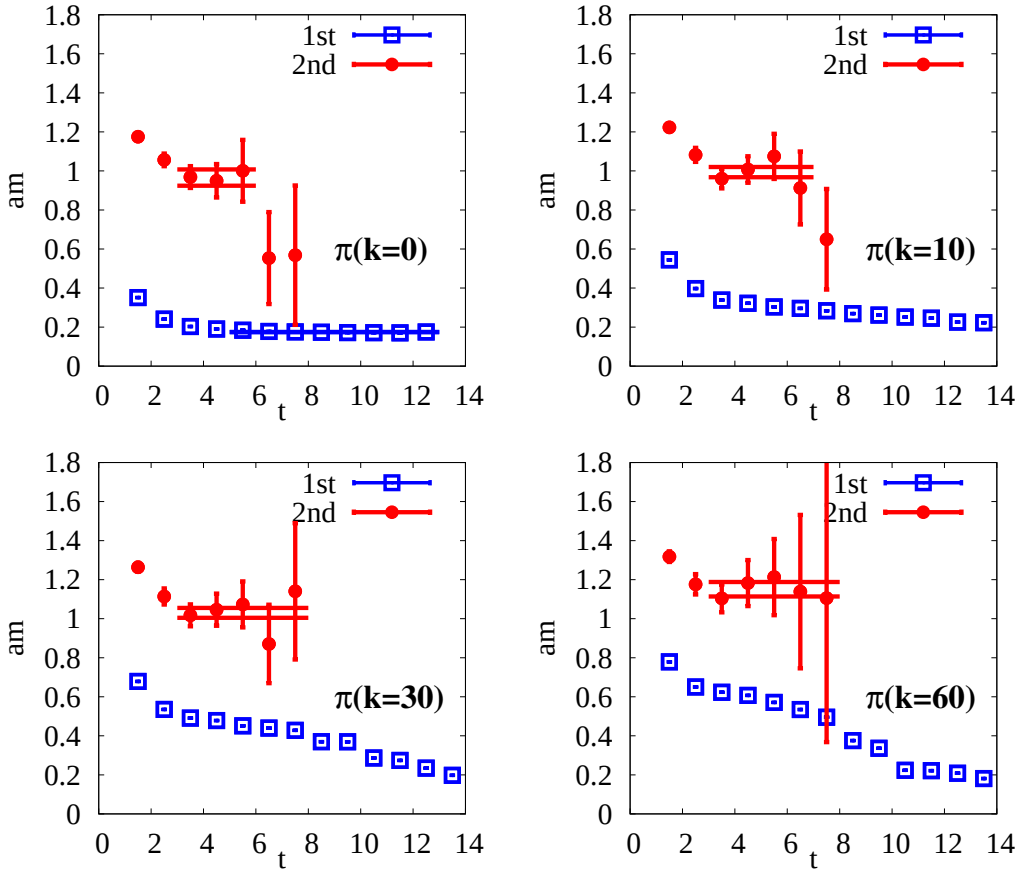

Figure 4.6: $\pi(I = 1, J^{PC} = 0^{-+})$ effective masses at $k = 0, 10, 30, 60$.

can extract the pion states with better statistics, see Figure 4.6. On the same figure we see that when we remove the low-lying modes the effective mass plateau disappears and further identification of the pion ground state is not possible. This has a far going implication. The pseudo-Goldstone boson nature of the pion ground state is primarily due to the chiral symmetry breaking effects. This state seize to exist as well as the corresponding σ, η and a_0 meson states upon removal of these effects. However, we see that the excited state π' survives the restoration and coincides with the first excited energy levels of the σ, a_0 η mesons.

4.2 $J = 1$ Mesons

In the previous section we demonstrated by studying the $J = 0$ meson correlators that the original $SU(2)_L \times SU(2)_R$ and $U(1)_A$ symmetries of the QCD Lagrangian are restored when a sufficient number of the low-lying eigenmodes of the Dirac operator is removed. In this chapter we confirm our finding by studying a large set of $J = 1$ meson states upon unbreaking chiral symmetry.

4.2.1 $J = 1$ Chiral Multiplets

Table 4.1 shows the $J = 1$ meson channels and corresponding interpolating fields classified with respect to the chiral representations of the parity-chiral group [24]. $J = 1$ meson states fall into four distinct multiplets

$$r : \ (0,0), (1/2,1/2)_a, \ (1/2,1/2)_b, \ (1,0)+(0,1), \tag{4.6}$$

see Figure 4.7.

There exist three pairs of the meson states $\rho \leftrightarrow a_1$, $\rho' \leftrightarrow b_1$ and $\omega' \leftrightarrow b_1$ which we use to test the restoration of the $SU(2)_L \times SU(2)_R$ symmetry. The $U(1)_A$ symmetry transformation mixes the state in two different chiral representations, namely $(1/2,1/2)_a$ and $(1/2,1/2)_b$. The following pairs of states $b_1 \leftrightarrow \rho'$ and $\omega' \leftrightarrow h_1$ can be used to test the $U(1)_A$ symmetry restoration.

I, J^{PC}	$\mathcal{O}$	r
$\rho(1,1^{--})$	$\bar{q}\gamma_i \frac{\vec{\tau}}{2} q$	$(1,0)+(0,1)$
$\rho'(1,1^{--})$	$\bar{q}\gamma_i\gamma_t \frac{\vec{\tau}}{2} q$	$(1/2,1/2)_b$
$\omega(0,1^{--})$	$\bar{q}\gamma_i q$	$(0,0)$
$\omega'(0,1^{--})$	$\bar{q}\gamma_i\gamma_t q$	$(1/2,1/2)_a$
$a_1(1,1^{++})$	$\bar{q}\gamma_i\gamma_5 \frac{\vec{\tau}}{2} q$	$(1,0)+(0,1)$
$f_1(0,1^{++})$	$\bar{q}\gamma_i\gamma_5 q$	$(0,0)$
$b_1(1,1^{+-})$	$\bar{q}\gamma_i\gamma_j \frac{\vec{\tau}}{2} q$	$(1/2,1/2)_a$
$h_1(0,1^{+-})$	$\bar{q}\gamma_i\gamma_j q$	$(1/2,1/2)_b$

Table 4.1: $J = 1$ meson interpolating fields classified with respect to the chiral representation r.

In the subsequent sections we discuss our results obtained with the $J = 1$ mesons upon unbreaking chiral symmetry. We extracted the meson states in each quantum

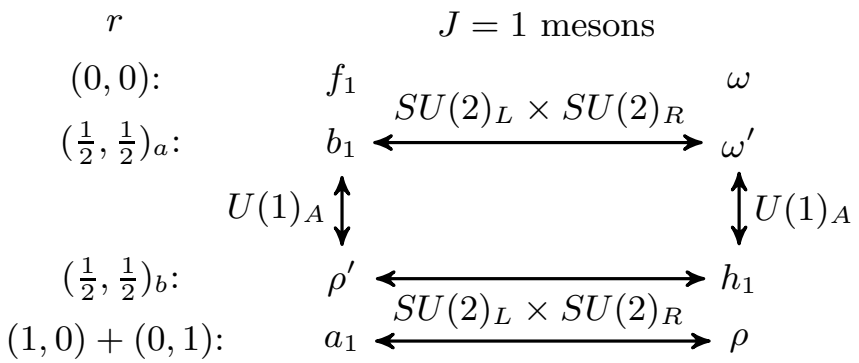

Figure 4.7: Symmetry relations among $J = 1$ mesons.

channel and studied their evolution under the exclusion of the low-lying modes. A few representative channels are selected to illustrate our main findings.

4.2.2 $a_1(I = 1, J^{PC} = 1^{++})$

We used the variational method discussed in Section 3.4 to extract the states in the $a_1(1, 1^{++})$ meson channel. Figure 4.8 provides the information on the determination of these states in the full case, i.e. $k = 0$. From the first two exponentially decaying eigenvalues $\lambda(t)$ we extract the masses of the ground and the first excited states, $n = 1$ and $n = 2$, respectively. Corresponding eigenvector components v_1^i and v_2^i introduced in (3.21) are stable in the fitting ranges t. The latter enables to evaluate which operator construction provides a better overlap with a given state n.

The plots for the a_1 states after the exclusion 10 low modes are shown in Figure 4.9. The a_1 states survive this truncation and the quality of the signals get improved. The latter is a generic feature and is not restricted to this specific channel. The eigenvectors of the original a_1 states become more stable. As we see the mass of the ground states is reduced as well as the mass of the first excited state at this truncation k.

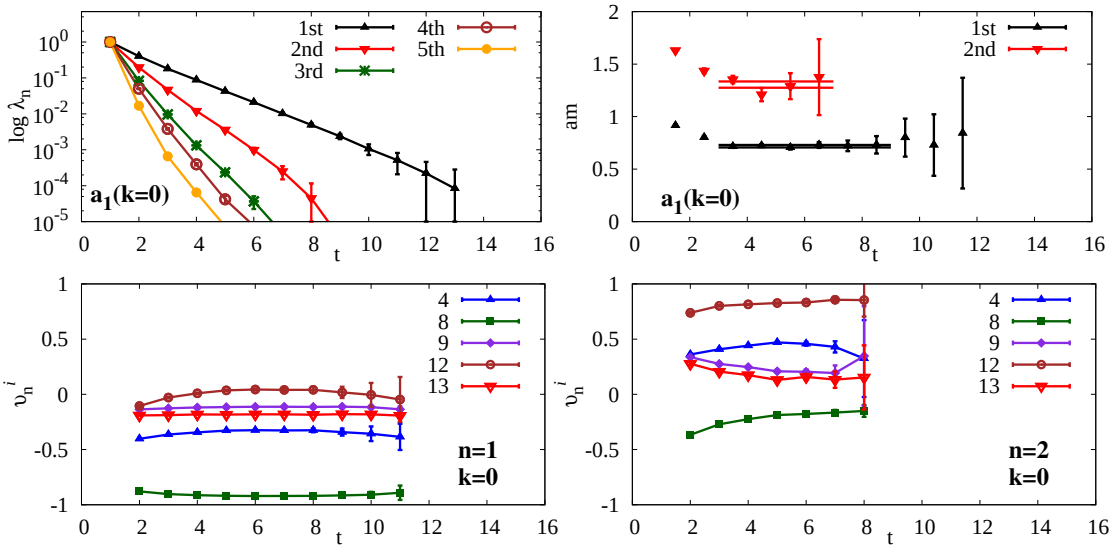

Figure 4.8: $a_1(I = 1, J^{PC} = 1^{++})$ full case: the eigenvalues for all states (upper left), effective mass plot for the first two states (upper right), eigenvectors corresponding to the ground state $n = 1$ (lower left) and the first excited state $n = 2$ (lower right).

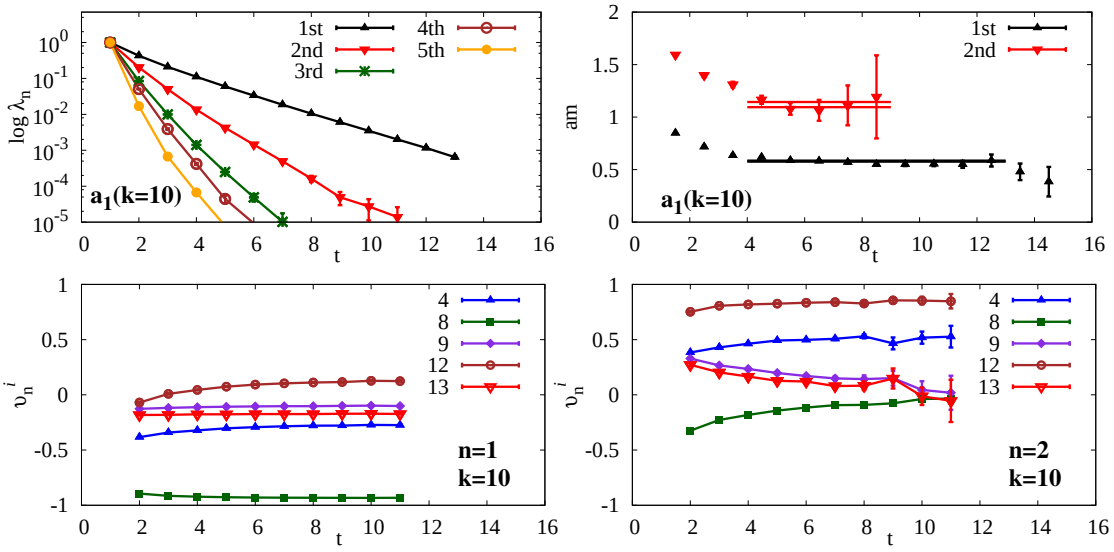

Figure 4.9: $a_1(I = 1, J^{PC} = 1^{++})$, 10 low modes excluded: the eigenvalues for all states (upper left), effective mass plot for the first two states (upper right), eigenvectors corresponding to the ground state $n = 1$ (lower left) and the first excited state $n = 2$ (lower right).

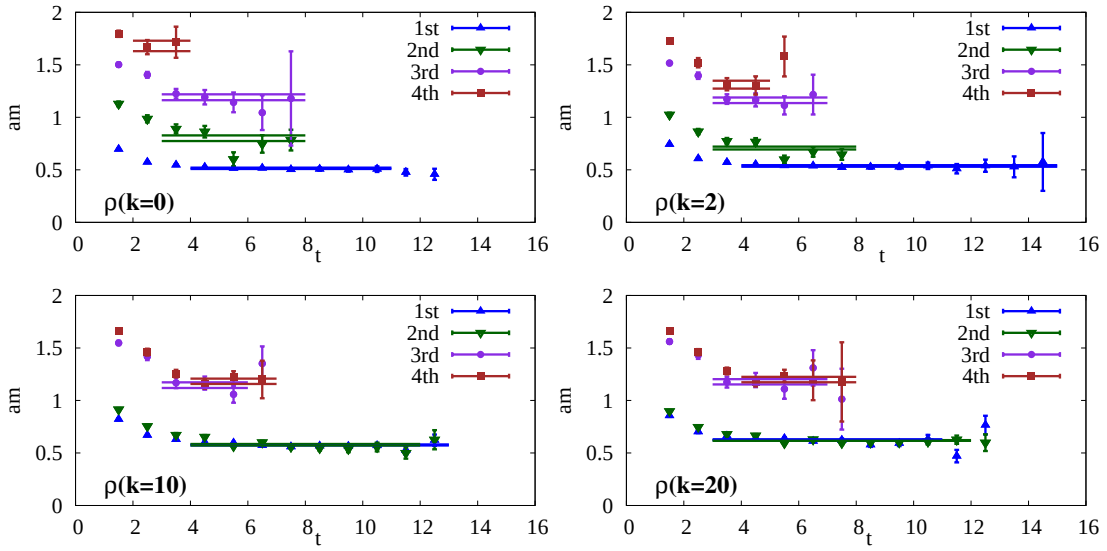

Figure 4.10: $\rho(I = 1, J^{PC} = 1^{--})$: effective masses, $k = 0, 2, 10, 20$ low modes excluded.

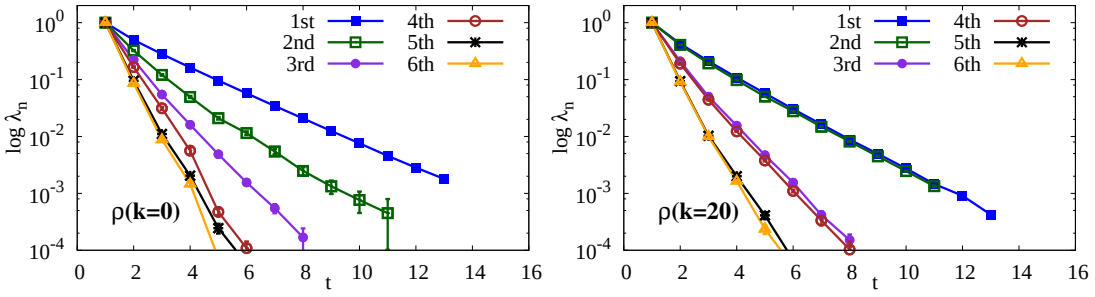

Figure 4.11: $\rho(I = 1, J^{PC} = 1^{--})$: eigenvalues, full case (left) 20 low modes excluded (right).

4.2.3 $\rho(I = 1, J^{PC} = 1^{--})$: Unmixing ρ and ρ'

Next, we extract the ρ meson states necessary to provide the first test of the $SU(2)_L \times SU(2)_R$ symmetry restoration in the $J = 1$ meson sector. This is done through the analysis of $a_1 - \rho$ mass splitting further in this section. Figure 4.10 shows the effective mass plots for the ρ meson at the truncations $k = 0, 2, 10, 20$. We find that the four states identified in the full case ($k = 0$) survive $k > 0$ truncations and become degenerate pairwise, i.e. each new energy level is doubly degenerate at the truncations $k \geq 10$. The mass gap between the first and the second doubly degenerate energy levels coincide with the energy of the first level. However, the lattice volume corrections have to be taken into account for a precise identification of the resulting energy levels. Moreover, this doubling phenomenon occurs for the high-lying states as well. The latter is illustrated by the eigenvalues $\lambda_n(t)$ shown in Figure 4.11.

This doubling phenomenon can be observed in the $\rho(1, 1^{--})$ channel only if the corresponding interpolator basis includes the interpolators belonging to two distinct chiral representations, $(1,0) + (0,1)$ and $(1/2, 1/2)_b$ respectively. Relative coupling of these two types of interpolators to different states n is different and changes on exclusion of the low-lying modes. This is the subject of the next section.

Unmixing ρ and ρ'

For this discussion we need to write down the cross-correlation matrix C_{ij} (see Equation (3.20)) in terms of the so-called *overlap factors* Z_i^n

$$\begin{aligned} C_{ij}(t) &= \sum_n \langle 0|\mathcal{O}_i|n\rangle\langle n|\mathcal{O}_j^\dagger|0\rangle e^{-E_n t} \\ &= \sum_n Z_i^n Z_j^{n\,*} e^{-E_n t}, \end{aligned} \tag{4.7}$$

where $Z_i^n = \langle 0|\mathcal{O}_i|n\rangle$ determines the relative coupling of an interpolator i with a given state n.

In our calculation we used 5 interpolators in the $(1,0) + (0,1)$ representation and the same number in the $(1/2, 1/2)_b$ representation of the ρ meson channel. The results of calculating the Z-factors for the first four states are shown in Figure 4.12 for the full case and at the truncation $k = 30$. For a given state n each of the overlap factor Z_i^n is normalized to the average value $\langle Z^n\rangle = 1/N \sum_i^N Z_i^n$, where $N = 10$ is the number of interpolators used in the construction of the cross-correlation matrix C_{ij}.

We find that without truncation, $k = 0$, the interpolators in both chiral representations contribute equally to the first state $n = 1$. However, the interpolators in the $(1/2, 1/2)_b$ representation dominate the contribution to the first state after exclusion of 30 low modes. On the other hand, those interpolators in $(1,0) + (0,1)$ representation have a relatively high contribution to the second state $n = 2$ in the full case. The latter contribution is even stronger at the truncation $k = 30$. The same discussion can be applied repeatedly to a higher states, $n = 3$ and $n = 4$ respectively.

We see that in the untruncated case the chiral symmetry is heavily broken in the ground state of the $I = 1, J^{PC} = 1^{--}$ quantum channel. The same strong mixing between the states in $(1,0) + (0,1)$ and $(1/2) + (1/2)_b$ chiral representations was found in [66–68]. However, this mixing weakens as we go higher in spectrum before any truncation and it reduces significantly in all four states after the exclusion of 30 low modes.

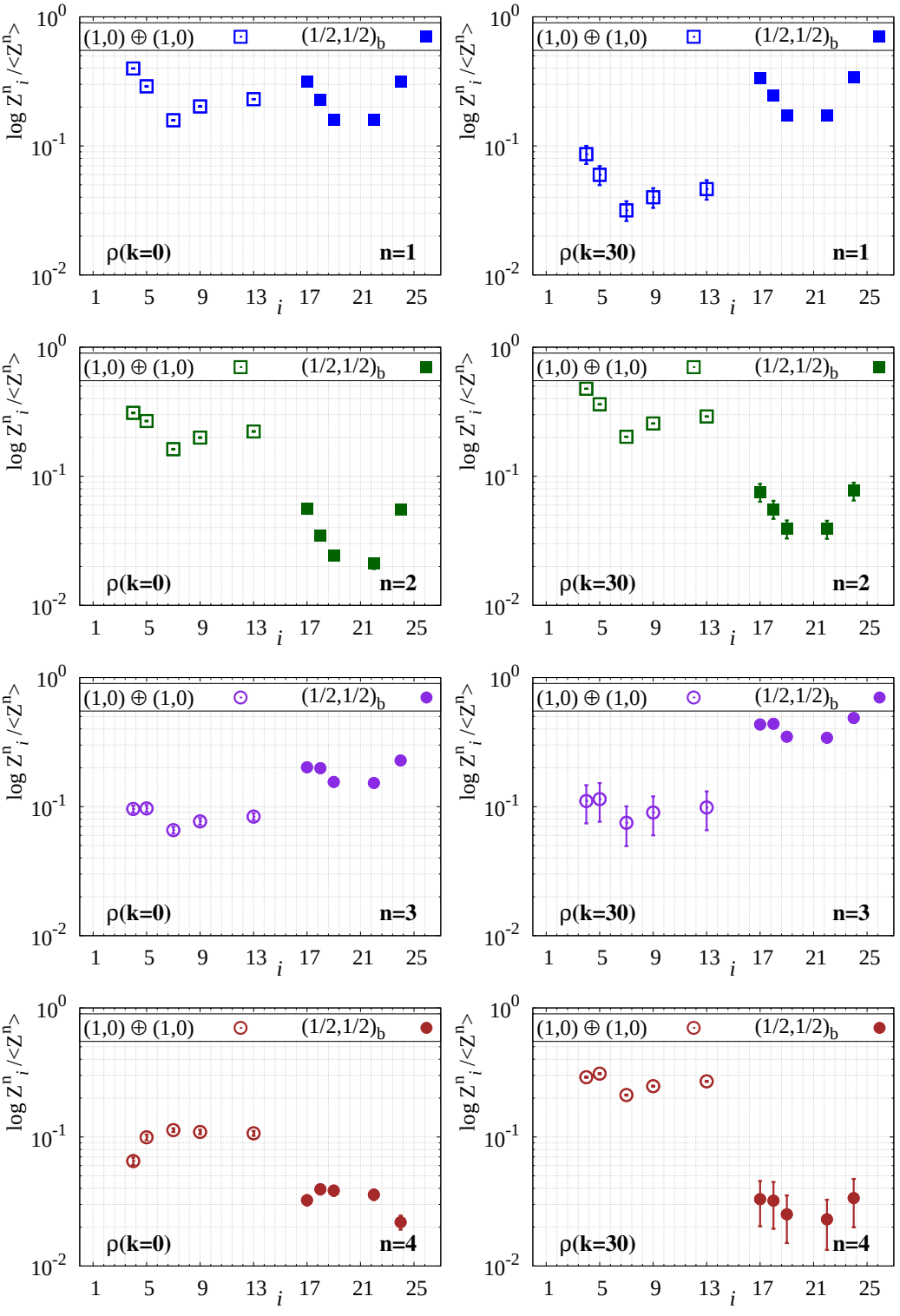

Figure 4.12: $\rho(I = 1, J^{PC} = 1^{--})$ overlap factors, i labels the interpolators according to Appendix B.

4.2.4 $h_1(J^{PC} = 1^{+-})$, $\omega(J^{PC} = 1^{--})$, $f_1(J^{PC} = 1^{++})$ Isoscalars

Here, we discuss the results for the isoscalar $J = 1$ mesons and concentrate on the h_1 meson. The latter can be used to probe both $SU(2)_L \times SU(2)_R$ and $U(1)_A$ symmetries in the chirally restored regime.

The computation of the $J = 1$ isoscalar mesons poses the same difficulties as in the case of the isoscalar $J = 0$ mesons on the lattice. Similar discussion we made in Section 4.1 is applicable here. The two-point correlator of any two interpolating currents of the h_1 meson contains the disconnected and connected contributions

$$F_{h_1} = C_{b_1} + D_{h_1}, \tag{4.8}$$

where the connected part of the h_1 correlator coincides with the $b_1(I = 1, J^{PC} = 1^{+-})$ meson correlator C_{b_1}, D_{h_1} is the disconnected piece. Corresponding correlators for $\omega(I = 0, J^{PC} = 1^{--})$ and $f_1(I = 0, J^{PC} = 1^{++})$ isoscalar mesons have the form identical to Equation (4.8), i.e. $C_{a_1} + D_{f_1}$ and $C_\rho + D_\omega$ respectively.

We find that the disconnected contributions in contrast to the connected contributions for all the $J = 1$ channels are very noisy. However, this noise reduces drastically if we eliminate the stochastically estimated part of the propagator S_{Stoch} in the computation of the disconnected pieces D. Corresponding connected and disconnected contributions are shown in Figure 4.13 for the h_1 meson. We see that inclusion of S_{Stoch} is vital for the connected pieces before as well as after exclusion of 10 low modes. A large noise appears in the disconnected contributions when S_{Stoch} is taken into account. Therefore, we approximate the disconnected contribution only by the low modes. The latter assumes that the contribution from the higher modes is negligible as it is in the $J = 0$ isoscalar channels. It is also shown in Figure 4.13 that the disconnected contribution D_{h_1} computed in this way goes to zero as we exclude $k = 10$ low modes. This implies that the h_1 meson correlator reduces to b_1 correlator as k gets larger.

We used 6 interpolators in the variational method to extract the h_1 states, see Figure 4.14. The h_1 states survive the low-mode truncation and the energy levels of the first two states can be extracted. Similar analysis is applied in the study of f_1 and ω meson correlators. We find that the disconnected pieces vanish when low modes are removed. Figure 4.15 shows the eigenvalues and effective masses of the h_1, ω and f_1 states at the truncation $k = 30$.

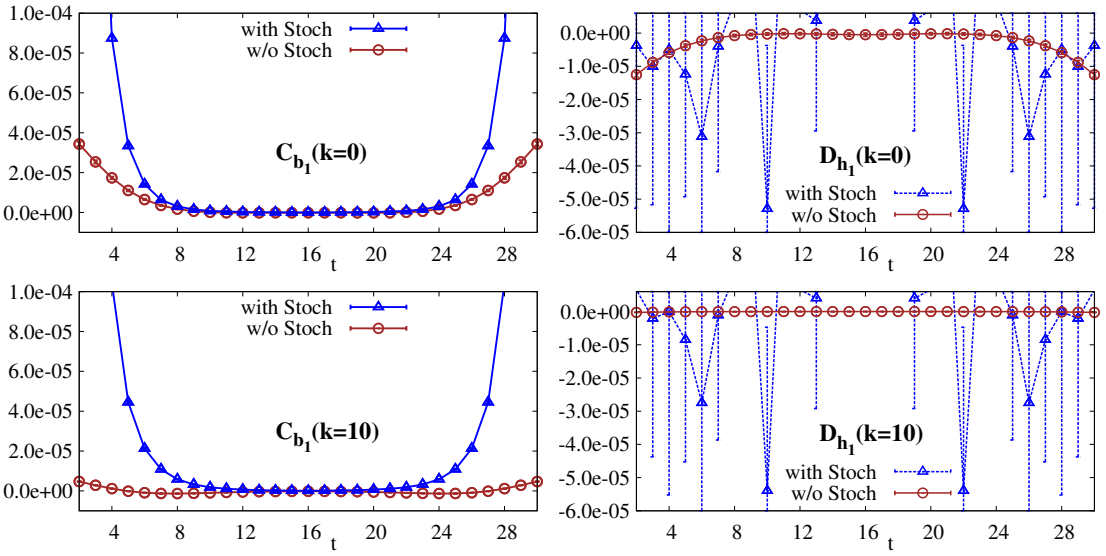

Figure 4.13: Connected (left) and disconnected (right) contributions to $h_1(I = 0, J^{PC} = 1^{+-})$ meson correlator with included or excluded stochastically estimated part of the quark propagator, $k = 0, 10$.

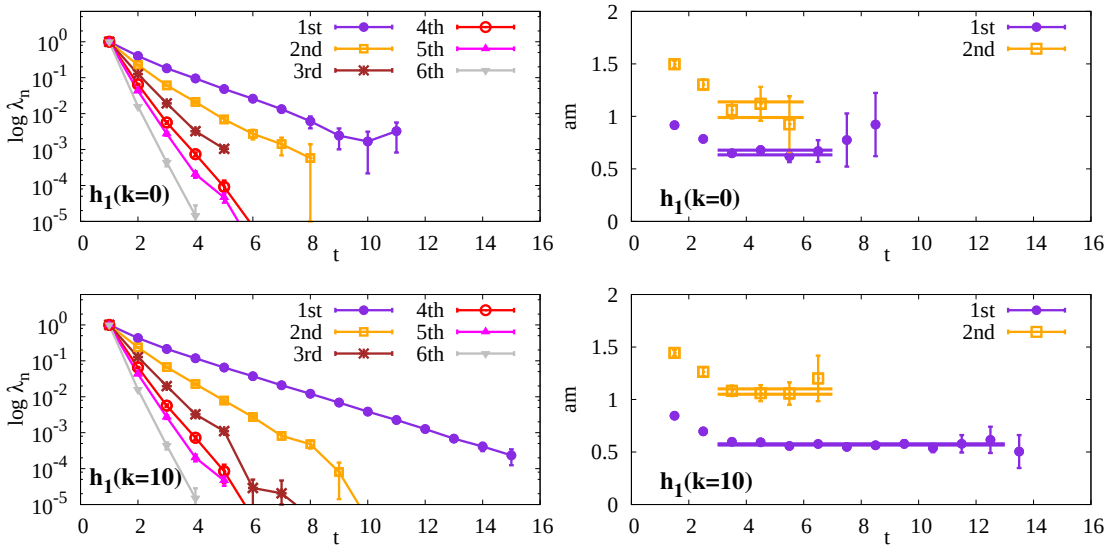

Figure 4.14: $h_1(I = 0, J^{PC} = 1^{+-})$: the eigenvalues (left), effective masses (right); the full case (upper panel), after the exclusion of 10 low-lying modes (lower panel)

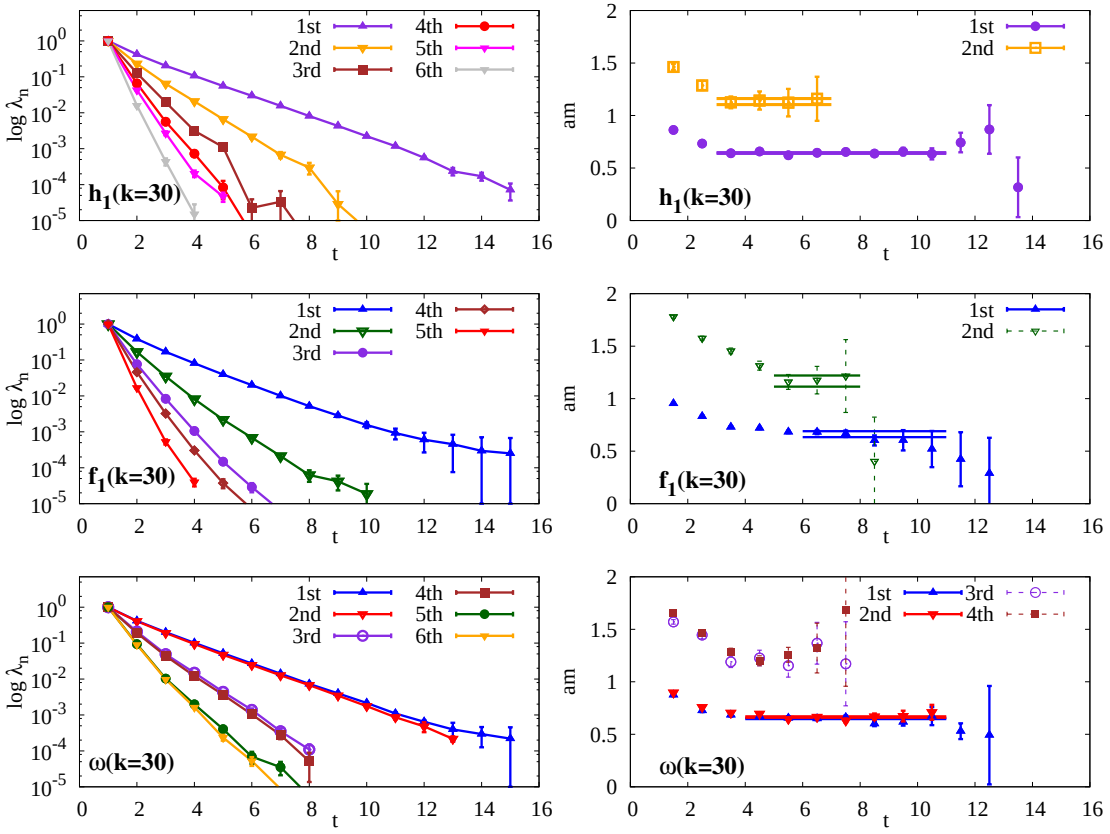

Figure 4.15: $h_1(I=0, J^{PC}=1^{+-})$ (upper panel), $\omega(I=0, J^{PC}=1^{--})$ (middle), $f_1(I=0, J^{PC}=1^{++})$ (lower panel) : the eigenvalues (left), effective masses (right), $k=30$.

We studied all possible $J=1$ isoscalar and isovector channels. Those correlators distinct in the untruncated case become identical on exclusion of the low-lying modes. Figure 4.16 shows corresponding eigenvalues in the full case and after exclusion of 30 low modes with the overlap fermions. We obtain identical results for the isovector mesons using the chirally improved fermions, see Figure 4.17.

4.2.5 Mass Spectrum of $J=1$ Mesons and String Interpretation

We extracted the masses of the states in every $J=1$ channel for a broad range of values k. The mass values of these states are plotted versus the number of the excluded low modes k in Figures [1] 4.18-4.19 . The energy gap produced due to reduction of k modes in the Dirac eigenvalue spectrum is denoted as σ, see Chapter 3. The statistical data and corresponding sets of interpolators used to extract the states are presented in the tables of Appendix E for a few selected truncations $k=0, 10, 20, 30$.

[1] Figure 4.19 is produced using the exact one-to-all overlap propagators. It provides an independent cross-check for the identical results obtained with the stochastic all-to-all propagators shown in Figure 4.18.

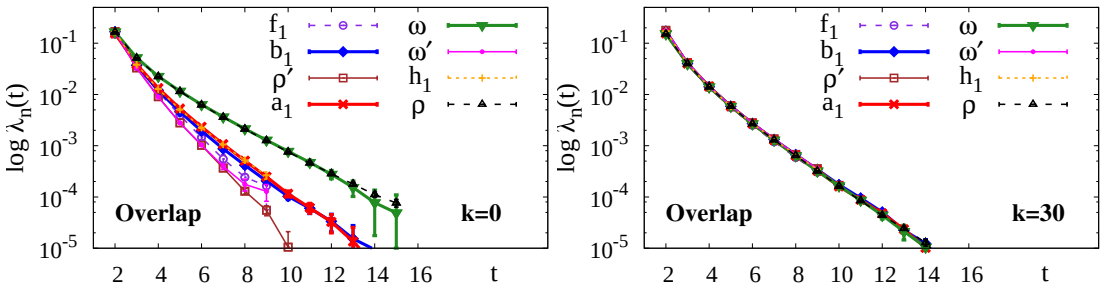

Figure 4.16: Overlap: $J = 1$ meson states eigenvalues in the full case (left), after the exclusion of 128 low modes (right).

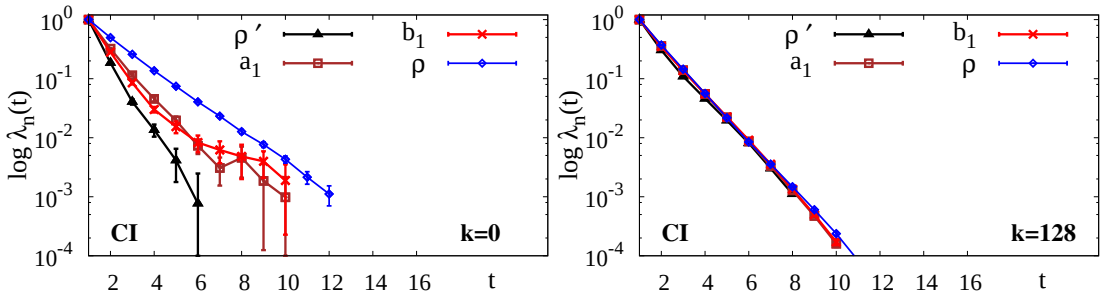

Figure 4.17: CI: $J = 1$ meson states eigenvalues in the full case (left), after the exclusion of 128 low modes (right).

We find an inset of the degeneracy of all the $J = 1$ meson ground states at $k = 10$. The degeneracy [2] of these states occurs and persists at larger truncations. In addition, we find that the following ρ' and ω' $n = 2$ meson states become degenerate with the ρ and ω ground states $n = 1$. Vanishing mass splittings of the following states

$$\rho - a_1, \ \omega' - b_1, \ \rho' - h_1 \tag{4.9}$$

demonstrate the restoration of the $SU(2)_L \times SU(2)_R$ symmetry in the $J = 1$ meson sector. The restoration of the $U(1)_A$ symmetry occurs as well via vanishing

$$\rho' - b_1 \text{ and } \omega' - h_1 \tag{4.10}$$

mass splittings.

We associate the $|(1/2, 1/2)_b; 1\ , 1^{--}\rangle$ and $|(1, 0) + (0, 1); 1\ , 1^{--}\rangle$ chiral states with two degenerate $n = 1$ and $n = 2$ ρ meson states in the chirally restored regime. At the same time, two degenerate $n = 1$ and $n = 2$ states in the ω channel can be associated with the $|(0, 0)_b; 0\ , 1^{--}\rangle$ and $|(1/2, 1/2)_a; 0\ , 1^{--}\rangle$ chiral states, see Figure 4.7. However,

[2] We call any two states degenerate if their absolute mass values are close to each other and there is a substantial overlap of the corresponding error bars.

$SU(2)_L \times SU(2)_R \times U(1)_A$ symmetry restoration cannot explain the degeneracies between the states in chiral representations r which are not connected by this symmetry. For example, we also observe degeneracies between ρ' and ρ states in the $(1/2, 1/2)_b$ and $(1,0)+(0,1)$ chiral multiplets, a_1 and f_1 states belonging to the $(1,0)+(0,1)$ and $(0,0)$ multiplets respectively. There must exist a larger symmetry group that can explain degeneracies of the

$$\rho,\ \omega,\ b_1,\ h_1,\ a_1,\ f_1,\ \rho',\ \omega' \tag{4.11}$$

$J = 1$ mesons after the removal of the chiral symmetry breaking effects. We propose a new $SU(4)$ symmetry group [2, 69, 70] to explain such huge degeneracy pattern, see related discussion in Section 4.2.6.

We find that the mass spectrum of any $J = 1$ meson can be expressed in the chirally restored regime as follows

$$M = (n_r + 1)M_\rho, \tag{4.12}$$

where $n_r = 0, 1, 2, ...$ - is the radial excitation quantum number, M_ρ is the mass of the ρ meson ground state.

Equation (4.12) is exact for $n_r = 0$, it holds for $n_r = 1$ on our lattice. However, we expect large lattice volume corrections to the $n_r \geq 1$ states. The latter may require the following substitution

$$(n_r + 1) \longrightarrow (n_r + 1)^\alpha, \quad \text{with } \alpha < 1. \tag{4.13}$$

We may think of Equation (4.12) as the energy quantization law for a single quark-antiquark dynamical system with the total angular momentum $J = 1$. The properties of the latter does not depend on the total isospin I, parity P or charge conjugation C. We argue that such system can be interpreted as a QCD dynamical string in the next section.

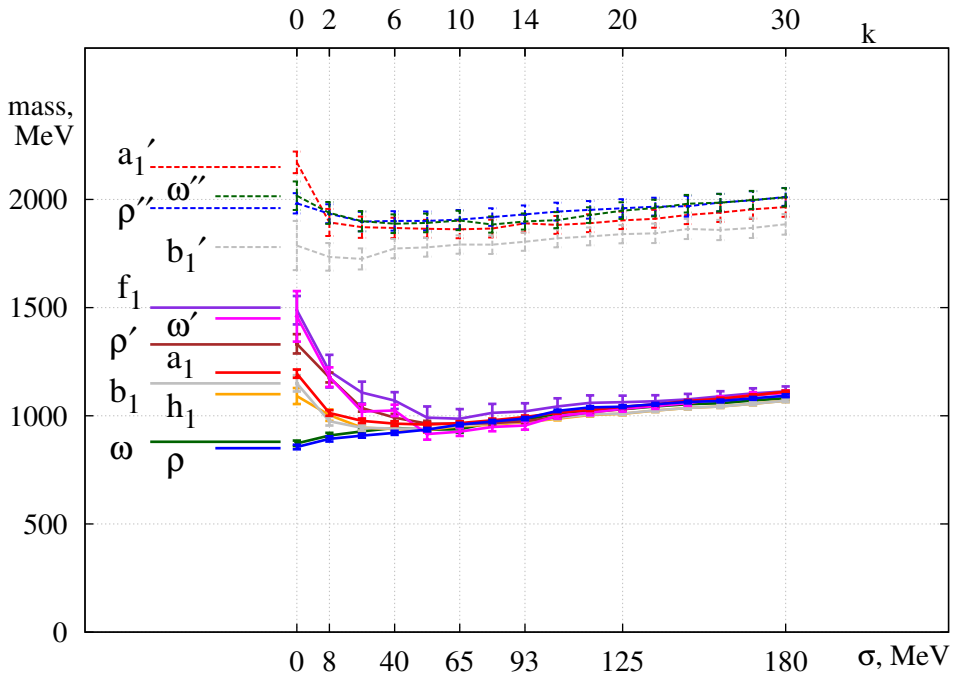

Figure 4.18: Mass evolution of $J = 1$ isoscalar and isovector mesons on exclusion of the low-lying modes. σ is the energy gap.

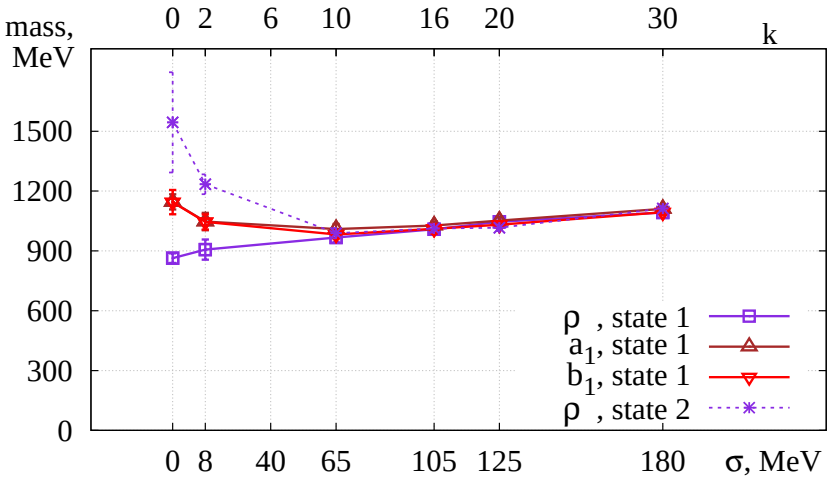

Figure 4.19: Mass evolution of isovector $J = 1$ mesons on exclusion of the low-lying modes.

String Interpretation

It is a common approach to use a basis of states $\{I,^{2S+1}L_J\}$ with a fixed orbital momenta L to classify the low-lying meson spectrum. The $J=1$ meson states in $\{I,^{2S+1}L_J\}$ basis can be decomposed into chiral states $\{r;I,J^{PC}\}$ of the relativistic basis [71] as follows:

$$\begin{aligned}
\rho: \quad |1;{}^3S_1\rangle &= \sqrt{\tfrac{2}{3}}\,|(0,1)+(1,0);1,1^{--}\rangle + \sqrt{\tfrac{1}{3}}\,|(1/2,1/2)_b;1,1^{--}\rangle\,,\\
\omega: \quad |0;{}^3S_1\rangle &= \sqrt{\tfrac{2}{3}}\,|(0,0);0,1^{--}\rangle + \sqrt{\tfrac{1}{3}}\,|(1/2,1/2)_a;0,1^{--}\rangle\,,\\
b_1: \quad |1;{}^1P_1\rangle &= |(1/2,1/2)_a;1,1^{+-}\rangle\,,\\
h_1: \quad |0;{}^1P_1\rangle &= |(1/2,1/2)_b;0,1^{+-}\rangle\,,\\
a_1: \quad |1;{}^3P_1\rangle &= |(0,1)+(1,0);1,1^{++}\rangle\,,\\
f_1: \quad |0;{}^3P_1\rangle &= |(0,0);0,1^{++}\rangle\,,\\
\rho': \quad |1;{}^3D_1\rangle &= \sqrt{\tfrac{1}{3}}\,|(0,1)+(1,0);1,1^{--}\rangle - \sqrt{\tfrac{2}{3}}\,|(1/2,1/2)_b;1,1^{--}\rangle\,,\\
\omega': \quad |0;{}^3D_1\rangle &= \sqrt{\tfrac{1}{3}}\,|(0,0);0,1^{--}\rangle - \sqrt{\tfrac{2}{3}}\,|(1/2,1/2)_a;0,1^{--}\rangle\,.
\end{aligned}$$

However, we showed that all these states are degenerate after unbreaking chiral symmetry. Degeneracy of the S, P and D states listed above:

- $^3S_1$ and $^3P_1$; $^1P_1$ and $^3P_1$; etc $\Rightarrow$ implies vanishing of spin-orbit forces,
- $^1P_1$ and $^3P_1$; $^3S_1$ and $^1P_1$ $\Rightarrow$ implies vanishing of spin-spin forces,
- $^3S_1$ and $^3D_1$ $\Rightarrow$ implies vanishing of tensor forces.

Hence, there are no coupling to color-magnetic field in the quark-antiquark system with the total angular momentum $J=1$ [72]. We define such a system as the *QCD dynamical string* . Equation (4.12) describes the excitation levels of this string with $J=1$, i.e.

$$E_{n_r} = (n_r+1)\hbar\omega, \qquad n_r = 0,1,2,\dots\,. \tag{4.14}$$

where $\hbar\omega = (960 \pm 20)$ MeV is the lowest quantum extracted at $k=10$.

In Section 4.2.3 we have shown that the ρ and ρ' meson states do not mix and belong to two distinct chiral representations in the chirally restored regime. The latter makes the description of the ρ and ρ' meson states in terms of fixed orbital momentum states, $|1;{}^3S_1\rangle$ and $|1;{}^3D_1\rangle$ impossible. The same argument applies to the ω and ω' states. The discussion above implies that the energy of the QCD dynamical string will depend on the total angular momentum J. The latter distinguishes it from the Nambu-Goto type string whose energies depend on the orbital momentum L [73, 74].

4.2.6 Emergent $SU(4)$ Symmetry

The degeneracy of all $J = 1$ mesons discussed earlier in this chapter may be understood as a signal for a new larger symmetry that includes $SU(2)_L \times SU(2)_R \times U(1)_A$ group as a subgroup. We employ a minimal $SU(4) \supset SU(2)_L \times SU(2)_R \times U(1)_A$ symmetry group [1, 69, 70] to explain our lattice observations in the $J = 1$ meson sector . For $N_f = 2$ flavors the four-component basis vector reads as follows

$$q = \begin{bmatrix} u_L \\ u_R \\ d_L \\ d_R \end{bmatrix} . \tag{4.15}$$

We see that the $SU(4)$ rotations mix the left/right components as well as different flavors. Resulting $J = 1$ $(q\bar{q})$ meson states fall in to the following irreducible representations

$$[\mathbf{4}] \times [\bar{\mathbf{4}}] = \mathbf{15} + \mathbf{1} \, , \tag{4.16}$$

and transform as a singlet or fifteen-plet under $SU(4)$. In our case, f_1 state transforms as a singlet and other 15 states as a fifteen-plet [70], i.e.

$$\begin{aligned} \mathbf{1} \; &: \quad f_1 \, , \\ \mathbf{15} \; &: \quad \rho, \; \omega, \; b_1, \; h_1, \; a_1, \; \rho', \; \omega' \, . \end{aligned} \tag{4.17}$$

However, this $SU(4)$ is not a symmetry of the QCD Lagrangian, hence it is an emergent symmetry in the $J = 1$ mesons sector. In addition, our lattice data supports that the singlet state is degenerate with the 15-plet states. This degeneracy could be an accidental one or there must exist a higher symmetry provided that the future lattice simulations support our current observations. In the next section we test the implications of both $SU(4)$ and $SU(2)_L \times SU(2)_R \times U(1)_A$ symmetry restorations with $J = 2$ tensor mesons.

4.3 $J = 2$ Tensor Mesons

In this section we present our lattice studies of $J = 2$ isovector mesons on unbreaking chiral symmetry. We provide an evidence for the $SU(4)$ and $SU(2)_L \times SU(2)_R \times U(1)_A$ symmetry restorations.

4.3.1 Symmetry Predictions

First, we start with the classification of the $J = 2$ tensor mesons with respect to the chiral multiplets shown in Figure 4.20. This classification is similar to the one we have with $J = 1$ mesons. Restoration of $SU(2)_L \times SU(2)_R \times U(1)_A$ symmetry implies the degeneracy between the following states:

$$\pi_2 \longleftrightarrow f_2' \longleftrightarrow \eta_2 \longleftrightarrow a_2' \tag{4.18}$$

in the $(1/2, 1/2)_a$ and $(1/2, 1/2)_b$ multiplets and separately for

$$a_2 \longleftrightarrow \rho_2 \tag{4.19}$$

states in the $(1, 0) + (0, 1)$ multiplet. However, there no constraints on f_2 of ω_2 masses with respect to the states above. The $SU(4)$ multiplet structure for the $J = 2$ mesons is similar to the one for the $J = 1$ mesons (4.17)

$$\begin{aligned} \mathbf{1} &: \quad \omega_2\,, \\ \mathbf{15} &: \quad a_2,\ f_2, \rho_2,\ \pi_2,\ \eta_2,\ a_2',\ f_2'. \end{aligned} \tag{4.20}$$

According to (4.20), $SU(4)$ symmetry predicts that all $J = 2$ mesons except for ω_2 state must be mass degenerate after removal of the low-lying modes. In the next section we test these symmetry predictions for $J = 2$ isovector states on the lattice.

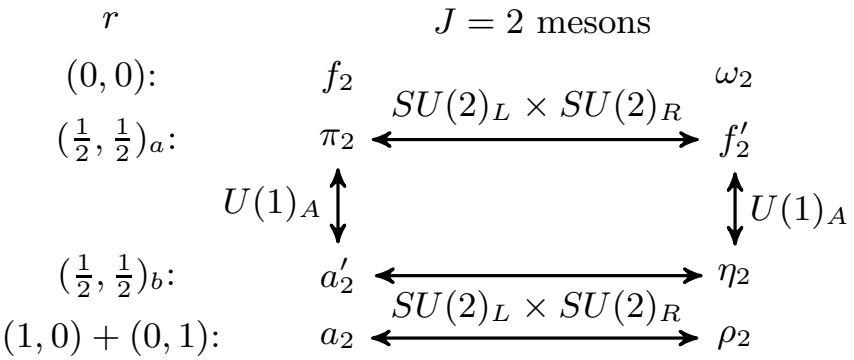

Figure 4.20: Symmetry relations among $J = 2$ mesons.

4.3.2 Results

There are two irreducible representations of the hyper-cubic group $O_{\rm h}$ for $J = 2$ tensor mesons, E and T_2 respectively [75]. We studied the $J = 2$ mesons using interpolators in each of these representations. In addition, we used the $J = 2$ interpolators with the derivative quark sources introduced in [76–78]. Those interpolators used in our work are classified with respect to chiral representations r, see Table 4.2. The latter enables us to access a_2, ρ_2, π_2 and a_2' isovector states on the lattice. We used 4×4 cross-correlation matrices to extract the states in the $a_2(1, 2^{++})$ channel. The corresponding interpolator basis includes the interpolators belonging to two possible chiral multiplets, i.e. $(1/2, 1/2)_b$ and $(1, 0) + (0, 1)$. The latter takes into account a possible mixing of the chiral states. We used 2 interpolators in each of the $(1, 0) + (0, 1)$ and $(1/2, 1/2)_b$ chiral representations to extract the states in the $\pi_2(1, 2^{--})$ and $\rho_2(1, 2^{--})$ isovector channels respectively.

First, we present results for the eigenvalues of the states in these channels in the full case and after exclusion of $k = 30$ low-lying modes, as shown in Figure 4.21. We find that the eigenvalues of $a_2(n = 1, n = 2)$, $\rho_2(n = 1)$ and $\pi_2(n = 1)$ states provide and additional support for the $SU(2)_L \times SU(2)_R \times U(1)_A$ symmetry restoration and are consistent with $SU(4)$ symmetry predictions, i.e.

$$\begin{aligned} SU(2)_L \times SU(2)_R : &\qquad \lambda_{a_2} = \lambda_{\rho_2} \ , \\ U(1)_A : &\qquad \lambda_{a_2'} = \lambda_{\pi_2} \ , \\ SU(4) : &\qquad \lambda_{a_2} = \lambda_{a_2'} = \lambda_{\pi_2} = \lambda_{\rho_2} \ . \end{aligned} \tag{4.21}$$

The same observation is made with the eigenvalues for the high-lying $a_2(n = 3, n = 4)$, $\rho_2(n = 2)$ and $\pi_2(n = 2)$ states. We analyzed the eigenvalues of the $J = 2$ states before and after the low-mode removal with the chirally improved fermions. We found an independent support for the restoration of the symmetries discussed above, see Figure 4.22. However, a larger amount of the low-lying modes has to be removed to observe this effect in this case. There are two main reasons for this. The first is that the number of the low-modes responsible for the symmetry breaking scales with the volume. The physical volume in the simulations with the chirally improved fermions is 0.4 fm greater than the physical volume used with the overlap fermions. The second, the chirally improved fermion discretization on the lattice suffer from the additive quark renormalization which contributes to the explicit chiral symmetry breaking.

I, J^{PC}	$\mathcal{O}$	r	O_h
$\rho_2(1, 2^{--})$	$Q_{ijk}\bar{a}_{\partial_k}\gamma_j\gamma_5 b_n - Q_{ijk}\bar{a}_n\gamma_j\gamma_5 b_{\partial_k}$ $Q_{ijk}\bar{a}_{\partial_k}\gamma_j\gamma_5 b_w - Q_{ijk}\bar{a}_w\gamma_j\gamma_5 b_{\partial_k}$	$(1,0)+(0,1)$	E
	$\lvert\epsilon_{ijk}\rvert\bar{a}_{\partial_k}\gamma_j\gamma_5 b_n - \lvert\epsilon_{ijk}\rvert\bar{a}_n\gamma_j\gamma_5 b_{\partial_k}$ $\lvert\epsilon_{ijk}\rvert\bar{a}_{\partial_k}\gamma_j\gamma_5 b_w - \lvert\epsilon_{ijk}\rvert\bar{a}_w\gamma_j\gamma_5 b_{\partial_k}$		T_2
$a_2(1, 2^{++})$	$Q_{ijk}\bar{a}_{\partial_k}\gamma_j b_n - Q_{ijk}\bar{a}_n\gamma_j b_{\partial_k}$ $Q_{ijk}\bar{a}_{\partial_k}\gamma_j b_w - Q_{ijk}\bar{a}_w\gamma_j b_{\partial_k}$	$(1,0)+(0,1)$	E
	$\lvert\epsilon_{ijk}\rvert\bar{a}_{\partial_k}\gamma_j b_n - \lvert\epsilon_{ijk}\rvert\bar{a}_n\gamma_j b_{\partial_k}$ $\lvert\epsilon_{ijk}\rvert\bar{a}_{\partial_k}\gamma_j b_w - \lvert\epsilon_{ijk}\rvert\bar{a}_w\gamma_j b_{\partial_k}$		T_2
$a_2'(1, 2^{++})$	$Q_{ijk}\bar{a}_{\partial_k}\gamma_j\gamma_t b_n - Q_{ijk}\bar{a}_n\gamma_j\gamma_t b_{\partial_k}$ $Q_{ijk}\bar{a}_{\partial_k}\gamma_j\gamma_t b_w - Q_{ijk}\bar{a}_w\gamma_j\gamma_t b_{\partial_k}$	$(1/2,1/2)_b$	E
	$\lvert\epsilon_{ijk}\rvert\bar{a}_{\partial_k}\gamma_j\gamma_t b_n - \lvert\epsilon_{ijk}\rvert\bar{a}_n\gamma_j\gamma_t b_{\partial_k}$ $\lvert\epsilon_{ijk}\rvert\bar{a}_{\partial_k}\gamma_j\gamma_t b_w - \lvert\epsilon_{ijk}\rvert\bar{a}_w\gamma_j\gamma_t b_{\partial_k}$		T_2
$\pi_2(1, 2^{-+})$	$Q_{ijk}\bar{a}_{\partial_k}\gamma_j\gamma_t\gamma_5 b_n - Q_{ijk}\bar{a}_n\gamma_j\gamma_t\gamma_5 b_{\partial_k}$ $Q_{ijk}\bar{a}_{\partial_k}\gamma_j\gamma_t\gamma_5 b_w - Q_{ijk}\bar{a}_w\gamma_j\gamma_t\gamma_5 b_{\partial_k}$	$(1/2,1/2)_a$	E
	$\lvert\epsilon_{ijk}\rvert\bar{a}_{\partial_k}\gamma_j\gamma_t\gamma_5 b_n - \lvert\epsilon_{ijk}\rvert\bar{a}_n\gamma_j\gamma_t\gamma_5 b_{\partial_k}$ $\lvert\epsilon_{ijk}\rvert\bar{a}_{\partial_k}\gamma_j\gamma_t\gamma_5 b_w - \lvert\epsilon_{ijk}\rvert\bar{a}_w\gamma_j\gamma_t\gamma_5 b_{\partial_k}$		T_2

Table 4.2: List of tensor meson interpolators $\mathcal{O}$ classified with respect to the chiral representations r and irreducible representations E, T_2 of the hyper-cubic group $O_{\rm h}$. Indices n, w and ∂_k stand for the narrow, wide and derivative quarks sources respectively, see [76, 78].

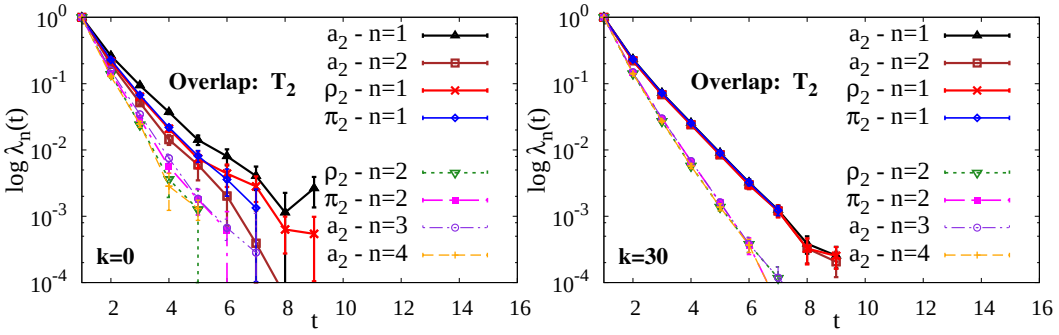

Figure 4.21: Eigenvalues of $J = 2$ tensor mesons in the T_2 irrep: full case (left), after excluding $k = 30$ low-lying modes (right) of the Overlap Dirac operator.

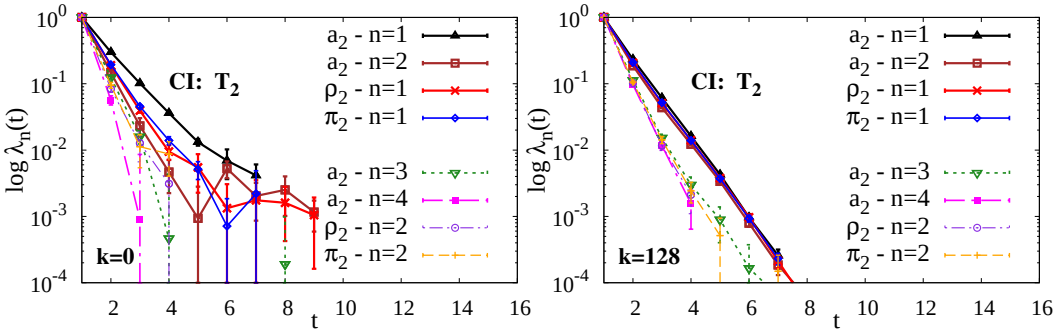

Figure 4.22: Eigenvalues of $J = 2$ tensor mesons in the T_2 irrep: full case (left), after excluding $k = 30$ low-lying modes (right) of the Chirally Improved Dirac operator.

We extracted the effective masses of the few lowest $J = 2$ states in the T_2 and E representations. In general, the signals in the E representation are noisier than in the T_2 representation. However, this noise gets reduced on the exclusion of the low-lying modes. This allows us to compare the states in the T_2 and E representation with each other after truncation. The effective masses for the two lowest states in $a_2(1, 2^{++})$ channel are shown in Figure 4.23 at truncations $k = 16$ and $k = 30$. We found an agreement between the distributions of points within the fit ranges of the states in the T_2 and E representations. The corresponding mass values agree with each other as well, see Appendix E. The same holds for the $\rho_2(1, 2^{--})$ states in the respective lattice representations. Hence, it is sufficient to consider meson states extracted in the T_2 lattice representation. Figure 4.25 shows the effective mass plots for the π_2 states in T_2.

We extracted the $J = 2$ meson masses at each level of the low-mode truncation. The corresponding mass evolution of these states is depicted in Figure 4.26. We see that the mass splittings between the $J = 2$ meson states vanish and degeneracy pattern appears at the truncation $k = 16$, numerical values are presented in Appendix E. These $J = 2$ states fall into the same energy level. Then, we may check the assumption of whether $J = 2$ mesons follow a similar quantization law as the $J = 1$ mesons, i.e. $E \sim (n_r + J)$.

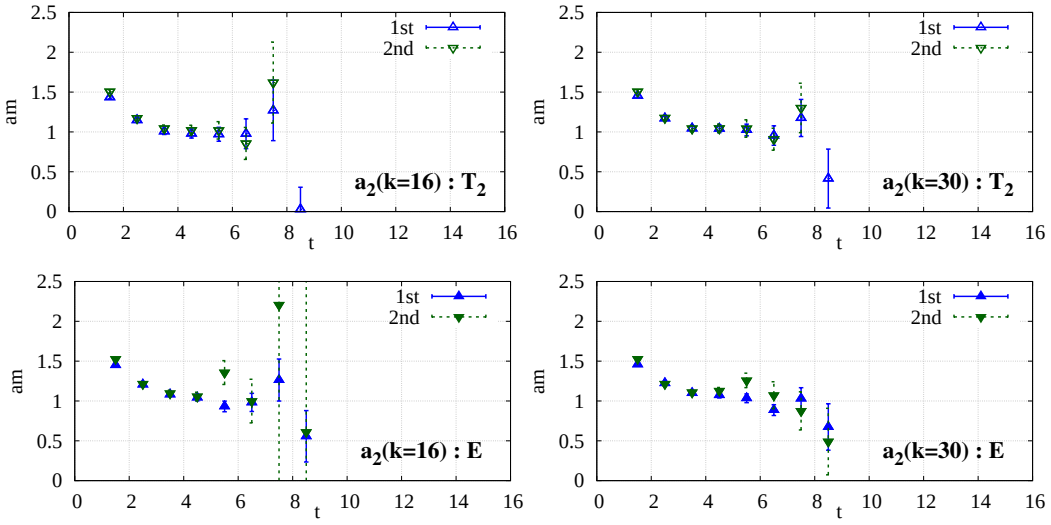

Figure 4.23: $a_2(I = 1, J^{PC} = 2^{++})$ states in T_2 (upper panel)and E (lower panel) after excluding $k = 16$ (left panel), $k = 30$ (right panel) low-lying modes.

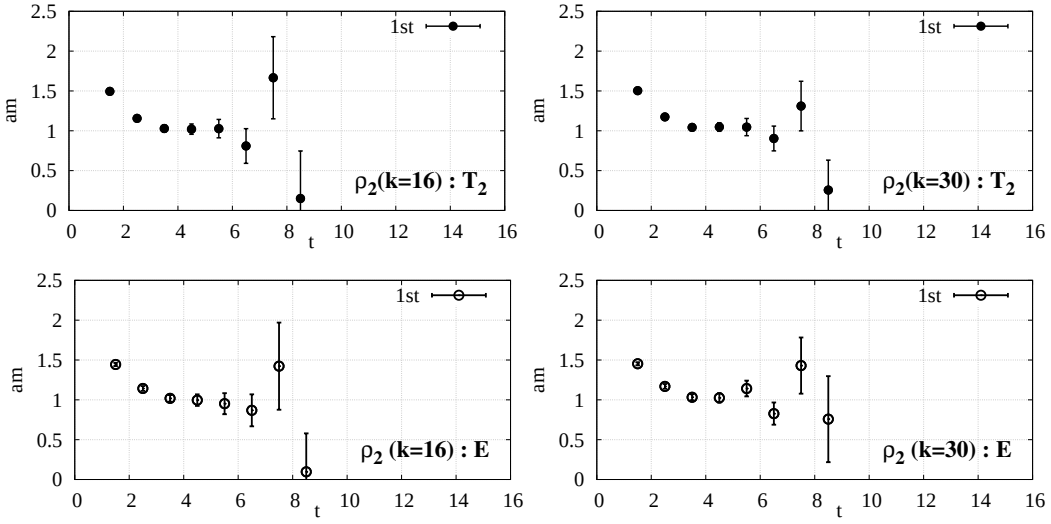

Figure 4.24: $\rho_2(I = 1, J^{PC} = 2^{--})$ states in T_2 (upper panel) and E (lower panel) after excluding $k = 16$ (left panel), $k = 30$ (right panel) low-lying modes.

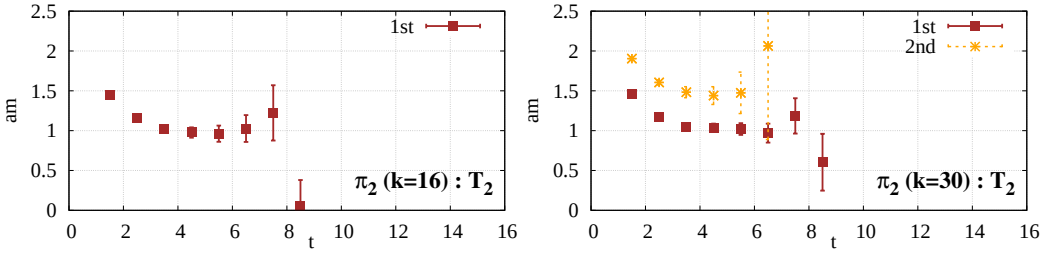

Figure 4.25: $\pi_2(I = 1, J^{PC} = 2^{-+})$ states in T_2 after excluding $k = 16$ (left panel), $k = 30$ (right panel) low-lying modes.

This implies that $n_r = 0$ level of the $J = 2$ mesons have to coincide with the $n_r = 1$ energy level of $J = 1$ mesons.

We compare the energy level $n_r = 0$ of the $J = 2$ mesons with the similar energy level of the $J = 1$ mesons in chirally restored regime, see Figure 4.27. We found that the energy level $n_r = 0$ of the $J = 2$ mesons is below the $n_r = 1$ level of the $J = 1$ mesons. At the same time the $n_r = 0$, $J = 2$ level is above $n_r = 0$ energy level of the $J = 1$ mesons. However, one needs to take into account the volume corrections to these energy levels to make a final conclusion.

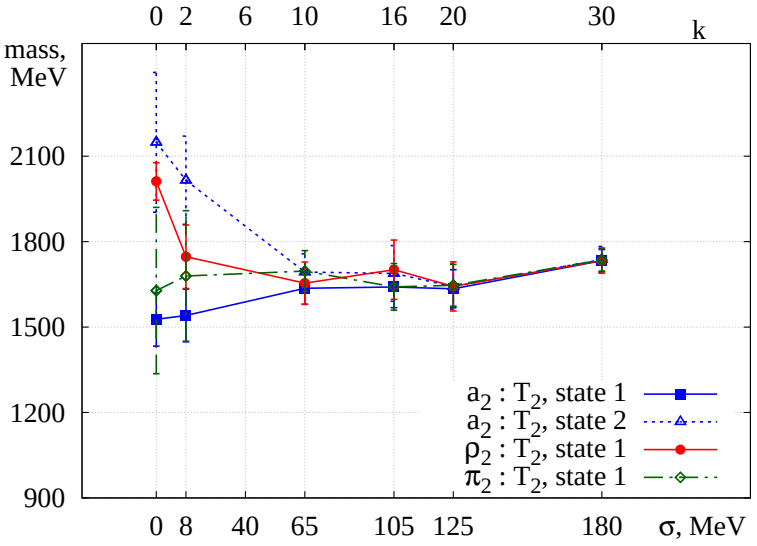

Figure 4.26: Ground state and excited state mass evolution of $J = 2$ mesons in the T_2 representation. The value k denotes the truncation step and σ the corresponding energy gap.

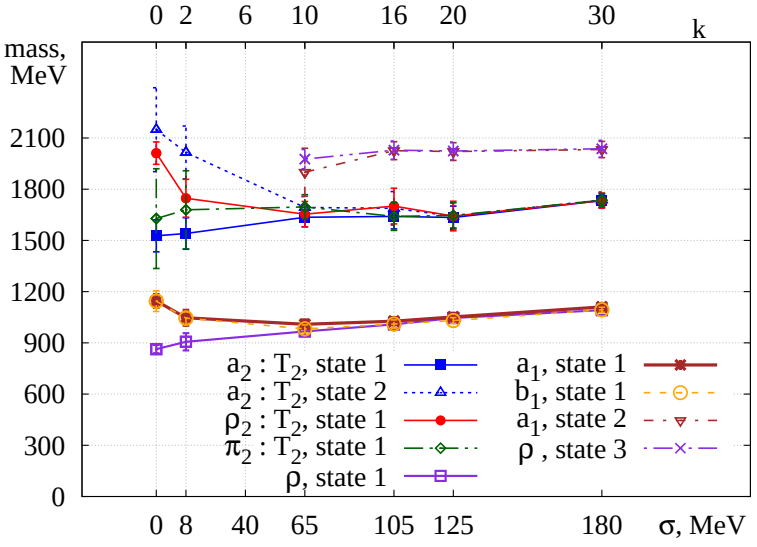

Figure 4.27: Ground state and excited state mass evolution of $J = 1$ and $J = 2$ mesons. The value k denotes the truncation step and σ the corresponding energy gap. For $J = 2$ mesons the results in the T_2 representation are used.

4.4 Summary and Outlook

In this chapter we studied the $J = 0$, $J = 1$ and $J = 2$ meson channels upon unbreaking of chiral symmetry. We have found that removal of the low-lying modes from the valence quark propagators results in the restoration of $SU(2)_L \times SU(2)_R$ chiral symmetry as well as the $U(1)_A$ symmetry. It has been demonstrated that the disconnected contributions vanish in the chirally restored regime. The latter implies that the t'Hooft type of the interactions [64] are no longer relevant for the disconnected contributions to the $\eta(\sigma)$ correlators. The later become identical to the π and a_0 correlators. The $J = 0$ meson ground states do not survive the chiral symmetry restoration.

On the contrary, the $J = 1$ mesons survive the chiral restoration. The energy levels of the $J = 1$ mesons become identical and depend only on the radial excitation quantum number n_r. We argue that the color-magnetic interactions are absent in the $J = 1$ mesons. We associate the energy levels of the $J = 1$ mesons with the energy levels of the QCD string. If the E energy of such a string is quantized as follows $E_{n_r} \sim (n_r + J)$ for any total angular momentum $J = 1, 2, ...$, then to compare the energy levels of the $J = 1$ and $J = 2$ mesons in the chirally restored regime requires the calculation of the finite volume corrections to the current energy levels. The latter is a subject for the future studies.

We employed a new $SU(4)$ symmetry to explain the large degeneracies in the mass spectra of the $J = 1$ and $J = 2$ mesons. The latter arranges the $J \geq (q\bar{q})$ meson states into a singlet and 15-plet representation of the $SU(4)$ group.

So far, we have studied $J = 0, 1, 2$ mesons with non-exotic quantum numbers. It is an interesting question whether the states with the exotic quantum numbers 0^{+-}, 1^{-+}, 2^{+-},... exist in the chirally restored regime.

Chapter 5

Restoration of $\mathbf{SU(2)_L \times SU(2)_R}$ Symmetry in Baryons

In this chapter we study the implications of chiral symmetry restoration on the baryon spectrum. We use the nucleon and Δ states of spin $J = 1/2, 3/2$ to test chiral symmetry predictions.

5.1 Experimental Data versus Baryon Chiral Multiplets

Chiral symmetry restoration predicts the nucleon and Δ parity doublets to be present in the spectrum. However, these parity doublets are absent in the low-lying baryon spectrum as it is clearly seen in the snapshot from the PDG [20], see Table 5.1. For example, there is an approximate 600 MeV mass splitting between the nucleon of positive and negative parities of spin $\frac{1}{2}$. Similar splitting can be found in the Δ spectrum. It is argued that there is a signal of the effective chiral symmetry restoration in the spectrum of baryons of the higher spin [79–83]. This phenomenological observation is understood in terms of the diminishing role of the chiral symmetry breaking effects in the high-lying baryon states. In our approach we can mimic this situation by the removal of the low-lying eigenmodes and look for the parity doublets in the resulting spectrum.

If the chiral symmetry is restored we can arrange baryons into chiral representations of the parity-chiral group. For each spin $J = 1/2, 3/2, 5/2, ...$ there exist the following classification with respect to the total isospin $I \leq 3/2$ presented in Table 5.2. According to this classification, $(1/2, 0) + (0, 1/2)$ contains only nucleon states of different parities. There are only $\Delta^{\pm}$ - states in the $(3/2, 0) + (0, 3/2)$ chiral multiplet. However, both nucleon and Δ states are present in the $(1/2, 1) + (1, 1/2)$ chiral representation.

I \ J^P	$\frac{1}{2}^+$	$\frac{1}{2}^-$	$\frac{3}{2}^+$	$\frac{3}{2}^-$
$\frac{1}{2}$	$N(940)$	$N(1535)$	$N(1720)$	$N(1520)$
	$N(1440)$	$N(1650)$	$N(1900)$	$N(1700)$
$\frac{3}{2}$	$\Delta(1910)$	$\Delta(1620)$	$\Delta(1232)$	$\Delta(1700)$
			$\Delta(1600)$	

Table 5.1: Experimental mass values of the lowest few N and Δ states.

Baryons (isospin)	r
$N^{\pm}(I = \frac{1}{2})$	$(1/2, 0) + (0, 1/2)$
$N^{\pm}(I = \frac{1}{2})$, $\Delta^{\pm}(I = \frac{3}{2})$	$(1/2, 1) + (1, 1/2)$
$\Delta^{\pm}(I = \frac{3}{2})$	$(3/2, 0) + (0, 3/2)$

Table 5.2: Chiral multiplets for baryons with fixed angular momentum J.

5.2 N and Δ Baryons on the Lattice

To extract the baryon states on the lattice we used the set of interpolators listed in Table 5.3. We classified the interpolators with respect to the chiral representations, see Table 5.3. These interpolators are local and include the diquark in the construction [78, 84–89]. Interpolators 1, 2 and 5 were used in the previous studies with the chirally improved fermions [26]. In our analysis with the overlap fermions we used operators 3 and 5 to access nucleons of $J = 3/2$ and deltas of $J = 1/2$ in addition. We used this set of baryon interpolators to construct cross-correlation matrices of dimensions varying from 3×3 to 6×6. Subsequently, we extracted the ground states and excited states in these baryon channels before and after exclusion of the low-lying modes. Corresponding mass values and statistics on the fitting procedure are collected in Appendix E. In general, there is a systematic improvement in the quality of the effective mass plateaus at each level of truncation considered here.

5.2.1 $J = 1/2$: $N^{\pm}$ and $\Delta^{\pm}$ States

The exclusion of the low modes enables us to extract the low-lying baryonic states with better accuracy. Figure 5.1 shows the eigenvalues and effective masses for the nucleon $J = 1/2$ states of positive parity in the full case as well as after the exclusion of $k = 30$ modes. In the latter case, we find doubly degenerate nucleon states. The situation here is of a similar nature as we had with the doubly degenerate states of the $\rho(1, 1^{--})$, $\omega(0, 1^{--})$ and $a_2(1, 2^{++})$ mesons in the chirally restored regime. We observe the same

I, J^P	$\mathcal{O}$	l	r
$N(\frac{1}{2}, \frac{1}{2}^{\pm})$	$\epsilon_{abc} i u_a (u_b^T C\gamma_5 d_c - d_b^T C\gamma_5 u_c)$	1	$(\frac{1}{2}, 0) + (0, \frac{1}{2})$
	$\epsilon_{abc} i u_a (u_b^T C\gamma_4\gamma_5 d_c - d_b^T C\gamma_4\gamma_5 u_c)$	2	$(1, \frac{1}{2}) + (1, \frac{1}{2})$ $(\frac{1}{2}, 0) + (0, \frac{1}{2})$
$N(\frac{1}{2}, \frac{3}{2}^{\pm})$	$\epsilon_{abc} i\gamma_5 u_a (u_b^T C\gamma_i\gamma_5 d_c - d_b^T C\gamma_i\gamma_5 u_c)$	3	$(1, \frac{1}{2}) + (1, \frac{1}{2})$ $(\frac{1}{2}, 0) + (0, \frac{1}{2})$
$\Delta(\frac{3}{2}, \frac{1}{2}^{\pm})$	$\epsilon_{abc} i\gamma_i\gamma_5 u_a (u_b^T C\gamma_i u_c)$	4	$(1, \frac{1}{2}) + (1, \frac{1}{2})$
$\Delta(\frac{3}{2}, \frac{3}{2}^{\pm})$	$\epsilon_{abc} i u_a (u_b^T C\gamma_i u_c)$	5	

Table 5.3: List of the baryon interpolators.

pattern in the nucleon channel of negative parity. Corresponding plots are shown in Figure 5.2. We compare the extracted mases of the nucleon of both parities along the low-mode truncation. The masses of the ground states and excited states are plotted in Figure 5.4. We see that after subtraction of $16 - 20$ modes the nucleon states of opposite parities become degenerate. This goes in line with the predictions of the chiral symmetry restoration. In addition, we perform the same analysis in the Δ channel of spin $J = 1/2$ and found parity doubling of these states. We provide a comparison of the $N(I = 1/2, J = 1/2)$ and $\Delta(I = 3/2, J = 1/2)$ ground states and find that the mass splitting of $N - \Delta$ vanishes as well. In other words, we observe the degeneracy of the $J = 1/2$ baryons states of different isospin and parities. We see that the states in the $(1/2, 0) + (0, 1/2)$ and $(1/2, 1) + (1, 1/2)$ chiral multiplets become degenerate.

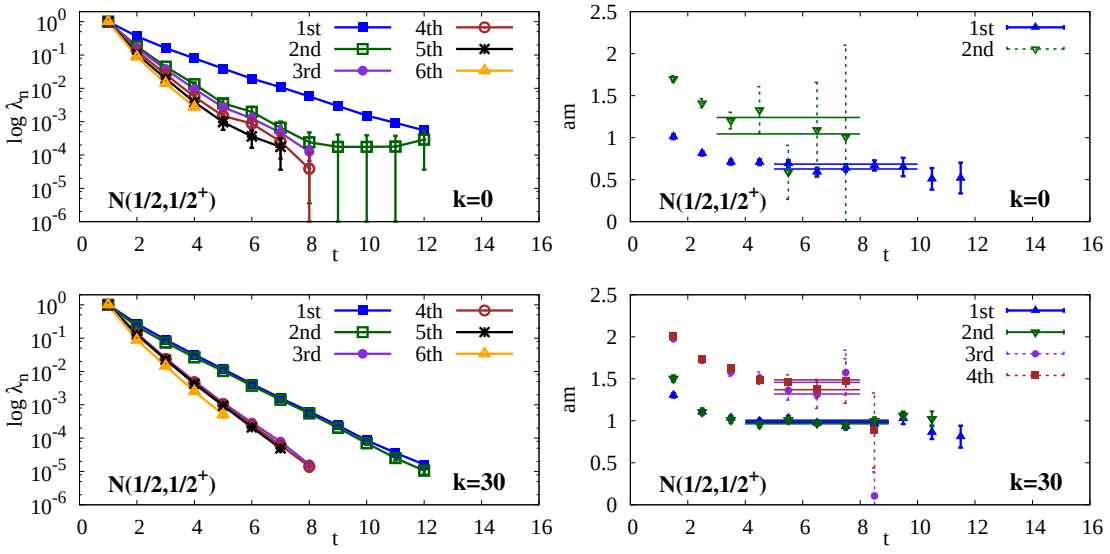

Figure 5.1: $N(I = \frac{1}{2}, J^P = \frac{1}{2}^+)$: eigenvalues (left), effective masses (right), $k = 0, 30$.

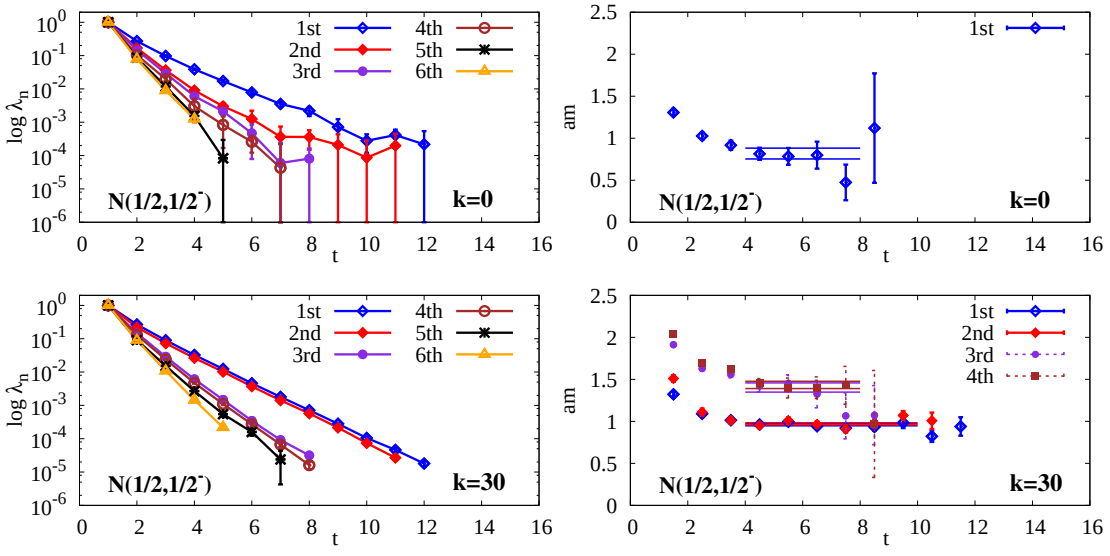

Figure 5.2: $N(I = \frac{1}{2}, J^P = \frac{1}{2}^-)$: eigenvalues (left), effective masses (right), $k = 0, 30$.

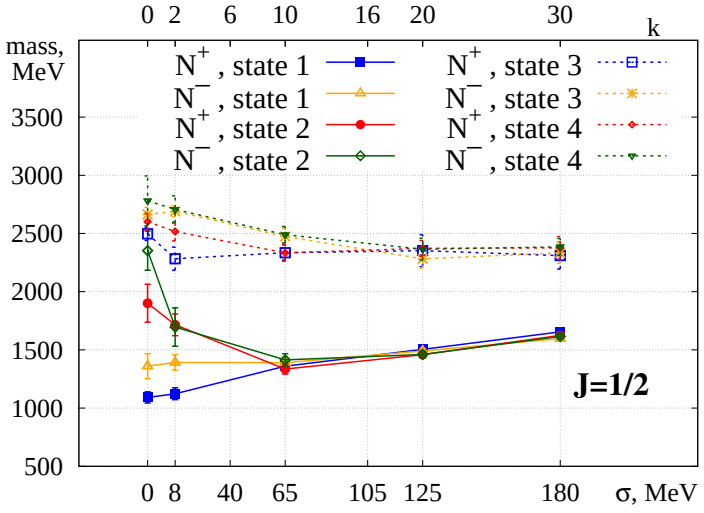

Figure 5.3: $N(I = \frac{1}{2}, J^P = \frac{1}{2}^{\pm})$: Mass evolution of nucleons on exclusion of the low-lying modes. The value σ denotes the energy gap.

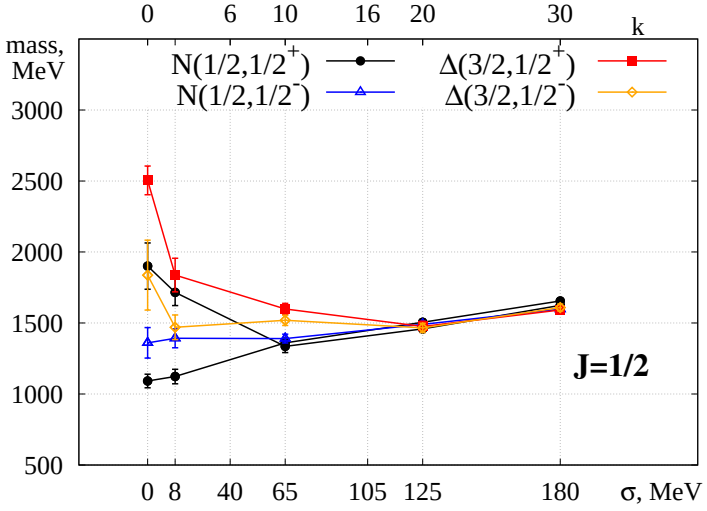

Figure 5.4: $J = \frac{1}{2}$ baryons: Mass evolution of nucleons on exclusion of the low-lying modes. The value σ denotes the energy gap.

5.2.2 $J = 3/2$: $N^{\pm}$ and $\Delta^{\pm}$ States

The analysis presented above can be easily extended to the case of the $J = 3/2$ nucleon and Δ. The signals in the untruncated case are rather noisy. However, they become more stable when the low modes get excluded as it is illustrated using $\Delta^{\pm}$ and $N^{\pm}$ in Figures 5.5-5.8. The identification of the states is more reliable as we approach the truncations with $k = 16 - 20$. Figure 5.9 shows the appearance of the $\Delta(J = 3/2)$ parity doublets exactly at these truncations. This degeneracy occurs for the ground as well as for the excited Δ states. The $N(J = 3/2)$ exhibit parity doubling at the similar truncations k. Additionally, we find that all $J = 3/2$ $\Delta^{\pm}$ and $N^{\pm}$ states degenerate in the chirally restored regime, as it is shown in Figure 5.10 . However, it turns out that the splitting between the baryons of different spin persists. Figure 5.11 shows that the splitting, for example, between $\Delta(J^P = 3/2^+) - N(J^P = 1/2^+)$ and $\Delta(J^P = 3/2^-) - N(J^P = 1/2^-)$ reduces by factor of 2 at the truncation $k = 30$ which is in agreement with the previous observations [26].

In our simulations we did not have the interpolators for the Δ states in the $(3/2, 0) + (0, 3/2)$ chiral representation. It is an interesting question whether such states are degenerate with the states in the $(1/2, 1) + (1, 1/2)$ chiral representation. Given a positive answer one can test whether $SU(4)$ symmetry emerges in the baryon spectrum as well. In this case, the direct product of the $SU(4)$ basis vectors for (qqq) can be decomposed into a sum of the following irreducible representations

$$[4] \times [4] \times [4] = 20 + 20 + 20 + 4 \, . \tag{5.1}$$

It is planned to implement a wider set of the baryon interpolators on the lattice representing all chiral representations. This will enable us to establish the $SU(4)$ emergent symmetry in the baryon sector and find a clue on the generic description of hadrons in the chirally restored as well as in the chirally broken regimes of QCD.

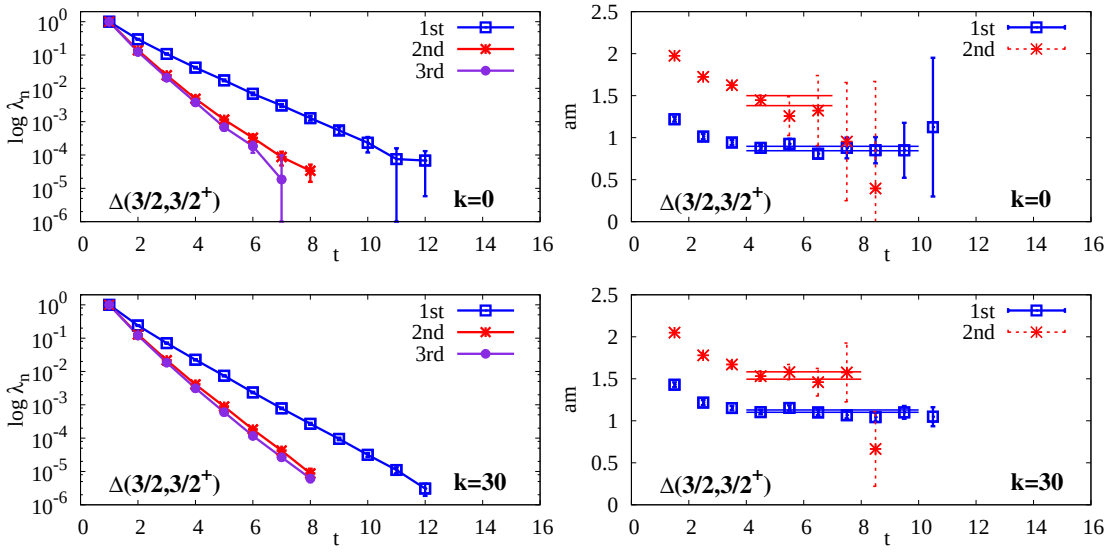

Figure 5.5: $\Delta(I = \frac{3}{2}, J^P = \frac{3}{2}^+)$: eigenvalues (left), effective masses (right), $k = 0, 30$.

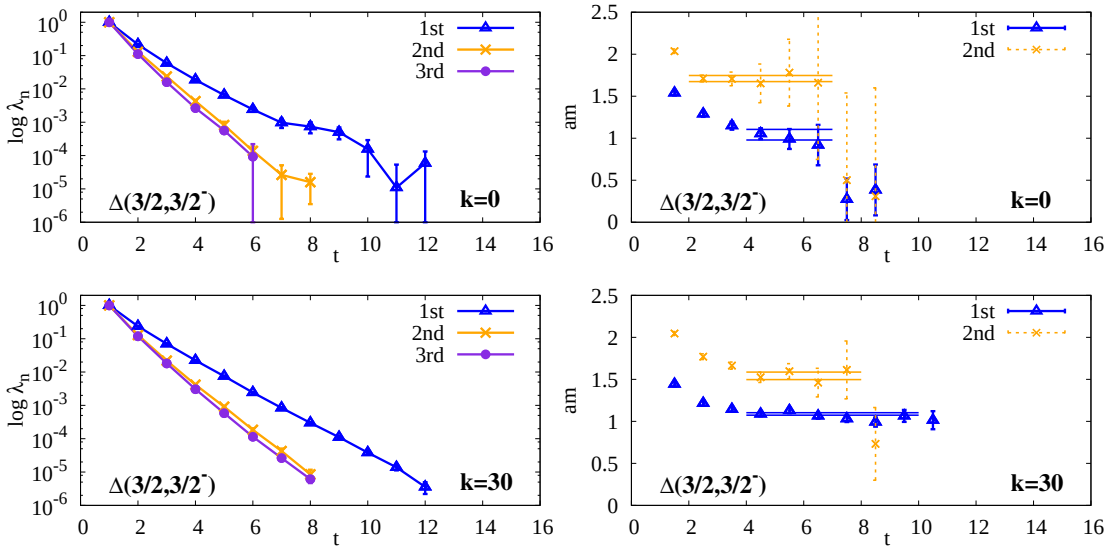

Figure 5.6: $\Delta(I = \frac{3}{2}, J^P = \frac{3}{2}^-)$: eigenvalues (left), effective masses (right), $k = 0, 30$.

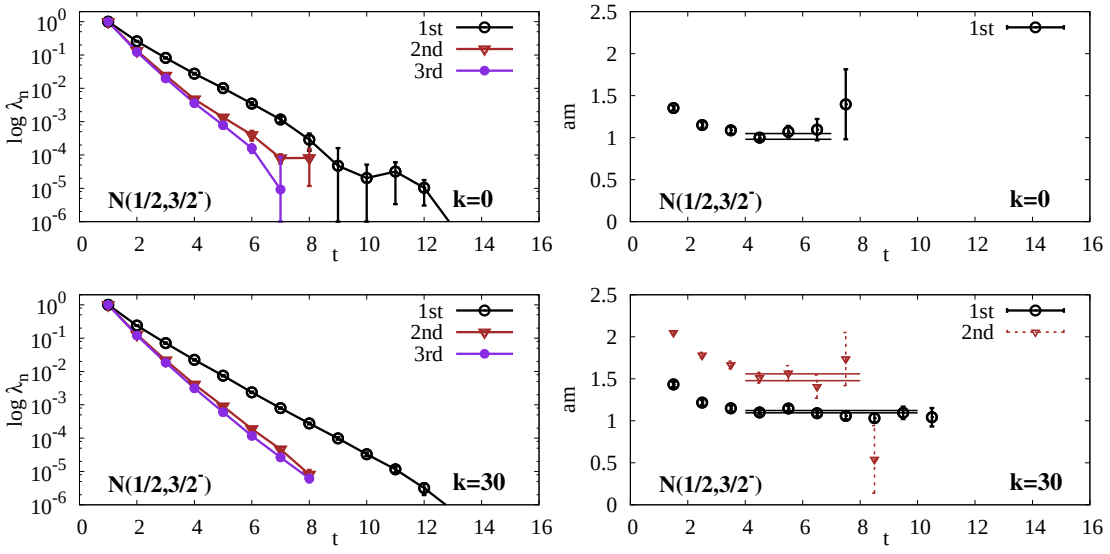

Figure 5.7: $N(I = \frac{1}{2}, J^P = \frac{3}{2}^-)$: eigenvalues (left), effective masses (right), $k = 0, 30$.

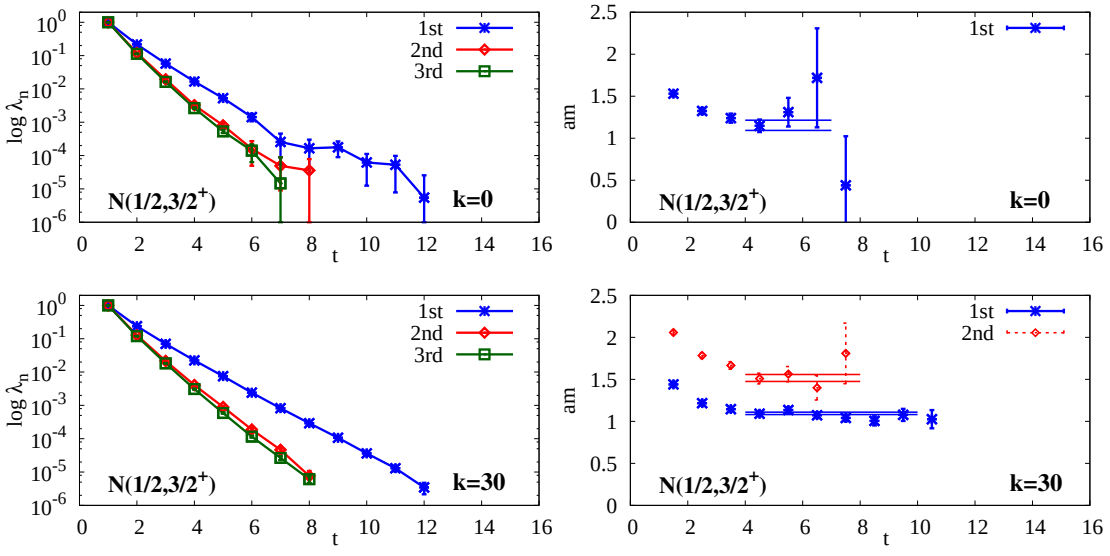

Figure 5.8: $N(I = \frac{1}{2}, J^P = \frac{3}{2}^+)$: eigenvalues (left), effective masses (right), $k = 0, 30$.

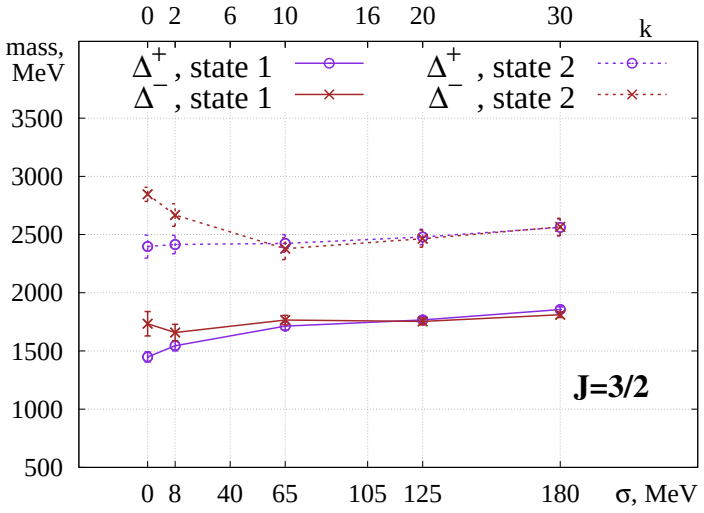

Figure 5.9: Mass evolution of N and Δ baryons on exclusion of the low-lying modes. The value σ denotes the energy gap.

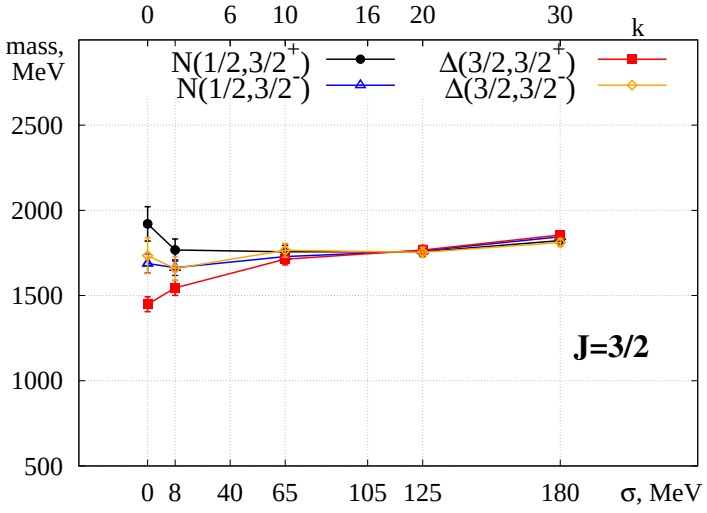

Figure 5.10: Mass evolution of N and Δ baryons on exclusion of the low-lying modes. The value σ denotes the energy gap.

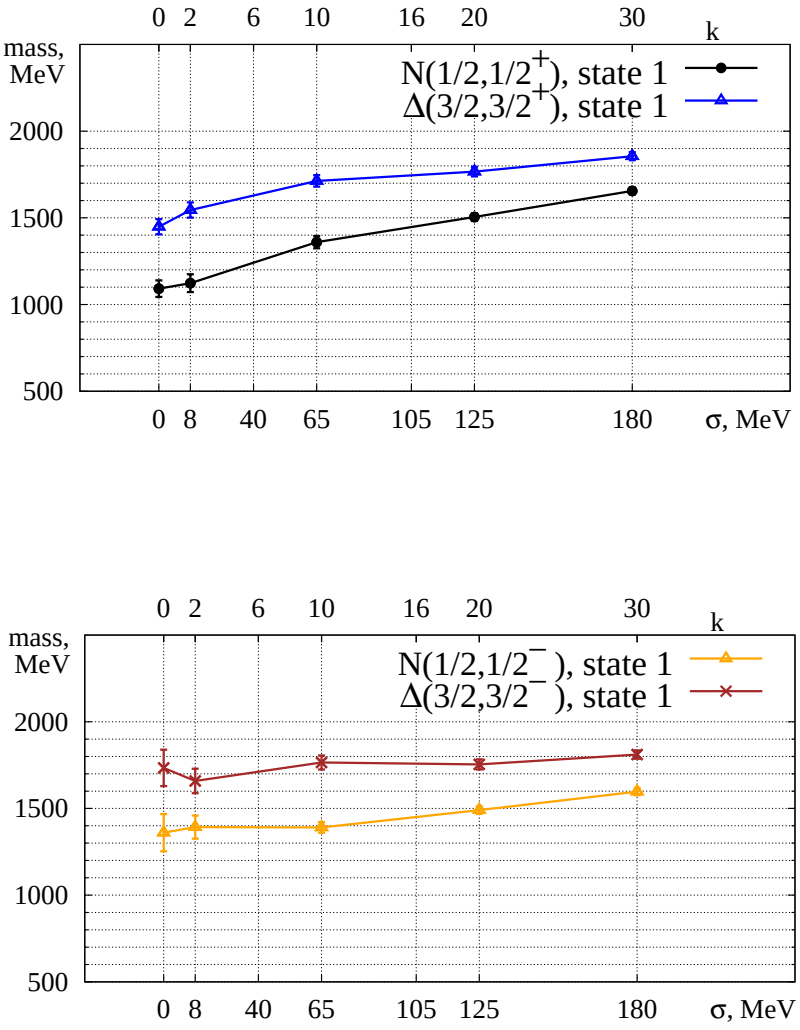

Figure 5.11: Mass evolution of N and Δ baryons on exclusion of the low-lying modes. The value σ denotes the energy gap.

Chapter 6

Conclusion

In this work we restored $SU(2)_L \times SU(2)_R$ and $U(1)_A$ symmetries in the hadron spectrum with exact chiral fermions on the lattice. We demonstrated that a large set of hadrons exhibit these symmetries upon elimination of the low-lying modes from the valence quark propagators. We have found that these low modes are responsible for the $SU(2)_L \times SU(2)_R$ and $U(1)_A$ symmetry breakings in the hadron spectrum. It was found that the ground states of the $J = 0$ mesons accessed with the standard interpolating currents do not survive this chiral restoration on the lattice. However, the isoscalar and isovector $J = 1$ mesons survive such a restoration. A larger degeneracy pattern is found in the $J = 1$ meson spectrum than it is predicted by chiral symmetry. We proposed a new $SU(4)$ symmetry to explain these lattice observations in the $J = 1$ mesons sector. Predictions of the $SU(4)$ symmetry were tested on the $J = 2$ tensor mesons. We suggested the string interpretation to explain the degeneracy between the $J = 1$ meson states.

We performed analogous studies of the nucleon and Δ baryons on the removal of the chiral symmetry breaking effects. We found the nucleon and Δ parity doublets in the spectrum which is in agreement with the predictions of chiral symmetry restoration. We showed that the parity doubling occurs in the nucleon and Δ spectrum for $J = 1/2, J = 3/2$ values of the total angular momentum. However, a non-zero mass splitting between the baryons of different angular momenta J persists in the chirally restored regime. Moreover, a new degeneracy between the baryon states in different chiral representations of $I = 1/2$ and $I = 3/2$ isospin was found which is a signal from the $SU(4)$ symmetry.

It is an interesting question whether our findings of the symmetry patterns in hadrons after unbreaking chiral symmetry can be found in the studies of chiral phase transitions at non-zero temperatures T and finite densities μ. It would be interesting to perform

the studies on unbreaking chiral symmetry with exotic mesons to extend our string interpretation to an arbitrary meson state.

Appendix A

Lattice Gauge Ensembles

In our work, we used the following gauge ensebles listed in Table A.1. The major bulk of the results were produced using the gauge ensembles **A**-**D** provided by JLQCD collaboration. These gauge ensembles were generated with the $N_f = 2$ dynamical overlap fermions using the Iwasaki action at a fixed topology. Exhaustive information on the implementation and generation of these gauge ensembles as well as the related studies can be found in the original works of the JLQCD colaboration [51, 90–95].

Ensemble	$N_s \times N_T$	a fm	M_π, MeV	#conf	Q_T
A	$16^3 \times 32$	0.1184(21)	289.0(1.8)	100	0
B	$16^3 \times 32$	0.1184(21)	365.6(1.2)	100	0
C	$16^3 \times 32$	0.1184(21)	520.8(1.2)	73	0
D	$16^3 \times 32$	0.1184(21)	520.8(1.2)	50	-2
E	$16^3 \times 32$	0.144(1)	322(5)	160	$\langle Q_T \rangle \approx 0$

Table A.1: List of the gauge ensembles. M_π is the mass of pion. Q_T denotes the topological charge of any gauge configuration. $\langle Q_T \rangle$ is the average value over the whole ensemle.

An ensemble **E** of the gauge configurations was generated with the $N_f = 2$ chirally-imroved fermions and Luescher-Weise gauge action by the BGR collaboration [77, 96]. The topological charge was not fixed in these simulations. Exactly the same ensemble was used in the pioneering studies on unbreaking chiral symmetry [25, 26]. In our work, we recompute the $J = 1$ correlators and present new results for the $J = 2$ meson correlators. The results obtained with this ensemble are in a full agreement with the similar observations at the fixed topologies. The latter implies that the conlusions we made in this work hold in general and can be extended to QCD with the physical θ-vacuum.

Appendix B

Stochastic Estimation Technique

In this section we present an outline of the meson two-point correlation function computation with the stochastic estimation technique. The list of quark vectors representing the quark sources and solution vectors according to [61, 91] is

$$\begin{aligned}\{v_k\} =&\Big\{u_1, u_2, ..., u_{N_e}, x_1, ..., x_{N_d}\Big\}\ ,\\ \{w_k\} =&\Big\{\frac{u_1}{\lambda_1}, \frac{u_2}{\lambda_2}, ..., \frac{u_{N_e}}{\lambda_{N_e}}, P_l\eta_1, ..., P_l\eta_{N_d}\Big\}\ ,\end{aligned} \tag{B.1}$$

where u_k are $N_e = 100$ low-lying modes and η_{N_d} single $Z(2)$ noise vector for each configuration. These noise vectors are diluted into $N_d = 3 \times 4 \times N_t/2$ vectors η_d ($d = 1, .., Nd$), which have nonzero elements only for a single combination of color and Dirac indices and at two consecutive time slices. The vectors x_d represent the solution of the linear equation

$$D_{\rm ov}(m)x_d = P_l\eta_d \tag{B.2}$$

with a low-mode projector $P_l = 1 - \sum_{n=1}^{N_e} u_n u_n^\dagger$. We use these vectors for the evaluation of the two-point functions in the isovector meson channel

$$\begin{aligned}G_\Gamma^{I=1}(t; \mathbf{p} = 0) =&\ \langle(\bar{q_1}\Gamma q_2)(t)(\bar{q_2}\Gamma^\dagger q_1)(0)\rangle\\ =&\ \sum_{n=1}^{N_e+N_d}\sum_{m=1}^{N_e+N_d}\mathcal{O}^{(m,n)}(t)\mathcal{O}^{(n,m)}(0) =\ C(t),\end{aligned} \tag{B.3}$$

and in the isoscalar meson channel,

$$\begin{aligned} G_{\Gamma}^{I=0}(t;\mathbf{p}=0) &= \langle(\bar{q}\Gamma q)(t)(\bar{q}\Gamma q)(0)\rangle \\ &= \sum_{n=1}^{N_e+N_d}\sum_{m=1}^{N_e+N_d}\mathcal{O}^{(m,n)}(t)\mathcal{O}^{(n,m)}(0) - 2\sum_{n=1}^{N_e+N_d}\mathcal{O}^{(n,n)}(t)\sum_{m=1}^{N_e+N_d}\mathcal{O}^{(m,m)}(0) \\ &= C(t)+D(t)\,, \end{aligned} \tag{B.4}$$

with

$$\mathcal{O}^{(n,m)}(t) = \sum_{\mathbf{r}}\phi(\mathbf{r})w_m(\mathbf{x}+\mathbf{r},t)\Gamma v_n(\mathbf{x},t) \tag{B.5}$$

defined as a smeared meson interpolating field at time t with Dirac matrices Γ and smearing functions ϕ [97–99]. We used the point, wall and exponential types of smearing functions ϕ_s presented in Table B.1 with the Γ structure combinations shown on Figure 4.1 for the $J=0$ mesons and listed in Table 4.1 for the $J=1$ mesons.

s	$\phi_s(\mathbf{r}) \propto$	s	$\phi_s(\mathbf{r}) \propto$
1	$\delta_{\mathbf{r},0}$	8	$\lvert\mathbf{r}\rvert e^{-\lvert\mathbf{r}\rvert}$
2	const	9	$\lvert\mathbf{r}\rvert e^{-\lvert\mathbf{r}\rvert^2}$
3	$e^{-0.4\lvert\mathbf{r}\rvert}$	10	$\lvert\mathbf{r}\rvert^2 e^{-0.2\lvert\mathbf{r}\rvert^2}$
4	$e^{-\lvert\mathbf{r}\rvert}$	11	$\lvert\mathbf{r}\rvert^2 e^{-0.4\lvert\mathbf{r}\rvert^2}$
5	$e^{-0.4\lvert\mathbf{r}\rvert^2}$	12	$\lvert\mathbf{r}\rvert^2 e^{-0.7\lvert\mathbf{r}\rvert^2}$
6	$e^{-0.7\lvert\mathbf{r}\rvert^2}$	13	$\lvert\mathbf{r}\rvert^2 e^{-\lvert\mathbf{r}\rvert^2}$
7	$e^{-\lvert\mathbf{r}\rvert^2}$	14-26	$\phi_s = \phi_{1-13}$

Table B.1: List of smearing functions used in the construction of the $J=0,1$ meson interpolators with $\sum_r |\phi_s(\mathbf{r})| = 1$ normalization. Index $s = 1-13$ labels the interpolators constructed with $\Gamma = 1, \gamma_5, \gamma_i, \gamma_i\gamma_5$ Dirac gamma matrices, $s = 14-26$ correspond to the $\Gamma = \gamma_i\gamma_t$ interpolators with the same set of smearing functions.

Appendix C

Reweighting the Fermion Determinant

The results presented in Chapters 4-5 were obtained by projecting out the low-lying modes of the Dirac operator from the hadron observables. In this way we modified the energy of a hadron state as well as the overlap of a given operator with this hadron state created from the original chirally broken vacuum. In principle, it is possible to modify the vacuum first and then apply standard operators to probe its structure. However, this requires the removal of the fermion determinant constructed from the low-lying eigenvalues $\{\lambda_k\}$ at each step of a Monte-Carlo simulation. The latter is computionally demanding on the lattice. Below we present our attempt to get a clue on what one might expect in this case using the reweighting technique [7, 100]. We rewrite the defenition of the observable on our lattice as follows

$$\langle \mathcal{O} \rangle = \frac{\int \mathcal{D}[U]\; e^{-S_G} (\det_{Low} D[U]\; \det_{High} D[U])^2\; \mathcal{O}[U]}{\int \mathcal{D}[U]\; e^{-S_G} (\det_{Low} D[U]\; \det_{High} D[U])^2}, \tag{C.1}$$

where $\det_{Low} D[U]\; \det_{High} D[U]$ is a factorization of the fermion determinant $\det D[U]$ into the low-mode and high-mode part. The latter are defined in terms of the product of eigenvalues of the Overlap operator:

$$\det_{Low} D[U] = \prod_{n=1}^{k} \lambda_n[U] \qquad \det_{High} D[U] = \prod_{n=k+1}^{N} \lambda_n[U]. \tag{C.2}$$

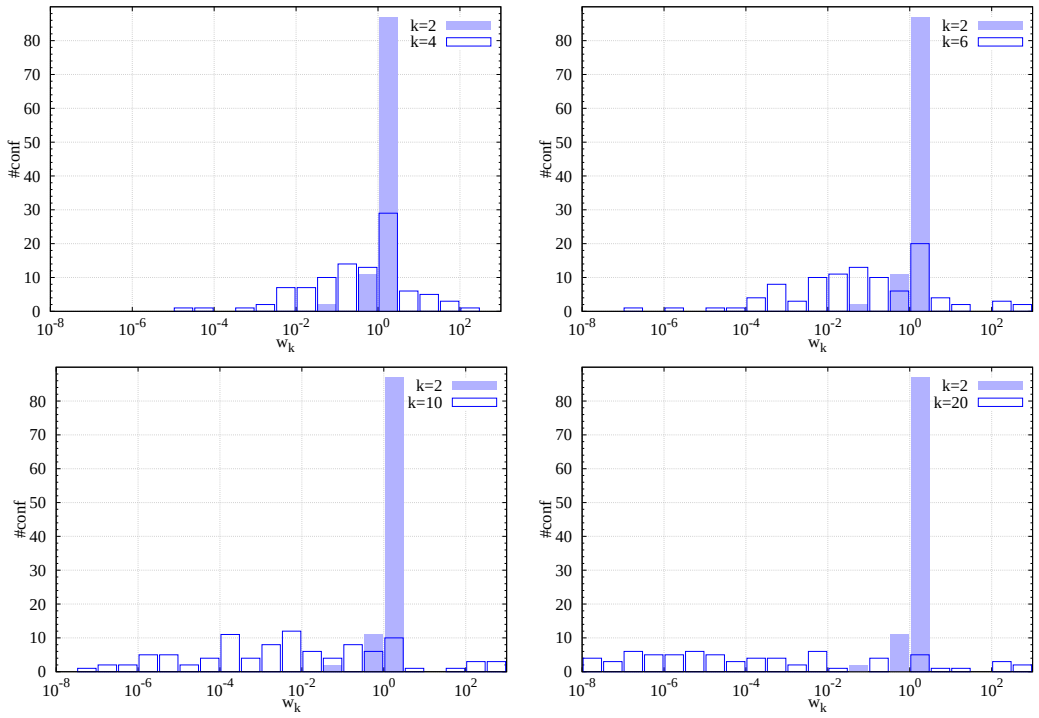

Figure C.1: Distribution of the reweighting coefficients

On a given gauge ensemble we may introduce the so-called reweighted observable

$$\langle \mathcal{O}[U] \rangle_{\mathrm{w}_k} \approx \frac{\sum_{i=1}^{N_{conf}} \mathcal{O}[U_i] \mathrm{w}_k[U_i]}{\sum_{i=1}^{N_{conf}} \mathrm{w}_k[U_i]} \quad \text{with} \quad \mathrm{w}_k = \frac{1}{(\det_{Low} D[U])^2} \tag{C.3}$$

where $w_k[U_i]$ are the reweighting coefficients computed on the gauge configuration U_i.

Figure C.1 shows the distribution of these coefficients over 100 gauge configurations at $k = 2, 4, 6, 10, 20$. It is clearly seen that the larger the amount of the removed eigenvalues, the larger is the spread of the weight factors w_k. Similar distributions were found in [7]. At a truncation $k = 10$ there are only ten gauge configurations which are of the same importance as those ones at the truncation level $k = 2$.

We performed the same analysis presented in Section 4.2 with the reweighted correlation functions for the isovector mesons with $J = 1$. We found similar degeneracies of the isovector mesons for $k \leq 20$ with much lower statistics, however. Taking this analysis into account, we expect that unbreaking chiral symmetry in the vacuum yields the identical results obtained in this work.

Appendix D

Zero-modes and Explicit Chiral Symmetry Breaking

In Section 4.1 we showed that the $U(1)_A$ symmetry is restored in the $J = 0$ meson sector after the exclusion of around 30 lowest eigenmodes of the Overlap Dirac operator. This result was obtained for the ensemble **A** with the lowest quark mass $m \approx 20$ MeV [1] in the trivial topological sector $Q = 0$. By construction there are no exact zero modes in this sector. To determine a possible effect of the exact zero modes on the $U(1)_A$ symmetry breaking at finite volume we analyzed the π and a_0 meson correlators on the gauge ensembles **C** and **D** at fixed $Q = 0$ and $Q = -2$ topologies respectively. The sea quark mass is $m \approx 70$ MeV and is the same in both of these ensembles, see Appendix A.

We find that the shape of the π (a_0) meson point-to-point correlators depends on the topological sector Q in the full case ($k = 0$), see Figure D.1 (upper left). The rest plots in Figure D.1 are shown for the truncations $k = 2, 30, 100$ of the near-zero modes [2]. Two zero modes were not excluded in the computation of the meson correlators in the $Q = -2$ topological sector. We find the degeneracy of the π and a_0 correlators at the maximal truncation of the near-zero modes $k = 100$. First, the differences between the π (a_0) meson correlators computed at a different topology vanishes. We see that the effects of the $U(1)_A$ symmetry breaking due to the presence of two exact zero modes is negligible at this finite volume and quark mass. Moreover, the contribution from the exact zero modes has to vanish in the thermodynamic and chiral limits, see Equation (3.6). To observe $U(1)_A$ symmetry restoration in the ensembles **C** and **D** with the largest quark mass m a larger amount of the low modes has to be excluded. It is due to the fact that

[1] The quark masses are in the physical units.

[2] Here, the term "near-zero modes" is introduced to distinguish the low-lying eigenmodes of the Dirac operator with the near-zero eigenvalue from the ones with the exact zero eigenvalue.

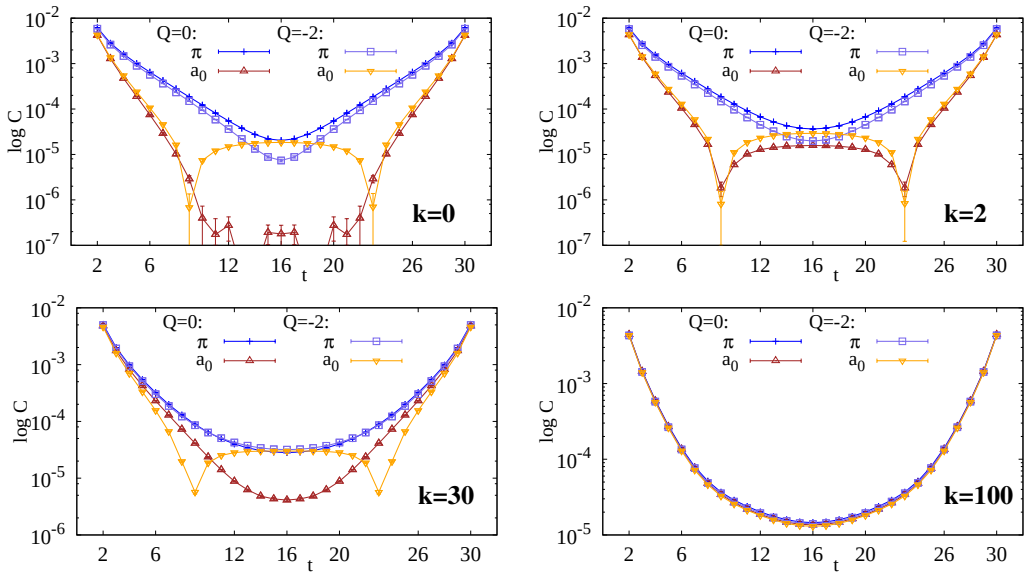

Figure D.1: π and a_0 point-to-point meson correlators on exclusion of the low-lying modes at the fixed topologies $Q = 0, -2$.

we are further away from the chiral limit which is necessary for the condensation of the Dirac modes near $\lambda = 0$.

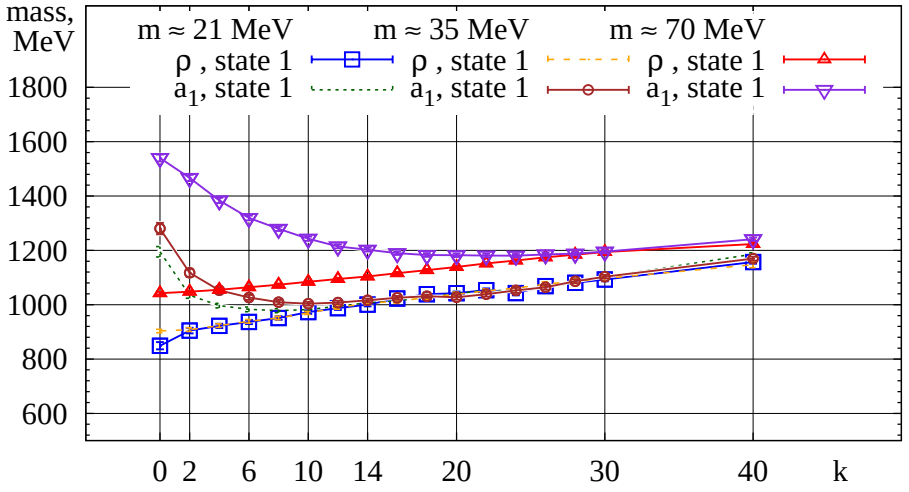

Figure D.2: Mass evolution of the ρ and a_1 meson ground states on exclusion of the low-lying modes at different sea quark masses m.

In addition, our studies shows that the removal of the near-zero modes removes the explicit $U(1)_A$ and $SU(2)_L \times SU(2)_R$ symmetry breaking due to the finite quark mass. The latter is illustrated in Figure D.2 by plotting the mass evolution of the ρ and a_1 meson ground states on exclusion of the near-zero modes for the **A**, **B**, **C** gauge ensembles with three different quark masses m (21, 35 and 70 MeV). The ρ and a_1 states become degenerate in each of these ensemble after the subtraction of different amount of the

near-zero modes. The larger the mass, the greater is the amount of the excluded near-zero modes k. The splitting between ρ (or a_1) states at different quark masses in the full case gets reduced on exclusion of the near-modes, see Figure D.2. However, the splitting between the ρ and a_1 meson states vanishes and is independent of the quark mass of a given ensemble. Analogous analysis of other $J = 1$ states supports the restoration of the $SU(2)_L \times SU(2)_R$ as well as the $U(1)_A$ symmetry on exclusion of the near-zero modes in all the gauge ensembles listed in Appendix A.

Appendix E

Fitting Details and Hadron Masses

Here, we present the numerical data visually depicted on the figures of Chapters 4-5. These data are the results of the hadron spectroscopy analysis performed on the gauge ensemble with the overlap fermions and the pion mass $M_\pi = 289.0(1.8)$, see Table A.1. The results are summarized in Tables E.1-E.10 that contain information on the masses of hadron states depending on the number of the excluded low-lying modes $k = 0, 10, 20, 30$. Hadron states were extracted by exploiting the variational method. Hadrons are labeled with the standard quantum numbers I, J^{PC} (I, J^P) with an index $n = 1, 2, ...$ which enumerates the states in a given quantum channel. For example, $n = 1$ corresponds to the ground state energy level, $n = 2$ corresponds to the first excited energy level, etc . Additional labels E and T_2 are provided to distinguish $J = 2$ mesons states extracted in the E and T_2 irreducible representations of the hypercubic group $\mathcal{O}_\mathrm{h}$. The mass of any state n is extracted using a single exponential fit to the respective eigenvalue $\lambda_n(t, t_0)$. A suitable fit range t is chosen for the χ^2 analysis by identifying a plateau in the effective mass plot. The masses of the states are presented in lattice units and the following multiplicative factor $197.327/a$ MeV can be used to convert these values into physical ones, where $a = 0.1184(21)$ fm. The set of interpolators used in the analysis of a given hadron state are listed as well. For the gauge ensemble **A** the hadron masses were computed using the one-to-all and stochastic all-to-all quark propagators. Hence, the tables are splitted into sections depending on the hadron sector and the type of propagators used in the computations.

Fit results to $J = 1$ meson states (stochastic all-to-all technique)

$\mathbf{k = 0}$					
I, J^{PC}	n	am	$\chi^2/d.o.f$	t	interpolators
$\rho(1, 1^{--})$	1	0.514 ± 0.006	1.37/6	4 - 11	4, 5, 7, 9, 13, 17, 18, 19, 22, 24
	2	0.801 ± 0.027	11.12/4	3 - 8	
	3	1.191 ± 0.028	1.66/4	3 - 8	
	4	1.680 ± 0.050	0.06/1	2 - 4	
$a_1(1, 1^{++})$	1	0.718 ± 0.012	0.12/5	3 - 9	4, 8, 9, 12, 13
	2	1.305 ± 0.030	2.86/3	3 - 7	
$b_1(1, 1^{+-})$	1	0.691 ± 0.023	0.67/3	3 - 7	4, 5, 6, 7, 8, 9
	2	1.074 ± 0.068	0.14/3	3 - 7	
$\omega(0, 1^{--})$	1	0.524 ± 0.008	5.28/9	3 - 13	4, 5, 7, 9, 13, 17, 18, 19, 22, 24
	2	0.877 ± 0.070	1.14/4	3 - 8	
	3	1.213 ± 0.040	0.22/3	3 - 7	
	4	1.607 ± 0.059	0.20/1	2 - 4	
$f_1(0, 1^{++})$	1	0.901 ± 0.035	1.00/4	3 - 8	5, 7, 9, 11, 12
	2	1.456 ± 0.131	0.01/1	4 - 6	
$h_1(0, 1^{+-})$	1	0.656 ± 0.022	0.22/3	3 - 7	4, 5, 6, 7, 8, 9
	2	1.064 ± 0.074	0.17/2	3 - 6	

Table E.1: $J = 1$ mesons: Results of the χ^2 fits to the eigenvalues at a truncation level $k = 0$. The mass am of any state n is given in lattice units; t denotes the fit interval.

k = 10					
I, J^{PC}	n	am	$\chi^2/d.o.f$	t	interpolators
$\rho(1, 1^{--})$	1	0.577 ± 0.005	10.31/8	4 - 13	4, 5, 7, 9, 13, 17, 18, 19, 22, 24
	2	0.579 ± 0.007	20.29/7	4 - 12	
	3	1.146 ± 0.027	1.07/2	3 - 6	
	4	1.183 ± 0.025	0.50/2	4 - 7	
$a_1(1, 1^{++})$	1	0.581 ± 0.005	24.59/8	4 - 13	4, 8, 9, 12, 13
	2	1.119 ± 0.025	1.69/4	4 - 9	
$b_1(1, 1^{+-})$	1	0.574 ± 0.005	4.45/6	3 - 10	4, 5, 6, 7, 8, 9
	2	1.077 ± 0.025	0.36/3	3 - 7	
$\omega(0, 1^{--})$	1	0.564 ± 0.009	2.81/4	5 - 10	4, 5, 7, 9, 13, 17, 18, 19, 22, 24
	2	0.557 ± 0.012	0.70/5	5 - 11	
	3	1.144 ± 0.027	1.43/2	3 - 6	
	4	1.117 ± 0.031	0.22/2	4 - 7	
$f_1(0, 1^{++})$	1	0.610 ± 0.025	0.59/2	5 - 8	5, 7, 9, 11, 12
	2	1.203 ± 0.035	2.17/1	4 - 6	
$h_1(0, 1^{+-})$	1	0.572 ± 0.006	5.30/9	3 - 13	4, 5, 6, 7, 8, 9
	2	1.076 ± 0.026	0.37/3	3 - 7	

Table E.2: $J = 1$ mesons: Results of the χ^2 fits to the eigenvalues at a truncation level $k = 10$. The mass am of any state n is given in lattice units; t denotes the fit interval.

k = 20					
I, J^{PC}	n	am	$\chi^2/d.o.f$	t	interpolators
$\rho(1, 1^{--})$	1	0.626 ± 0.004	21.46/7	3 - 11	4, 5, 7, 9, 13, 17, 18, 19, 22, 24
	2	0.619 ± 0.004	35.16/8	3 - 12	
	3	1.178 ± 0.025	0.70/3	3 - 7	
	4	1.199 ± 0.026	0.33/3	4 - 8	
$a_1(1, 1^{++})$	1	0.626 ± 0.003	31.82/10	3 - 14	4, 8, 9, 12, 13
	2	1.144 ± 0.024	2.48/3	4 - 8	
$b_1(1, 1^{+-})$	1	0.607 ± 0.004	1.88/6	3 - 10	4, 5, 6, 7, 8, 9
	2	1.106 ± 0.025	0.19/3	3 - 7	
$\omega(0, 1^{--})$	1	0.619 ± 0.005	9.90/6	4 - 11	4, 5, 7, 9, 13, 17, 18, 19, 22, 24
	2	0.621 ± 0.008	4.81/5	4 - 10	
	3	1.171 ± 0.023	0.41/4	3 - 8	
	4	1.172 ± 0.030	0.20/3	4 - 8	
$f_1(0, 1^{++})$	1	0.631 ± 0.036	0.87/3	6 - 10	5, 7, 9, 11, 12
	2	1.105 ± 0.054	0.03/2	5 - 8	
$h_1(0, 1^{+-})$	1	0.607 ± 0.004	2.28/8	3 - 12	4, 5, 6, 7, 8, 9
	2	1.105 ± 0.025	0.18/3	3 - 7	

Table E.3: $J = 1$ mesons: Results of the χ^2 fits to the eigenvalues at a truncation level $k = 20$. The mass am of any state n is given in lattice units; t denotes the fit interval.

k = 30					
I, J^{PC}	n	am	$\chi^2/d.o.f$	t	interpolators
$\rho(1, 1^{--})$	1	0.657 ± 0.004	13.66/7	3 - 11	4, 5, 7, 9, 13, 17, 18, 19, 22, 24
	2	0.668 ± 0.003	15.73/7	3 - 11	
	3	1.209 ± 0.025	0.87/4	3 - 8	
	4	1.241 ± 0.028	0.60/2	4 - 7	
$a_1(1, 1^{++})$	1	0.668 ± 0.003	9.93/10	3 - 14	4, 8, 9, 12, 13
	2	1.181 ± 0.027	1.62/2	4 - 7	
$b_1(1, 1^{+-})$	1	0.643 ± 0.004	1.19/6	3 - 10	4, 5, 6, 7, 8, 9
	2	1.133 ± 0.029	0.03/3	3 - 7	
$\omega(0, 1^{--})$	1	0.650 ± 0.005	7.24/6	4 - 11	4, 5, 7, 9, 13, 17, 18, 19, 22, 24
	2	0.664 ± 0.007	4.99/6	4 - 11	
	3	1.208 ± 0.026	0.79/4	3 - 8	
	4	1.226 ± 0.031	0.50/2	4 - 7	
$f_1(0, 1^{++})$	1	0.662 ± 0.028	1.28/4	6 - 11	5, 7, 9, 11, 12
	2	1.168 ± 0.053	0.03/2	5 - 8	
$h_1(0, 1^{+-})$	1	0.643 ± 0.004	1.21/7	3 - 11	4, 5, 6, 7, 8, 9
	2	1.133 ± 0.029	0.03/3	3 - 7	

Table E.4: $J = 1$ mesons: Results of the χ^2 fits to the eigenvalues at a truncation level $k = 30$. The mass am of any state n is given in lattice units; t denotes the fit interval.

Fit results to $J = 1$ and $J = 2$ meson states (one-to-all technique)

I, J^{PC}	n	am	$\chi^2/d.o.f$	t	interpolators [1]
k = 0					
$a_2(1, 2^{++}) : T_2$	1	0.918 ± 0.056	6.28/5	3 - 9	2, 4, 6, 8
	2	1.292 ± 0.147	1.10/3	3 - 7	
$\rho_2(1, 2^{--}) : T_2$	1	1.209 ± 0.040	1.24/2	2 - 5	2, 4
$\pi_2(1, 2^{-+}) : T_2$	1	0.979 ± 0.176	0.19/2	4 - 7	6, 8
$a_2(1, 2^{++}) : E$	1	0.913 ± 0.078	0.37/2	4 - 7	2, 8
$\rho_2(1, 2^{--}) : E$	1	1.212 ± 0.034	2.80/3	2 - 6	8, 10
$\rho(1, 1^{--})$	1	0.519 ± 0.014	1.82/7	4 - 12	1, 4, 5, 8
	2	0.928 ± 0.151	1.61/4	4 - 9	
$a_1(1, 1^{++})$	1	0.689 ± 0.023	4.25/3	3 - 7	1, 4
$b_1(1, 1^{+-})$	1	0.688 ± 0.036	2.11/3	3 - 7	22, 25
k = 10					
I, J^{PC}	n	am	$\chi^2/d.o.f$	t	interpolators
$a_2(1, 2^{++}) : T_2$	1	0.983 ± 0.034	2.06/4	3 - 8	2, 4, 6, 8
	2	1.018 ± 0.038	0.51/3	3 - 7	
$\rho_2(1, 2^{--}) : T_2$	1	0.994 ± 0.045	2.69/3	3 - 7	2, 4
$\pi_2(1, 2^{-+}) : T_2$	1	1.020 ± 0.043	0.62/3	3 - 7	6, 8
$a_2(1, 2^{++}) : E$	1	1.024 ± 0.045	0.76/4	4 - 9	2, 8
$\rho_2(1, 2^{--}) : E$	1	1.022 ± 0.039	1.91/6	3 - 10	8, 10
$\rho(1, 1^{--})$	1	0.581 ± 0.014	6.92/5	6 - 12	1, 4, 5, 8
	2	0.594 ± 0.016	6.20/5	5 - 11	
$a_1(1, 1^{++})$	1	0.607 ± 0.015	1.36/3	5 - 9	1, 4
$b_1(1, 1^{+-})$	1	0.590 ± 0.014	5.99/5	4 - 10	22, 25

Table E.5: $J = 1, 2$ mesons: Results of the χ^2 fits to the eigenvalues at the truncation levels $k = 0, 10$. The mass am of any state n is given in lattice units; t denotes the fit interval.

[1] The interpolators are labeled according to Ref. [78]

k = 20					
I, J^{PC}	n	am	$\chi^2/d.o.f$	t	interpolators
$a_2(1, 2^{++}) : T_2$	1	0.982 ± 0.040	1.04/3	4 - 8	2, 4, 6, 8
	2	0.987 ± 0.047	1.61/3	4 - 8	
	3	1.456 ± 0.061	1.54/3	3 - 7	
	4	1.550 ± 0.071	1.62/3	3 - 7	
$\rho_2(1, 2^{--}) : T_2$	1	0.987 ± 0.052	3.31/3	4 - 8	2, 4
	2	1.552 ± 0.072	1.72/3	3 - 7	
$\pi_2(1, 2^{-+}) : T_2$	1	0.990 ± 0.044	0.62/3	4 - 8	6, 8
	2	1.467 ± 0.065	1.74/3	3 - 7	
$a_2(1, 2^{++}) : E$	1	1.044 ± 0.040	9.25/3	4 - 8	2, 8
	2	1.102 ± 0.045	7.86/3	4 - 8	
$\rho_2(1, 2^{--}) : E$	1	1.029 ± 0.031	5.62/4	3 - 8	8, 10
	2	1.470 ± 0.060	4.91/3	3 - 7	
$\rho(1, 1^{--})$	1	0.629 ± 0.011	4.87/5	5 - 11	1, 4, 5, 8
	2	0.611 ± 0.010	4.69/5	5 - 11	
	3	1.216 ± 0.032	0.37/2	3 - 6	
	4	1.278 ± 0.053	0.85/2	3 - 6	
$a_1(1, 1^{++})$	1	0.632 ± 0.011	1.41/5	5 - 11	1, 4
	2	1.215 ± 0.031	0.94/3	3 - 7	
$b_1(1, 1^{+-})$	1	0.620 ± 0.010	11.77/6	4 - 11	22, 25
	2	1.287 ± 0.056	1.97/3	3 - 7	

Table E.6: $J = 1, 2$ mesons: Results of the χ^2 fits to the eigenvalues at a truncation level $k = 20$. The mass am of any state n is given in lattice units; t denotes the fit interval.

k = 30					
I, J^{PC}	n	am	$\chi^2/d.o.f$	t	interpolators
$a_2(1, 2^{++}) : T_2$	1	1.042 ± 0.023	0.80/4	3 - 8	2, 4, 6, 8
	2	1.044 ± 0.028	0.93/3	3 - 7	
	3	1.459 ± 0.046	0.50/3	3 - 7	
	4	1.507 ± 0.048	1.97/3	3 - 7	
$\rho_2(1, 2^{--}) : T_2$	1	1.042 ± 0.026	2.00/4	3 - 8	2, 4
	2	1.502 ± 0.052	2.17/3	3 - 7	
$\pi_2(1, 2^{-+}) : T_2$	1	1.043 ± 0.024	0.86/4	3 - 8	6, 8
	2	1.477 ± 0.048	0.65/3	3 - 7	
$a_2(1, 2^{++}) : E$	1	1.053 ± 0.035	5.62/3	4 - 8	2, 8
	2	1.138 ± 0.037	3.61/3	4 - 8	
$\rho_2(1, 2^{--}) : E$	1	1.047 ± 0.024	8.32/6	3 - 10	8, 10
	2	1.466 ± 0.042	4.59/3	3 - 7	
$\rho(1, 1^{--})$	1	0.657 ± 0.008	8.82/6	4 - 11	1, 4, 5, 8
	2	0.669 ± 0.007	8.85/6	4 - 11	
	3	1.224 ± 0.030	2.55/2	3 - 6	
	4	1.245 ± 0.044	2.63/2	3 - 6	
$a_1(1, 1^{++})$	1	0.668 ± 0.009	4.73/5	5 - 11	1, 4
	2	1.222 ± 0.029	2.59/3	3 - 7	
$b_1(1, 1^{+-})$	1	0.657 ± 0.009	8.38/7	4 - 12	22, 25
	2	1.240 ± 0.045	3.94/4	3 - 8	

Table E.7: $J = 1, 2$ mesons: Results of the χ^2 fits to the eigenvalues at a truncation level $k = 30$. The mass am of any state n is given in lattice units; t denotes the fit interval.

Fit results for the N and Δ baryon states (one-to-all technique)

k = 0					
state	n	am	$\chi^2/d.o.f$	t	interpolators [2]
$N(1/2,1/2^+)$	1	0.656 ± 0.029	3.28/4	5 - 10	1, 7, 8, 18, 19, 20
	2	1.142 ± 0.098	4.02/4	3 - 8	
$N(1/2,1/2^-)$	1	0.818 ± 0.065	1.82/3	4 - 8	1, 3, 7, 18, 20, 23
	2	1.414 ± 0.101	1.76/3	3 - 7	
$\Delta(3/2,1/2^+)$	1	1.505 ± 0.061	1.61/3	2 - 6	1, 2, 3
$\Delta(3/2,1/2^-)$	1	1.104 ± 0.148	4.94/2	3 - 6	1, 2, 3
$N(1/2,3/2^+)$	1	1.154 ± 0.061	3.60/2	4 - 7	1, 2, 3
$N(1/2,3/2^-)$	1	1.015 ± 0.034	1.56/2	4 - 7	1, 2, 3
$\Delta(3/2,3/2^-)$	1	0.871 ± 0.026	2.03/5	4 - 10	1, 2, 3
$\Delta(3/2,3/2^-)$	1	1.042 ± 0.063	0.37/2	4 - 7	1, 2, 3
k = 10					
state	n	am	$\chi^2/d.o.f$	t	interpolators
$N(1/2,1/2^+)$	1	0.817 ± 0.021	2.32/4	6 - 11	1, 7, 8, 18, 19, 20
	2	0.802 ± 0.026	10.65/5	5 - 11	
$N(1/2,1/2^-)$	1	0.836 ± 0.018	2.97/5	5 - 11	1, 3, 7, 18, 20, 23
	2	0.850 ± 0.032	13.53/5	5 - 11	
$\Delta(3/2,1/2^+)$	1	0.961 ± 0.024	4.78/4	3 - 8	1, 2, 3
$\Delta(3/2,1/2^-)$	1	0.913 ± 0.022	6.21/4	3 - 8	1, 2, 3
$N(1/2,3/2^+)$	1	1.056 ± 0.023	9.88/6	4 - 11	1, 2, 3
$N(1/2,3/2^-)$	1	1.039 ± 0.021	7.39/6	4 - 11	1, 2, 3
$\Delta(3/2,3/2^-)$	1	1.030 ± 0.020	6.90/6	4 - 11	1, 2, 3
$\Delta(3/2,3/2^-)$	1	1.061 ± 0.024	10.95/6	4 - 11	1, 2, 3

Table E.8: N and Δ baryons: Results of the χ^2 fits to the eigenvalues at the truncation levels $k = 0, 10$. The mass am of any state n is given in lattice units; t denotes the fit interval.

[2] interpolators are labeled according to Ref. [89].

k = 20					
state	n	am	$\chi^2/d.o.f$	t	interpolators
$N(1/2,1/2^+)$	1	0.904 ± 0.014	7.48/7	5 - 13	1, 7, 8, 18, 19, 20
	2	0.877 ± 0.015	11.09/7	5 - 13	
	3	1.414 ± 0.082	8.11/3	4 - 8	
	4	1.426 ± 0.041	4.96/3	4 - 8	
$N(1/2,1/2^-)$	1	0.896 ± 0.013	6.50/6	4 - 11	1, 3, 7, 18, 20, 23
	2	0.878 ± 0.017	10.20/6	4 - 11	
	3	1.371 ± 0.048	2.29/3	4 - 8	
	4	1.421 ± 0.057	2.63/4	4 - 9	
$\Delta(3/2,1/2^+)$	1	0.887 ± 0.022	7.07/4	4 - 9	1, 2, 3
	2	1.439 ± 0.043	2.34/3	4 - 8	
$\Delta(3/2,1/2^-)$	1	0.881 ± 0.019	6.72/4	4 - 9	1, 2, 3
	2	1.433 ± 0.046	2.47/3	4 - 8	
$N(1/2,3/2^+)$	1	1.056 ± 0.018	9.70/4	4 - 9	1, 2, 3
	2	1.478 ± 0.044	1.29/3	4 - 8	
$N(1/2,3/2^-)$	1	1.060 ± 0.017	8.73/4	4 - 9	1, 2, 3
	2	1.469 ± 0.042	1.27/3	4 - 8	
$\Delta(3/2,3/2^-)$	1	1.062 ± 0.017	8.40/4	4 - 9	1, 2, 3
	2	1.490 ± 0.040	1.38/3	4 - 8	
$\Delta(3/2,3/2^-)$	1	1.054 ± 0.018	10.31/4	4 - 9	1, 2, 3
	2	1.481 ± 0.044	1.35/3	4 - 8	

Table E.9: N and Δ baryons: Results of the χ^2 fits to the eigenvalues at a truncation level $k = 20$. The mass am of any state n is given in lattice units; t denotes the fit interval.

k = 30					
state	n	am	$\chi^2/d.o.f$	t	interpolators
$N(1/2,1/2^+)$	1	0.995 ± 0.012	4.83/4	4 - 9	1, 7, 8, 18, 19, 20
	2	0.976 ± 0.012	1.69/4	4 - 9	
	3	1.388 ± 0.069	0.54/2	5 - 8	
	4	1.428 ± 0.059	0.26/2	5 - 8	
$N(1/2,1/2^-)$	1	0.960 ± 0.013	4.38/5	4 - 10	1, 3, 7, 18, 20, 23
	2	0.971 ± 0.013	9.49/5	4 - 10	
	3	1.403 ± 0.055	2.32/3	4 - 8	
	4	1.434 ± 0.044	0.37/3	4 - 8	
$\Delta(3/2,1/2^+)$	1	0.957 ± 0.016	3.60/5	4 - 10	1, 2, 3
	2	1.539 ± 0.036	0.61/3	4 - 8	
$\Delta(3/2,1/2^-)$	1	0.967 ± 0.015	3.40/5	4 - 10	1, 2, 3
	2	1.528 ± 0.037	0.72/3	4 - 8	
$N(1/2,3/2^+)$	1	1.095 ± 0.014	7.88/5	4 - 10	1, 2, 3
	2	1.517 ± 0.042	1.31/3	4 - 8	
$N(1/2,3/2^-)$	1	1.109 ± 0.014	6.32/5	4 - 10	1, 2, 3
	2	1.519 ± 0.040	1.10/3	4 - 8	
$\Delta(3/2,3/2^-)$	1	1.115 ± 0.014	5.63/5	4 - 10	1, 2, 3
	2	1.539 ± 0.044	0.43/3	4 - 8	
$\Delta(3/2,3/2^-)$	1	1.088 ± 0.014	8.78/5	4 - 10	1, 2, 3
	2	1.542 ± 0.044	0.64/3	4 - 8	

Table E.10: N and Δ baryons: Results of the χ^2 fits to the eigenvalues at a truncation level $k = 30$. The mass am of any state n is given in lattice units; t denotes the fit interval.

List of Figures

List of Tables

Bibliography

[1] M. Denissenya, L. Y. Glozman, and M. Pak, (2015), arXiv:1505.03285 [hep-lat] .

[2] M. Denissenya, L. Glozman, and C. Lang, Phys.Rev. **D91**, 034505 (2015), arXiv:1410.8751 [hep-lat] .

[3] M. Denissenya, L. Y. Glozman, and C. Lang, PoS **LATTICE2014**, 068 (2014), arXiv:1411.1578 [hep-lat] .

[4] M. Denissenya, L. Y. Glozman, and C. Lang, Phys.Rev. **D89**, 077502 (2014), arXiv:1402.1887 [hep-lat] .

[5] M. Denissenya and L. Y. Glozman, (2014), arXiv:1401.6034 [hep-lat] .

[6] M. Denissenya, L. Y. Glozman, C. Lang, and M. Schröck, PoS **LATTICE2013**, 115 (2014), arXiv:1310.8584 [hep-lat] .

[7] M. Schröck, M. Denissenya, L. Y. Glozman, and C. Lang, PoS **LATTICE2013**, 116 (2014), arXiv:1309.0202 [hep-lat] .

[8] H. Fritzsch and M. Gell-Mann, *50 Years of Quarks* (2015) pp. 1–516.

[9] T. Y. Cao, *From current algebra to quantum chromodynamics* (2010) pp. 1–318.

[10] S. Chatrchyan *et al.* (CMS), Nature Phys. **10**, 557 (2014).

[11] C. D. Roberts and A. G. Williams, Prog.Part.Nucl.Phys. **33**, 477 (1994), arXiv:hep-ph/9403224 [hep-ph] .

[12] R. Alkofer and L. von Smekal, Phys.Rept. **353**, 281 (2001), arXiv:hep-ph/0007355 [hep-ph] .

[13] K. G. Wilson, Phys.Rev. **D10**, 2445 (1974).

[14] M. Creutz, Phys.Rev. **D15**, 1128 (1977).

[15] A. S. Kronfeld and P. B. Mackenzie, Ann.Rev.Nucl.Part.Sci. **43**, 793 (1993), arXiv:hep-ph/9303305 [hep-ph] .

[16] M. A. Shifman, A. Vainshtein, and V. I. Zakharov, Nucl.Phys. **B147**, 385 (1979).

[17] L. Reinders, H. Rubinstein, and S. Yazaki, Phys.Rept. **127**, 1 (1985).

[18] D. Bugg, Physics Reports **397**, 257 (2004).

[19] A. Anisovich, V. Anisovich, and A. Sarantsev, Phys.Rev. **D62**, 051502 (2000), arXiv:hep-ph/0003113 [hep-ph] .

[20] K. Olive *et al.* (Particle Data Group), Chin.Phys. **C38**, 090001 (2014).

[21] L. Glozman, Phys.Lett. **B539**, 257 (2002), arXiv:hep-ph/0205072 [hep-ph] .

[22] L. Y. Glozman, Phys.Lett. **B587**, 69 (2004), arXiv:hep-ph/0312354 [hep-ph] .

[23] S. Afonin, Phys.Lett. **B639**, 258 (2006), arXiv:hep-ph/0603166 [hep-ph] .

[24] L. Y. Glozman, Phys.Rept. **444**, 1 (2007), arXiv:hep-ph/0701081 [hep-ph] .

[25] C. Lang and M. Schrock, Phys.Rev. **D84**, 087704 (2011).

[26] L. Y. Glozman, C. Lang, and M. Schrock, Phys.Rev. **D86**, 014507 (2012).

[27] M. Schröck, PhD thesis (2013).

[28] C. Gattringer and C. B. Lang, *Quantum chromodynamics on the lattice*, Vol. 788 (2010) pp. 1–343.

[29] H. Nielsen and M. Ninomiya, Physics Letters B **105**, 219 (1981).

[30] P. H. Ginsparg and K. G. Wilson, Phys.Rev. **D25**, 2649 (1982).

[31] H. Neuberger, Phys.Lett. **B417**, 141 (1998), arXiv:hep-lat/9707022 [hep-lat] .

[32] H. Neuberger, Phys.Lett. **B427**, 353 (1998), arXiv:hep-lat/9801031 [hep-lat] .

[33] Y. Shamir, Nucl.Phys. **B406**, 90 (1993), arXiv:hep-lat/9303005 [hep-lat] .

[34] D. B. Kaplan, , 223 (2009), arXiv:0912.2560 [hep-lat] .

[35] M. Luscher, Phys.Lett. **B428**, 342 (1998), arXiv:hep-lat/9802011 [hep-lat] .

[36] K. Fujikawa, Phys.Rev.Lett. **42**, 1195 (1979).

[37] G. Christos, Z.Phys. **C18**, 155 (1983).

[38] A. V. Smilga, *Lectures on quantum chromodynamics* (2001) pp. 1–352.

[39] G. Christos, Phys.Rept. **116**, 251 (1984).

[40] H. Fukaya *et al.* (JLQCD), Phys.Rev.Lett. **104**, 122002 (2010), arXiv:0911.5555 [hep-lat] .

[41] H. Fukaya *et al.* (JLQCD, TWQCD), Phys.Rev. **D83**, 074501 (2011), arXiv:1012.4052 [hep-lat] .

[42] G. P. Engel, L. Giusti, S. Lottini, and R. Sommer, PoS **LATTICE2013**, 119 (2014), arXiv:1309.4537 [hep-lat] .

[43] G. P. Engel, L. Giusti, S. Lottini, and R. Sommer, Phys.Rev. **D91**, 054505 (2015), arXiv:1411.6386 [hep-lat] .

[44] T. A. DeGrand and A. Hasenfratz, Phys.Rev. **D64**, 034512 (2001), arXiv:hep-lat/0012021 [hep-lat] .

[45] T. A. DeGrand, Phys.Rev. **D69**, 074024 (2004), arXiv:hep-ph/0310303 [hep-ph] .

[46] C. Gattringer, M. Gockeler, P. E. Rakow, S. Schaefer, and A. Schafer, Nucl.Phys. **B617**, 101 (2001), arXiv:hep-lat/0107016 [hep-lat] .

[47] H. Neff, N. Eicker, T. Lippert, J. W. Negele, and K. Schilling, Phys.Rev. **D64**, 114509 (2001), arXiv:hep-lat/0106016 [hep-lat] .

[48] I. Horvath, N. Isgur, J. McCune, and H. Thacker, Phys.Rev. **D65**, 014502 (2002), arXiv:hep-lat/0102003 [hep-lat] .

[49] T. Ivanenko and J. W. Negele, Nucl.Phys.Proc.Suppl. **63**, 504 (1998), arXiv:hep-lat/9709130 [hep-lat] .

[50] C. Gattringer, Phys.Rev. **D63**, 114501 (2001), arXiv:hep-lat/0003005 [hep-lat] .

[51] J. Noaki *et al.* (JLQCD, TWQCD), Phys.Rev.Lett. **101**, 202004 (2008), arXiv:0806.0894 [hep-lat] .

[52] B. Blossier, M. Della Morte, G. von Hippel, T. Mendes, and R. Sommer, JHEP **0904**, 094 (2009), arXiv:0902.1265 [hep-lat] .

[53] M. Luscher and U. Wolff, Nucl.Phys. **B339**, 222 (1990).

[54] C. Michael, Nucl.Phys. **B259**, 58 (1985).

[55] T. D. Cohen and X.-D. Ji, Phys.Rev. **D55**, 6870 (1997), arXiv:hep-ph/9612302 [hep-ph] .

[56] C. McNeile, C. Michael, and K. Sharkey (UKQCD), Phys.Rev. **D65**, 014508 (2002), arXiv:hep-lat/0107003 [hep-lat] .

[57] T. Kunihiro *et al.* (SCALAR), Phys.Rev. **D70**, 034504 (2004), arXiv:hep-ph/0310312 [hep-ph] .

[58] K. Hashimoto and T. Izubuchi, Prog.Theor.Phys. **119**, 599 (2008), arXiv:0803.0186 [hep-lat] .

[59] S. Bernardson, P. McCarty, and C. Thron, Comput.Phys.Commun. **78**, 256 (1993).

[60] M. Peardon *et al.* (Hadron Spectrum), Phys.Rev. **D80**, 054506 (2009), arXiv:0905.2160 [hep-lat] .

[61] J. Foley, K. Jimmy Juge, A. O'Cais, M. Peardon, S. M. Ryan, *et al.*, Comput.Phys.Commun. **172**, 145 (2005), arXiv:hep-lat/0505023 [hep-lat] .

[62] E. V. Shuryak, Nucl.Phys. **B203**, 93 (1982).

[63] E. V. Shuryak, *The QCD vacuum, hadrons and the superdense matter*, Vol. 71 (2004) pp. 1–618.

[64] G. 't Hooft, Phys.Rept. **142**, 357 (1986).

[65] D. Diakonov and V. Y. Petrov, Nucl.Phys. **B272**, 457 (1986).

[66] L. Y. Glozman, C. Lang, and M. Limmer, Phys.Rev. **D82**, 097501 (2010), arXiv:1007.1346 [hep-lat] .

[67] L. Y. Glozman, C. Lang, and M. Limmer, Phys.Lett. **B705**, 129 (2011), arXiv:1106.1010 [hep-ph] .

[68] L. Y. Glozman, C. Lang, and M. Limmer, Prog.Part.Nucl.Phys. **67**, 312 (2012), arXiv:1111.2562 [hep-ph] .

[69] L. Y. Glozman, Eur.Phys.J. **A51**, 27 (2015), arXiv:1407.2798 [hep-ph] .

[70] L. Y. Glozman and M. Pak, (2015), arXiv:1504.02323 [hep-lat] .

[71] L. Y. Glozman and A. Nefediev, Phys.Rev. **D76**, 096004 (2007), arXiv:0704.2673 [hep-ph] .

[72] L. Y. Glozman, Phys.Lett. **B541**, 115 (2002), arXiv:hep-ph/0204006 [hep-ph] .

[73] Y. Nambu, Phys.Lett. **B80**, 372 (1979).

[74] M. Shifman and A. Vainshtein, Phys.Rev. **D77**, 034002 (2008), arXiv:0710.0863 [hep-ph] .

[75] R. Johnson, Physics Letters B **114**, 147 (1982).

[76] C. Gattringer, L. Y. Glozman, C. Lang, D. Mohler, and S. Prelovsek, Phys.Rev. **D78**, 034501 (2008), arXiv:0802.2020 [hep-lat] .

[77] G. P. Engel, C. Lang, M. Limmer, D. Mohler, and A. Schafer (BGR [Bern-Graz-Regensburg]), Phys.Rev. **D82**, 034505 (2010), arXiv:1005.1748 [hep-lat] .

[78] G. P. Engel, C. Lang, M. Limmer, D. Mohler, and A. Schafer, Phys.Rev. **D85**, 034508 (2012), arXiv:1112.1601 [hep-lat] .

[79] T. D. Cohen and L. Y. Glozman, Phys.Rev. **D65**, 016006 (2001), arXiv:hep-ph/0102206 [hep-ph] .

[80] T. D. Cohen and L. Y. Glozman, Int.J.Mod.Phys. **A17**, 1327 (2002), arXiv:hep-ph/0201242 [hep-ph] .

[81] L. Y. Glozman, Acta Phys.Polon. **B35**, 2985 (2004), arXiv:hep-ph/0410194 [hep-ph] .

[82] L. Y. Glozman, Nucl.Phys. **A755**, 17 (2005), arXiv:hep-ph/0501043 [hep-ph] .

[83] T. D. Cohen and L. Y. Glozman, (2006), arXiv:hep-ph/0603240 [hep-ph] .

[84] D. Brommel *et al.* (Bern-Graz-Regensburg), Nucl.Phys.Proc.Suppl. **129**, 251 (2004), arXiv:hep-lat/0309036 [hep-lat] .

[85] D. Brommel *et al.* (Bern-Graz-Regensburg), Phys.Rev. **D69**, 094513 (2004), arXiv:hep-ph/0307073 [hep-ph] .

[86] T. Burch *et al.* (Bern-Graz-Regensburg), Phys.Rev. **D70**, 054502 (2004), arXiv:hep-lat/0405006 [hep-lat] .

[87] T. Burch, C. Gattringer, L. Y. Glozman, C. Hagen, D. Hierl, *et al.*, Phys.Rev. **D74**, 014504 (2006), arXiv:hep-lat/0604019 [hep-lat] .

[88] T. DeGrand, Z. Liu, and S. Schaefer, Phys.Rev. **D77**, 034505 (2008), arXiv:0712.0254 [hep-ph] .

[89] G. P. Engel, C. Lang, D. Mohler, and A. Schäfer (BGR), Phys.Rev. **D87**, 074504 (2013), arXiv:1301.4318 [hep-lat] .

[90] S. Aoki *et al.* (JLQCD), Phys.Rev. **D78**, 014508 (2008).

[91] S. Aoki *et al.* (JLQCD, TWQCD), Phys.Rev. **D80**, 034508 (2009), arXiv:0905.2465 [hep-lat] .

[92] H. Fukaya, (2006), arXiv:hep-lat/0603008 [hep-lat] .

[93] H. Matsufuru, *Linear problem of overlap fermion operator in lattice QCD* (2010) pp. 1–15p.

[94] H. Matsufuru, *Implementation of the overlap fermion simulation* (2010) pp. 1–25p.

[95] S. Aoki, T.-W. Chiu, G. Cossu, X. Feng, H. Fukaya, *et al.*, PTEP **2012**, 01A106 (2012).

[96] C. Gattringer, C. Hagen, C. Lang, M. Limmer, D. Mohler, *et al.*, Phys.Rev. **D79**, 054501 (2009), arXiv:0812.1681 [hep-lat] .

[97] S. Aoki *et al.* (CP-PACS), Nucl.Phys.Proc.Suppl. **60A**, 14 (1998), arXiv:hep-lat/9710056 [hep-lat] .

[98] P. de Forcrand *et al.* (QCD-TARO), Phys.Rev. **D63**, 054501 (2001), arXiv:hep-lat/0008005 [hep-lat] .

[99] T. Kaneko *et al.* (TWQCD, JLQCD), PoS **LAT2009**, 107 (2009), arXiv:0910.4648 [hep-lat] .

[100] A. Hasenfratz, R. Hoffmann, and S. Schaefer, Phys.Rev. **D78**, 014515 (2008), arXiv:0805.2369 [hep-lat] .

Acknowledgments

I would like to thank my supervisor Prof. Leonid Glozman for giving me the opportunity to do the research on the very interesting topics at the Institute of Theoretical Physics at Karl-Franzens University of Graz. I'm grateful to Prof. Christian Lang and Mario Schröck for bringing me into the field of the lattice QCD and sharing their valuable experience.

My 3 years of PhD studies would be less exciting without the joy and fun I had with my colleagues Mario, Ydalia, Joseph , Valentina, Vasily, Markus, Ana, Milan, Christian, Pascal and many others. I'm grateful to Vasily Sazonov and Markus Pak for the interesting physics discussions and proof reading my thesis. I was happy to participate in the lattice group meeting where I've got a constructive feedback and motivation for the further improvements in my research strategy.

I'm grateful to Prof. Sinya Aoki, Prof. Shoji Hashimoto and Takashi Kaneko for their initiative in sharing their data and experience on the overlap fermions. I would like to express my gratitude to the Lattice Group at KEK National High Energy Accelerator Research Organization for their hospitality and support during my stay in Tsukuba, Japan. I'm also happy to thank Prof. Silvano Simula and Mario Schröck for their kind hospitality during my secondment at Roma Tre University in Italy.

It's hard to imagine my scientific life without the computer cluster support from Dr. Ursula Winkler. I would like to thank Martin Volk for managing the hardware and software resources necessary for the research.

I'm also immensely grateful to Mag. Claudia Spidla and Prof. Christof Gattringer for their administrative support which enabled me to present my results at the numerous international conferences and workshops. Finally, I want to thank the Austrian Science Fund (FWF) organization for funding my PhD program within the Doktoratskolleg Graz "Hadrons in Vacuum, Nuclei and Stars" graduate school.